

**PROPAGATION OF LF AND VLF LIGHTNING
ELECTROMAGNETIC WAVES: THE GROUND EFFECTS**
**Applications to Lightning Locating Systems in Mountainous
Regions**

A Dissertation Submitted to the Department of Electrical, Electronic and
Computer Engineering of the Universidad Nacional de Colombia in
Partial Fulfillment of the Requirements for the Degree of:
Doctor of Engineering

Author:
Juan Diego Pulgarín Rivera

March 2020

**PROPAGACIÓN DE ONDAS ELECTROMAGNÉTICAS DE
RAYO EN BF Y MBF: EFECTOS DEL SUELO**
Aplicaciones a sistemas de localización de rayos en regiones
montañosas

Disertación presentada al Departamento de Ingeniería Eléctrica,
Electrónica y Computación de la Universidad Nacional de Colombia como
requisito parcial para obtener al título de:
Doctor en Ingeniería

Autor:
Juan Diego Pulgarín Rivera

Marzo de 2020

Copyright © 2020 by Juan Diego Pulgarín Rivera
All Rights Reserved

A mis Padres:

Jesús Ernelso & María del Socorro

Abstract

The problem of radiowave propagation over ground has been subject of interest for more than one century. As an electromagnetic problem in nature, it is completely described by Maxwell's equations. However, given specific boundary conditions and source of the fields, the solution of these equations can be of extreme complexity and numerical solutions have to be pursued. The applications are numerous; the problem of this work being the modelling of lightning electromagnetic waves propagation over irregular ground for its application to lightning locating systems. A particular question arises: what is the effect that the ground irregularities have on the propagation of these kind of waves? Also, what is the consequence of these propagation effects on lightning locating systems that operate over mountainous regions of altitudes that are comparable to the source wavelength? These are the questions that were stated to be answered with this work.

The methodological approach for answering the questions stated consisted in the development of a numerical simulation model, specifically the use of the Finite-Difference Time-Domain Method (FDTD). Due to the requirements in computer memory of this method, it was necessary to obtain a two-dimensional approximation to Maxwell's equations, considering the azimuthal symmetry of the problem. After the model was validated and tested with canonical models, it was used to observe the propagation of lightning electromagnetic waves under different scenarios. Furthermore, six different relief profiles over the Colombian territory were modelled and used to determine their effects on the propagation of lightning-generated electromagnetic waves. Also, the onset times of the waves to different observation points were measured and compared for propagation over flat ground and over irregular ground.

The results showed that the overall effect of ground irregularities on the propagation of waves can be of two types: increase or attenuation of the signal peak. However, the time derivative or rise time of the waves was not modified in an important manner. That is, the ground irregularities alone, without the effect of ground conductivity, can only modify the signal amplitude. The attenuation of the signal peak is obtained as a result of propagation over electrically large obstacles due to wave reflection. The increase of the signal peak is explained by the phenomenon of constructive interference of waves when the observation point is located at an altitude. Some numbers can be given; for example, for a source wavelength of about 5000 m, and an obstacle of about 0.8 times this wavelength, the vertical electric field peak was reduced around 22% of the value obtained for propagation over flat ground. For a source wavelength of about 790 m, the vertical electric field peak suffered a reduction of about 43% of its value when it propagated over flat ground. The mentioned results were obtained for propagation over an obstacle of the same height, but for different source wavelengths, showing that the discussion has to be given in terms of wavelengths. The important point is that the change in the signal peak when it propagates over mountains of important altitude—like the ones that exist in Colombia due to the Cordillera of the Andes—has to be considered if a precise modelling of propagation is required. The results also showed that the signal onset times were not modified beyond 4% with respect to the onset times for propagation over flat ground. In fact, five out of six of the real relief profiles analysed showed that the error in calculation of the onset time was under 1% when the terrain irregularities were included in the propagation model.

When the research started, it was believed that the major effect of ground irregularities on the propagation of lightning-generated electromagnetic waves was on the location accuracy of lightning locating systems. However, the results suggested a change of direction when thinking about these effects, since signal onset times strongly depend on the signal risetime, but this parameter is not modified at a great extent by the terrain irregularities alone. In this regard, the propagation effects of ground conductivity are actually more important because it causes selective attenuation of certain frequency components, as it has been shown by several authors in the scientific literature. Then, this thesis showed

that the propagation effects of terrain irregularities have a major effect in other aspects of the application to lightning locating systems, as for example the detection efficiency and mainly, the estimation of lightning parameters from lightning locating systems data.

Keywords

FDTD Analysis, Irregular Ground, Lightning Locating Systems, Propagation Effects, Radiowave Propagation.

Resumen

El problema de propagación de ondas de radio sobre el suelo ha sido tema de interés por más de un siglo. Dado que el problema es de naturaleza electromagnética, su descripción está dada completamente por las ecuaciones de Maxwell. Sin embargo, dadas una condiciones de frontera específicas y según el tipo de fuente de los campos, la solución de dichas ecuaciones puede ser extremadamente compleja y casi siempre se tienen que buscar soluciones numéricas. Existe una gran cantidad de aplicaciones; el problema abordado en este trabajo trata sobre el modelado de la propagación sobre suelo irregular de las ondas electromagnéticas generadas por rayos, para su aplicación a sistemas de localización de rayos. Se puede pensar inmediatamente en la siguiente pregunta: ¿cuál es el efecto que tienen las irregularidades del suelo sobre la propagación de este tipo de ondas? Además, ¿cuál es la consecuencia de estos efectos de propagación sobre los sistemas de localización de rayos que funcionan sobre regiones montañosas de altitudes que son comparables a la longitud de onda de la fuente de los campos? Estas son las preguntas de investigación que fueron planteadas para ser respondidas mediante el presente trabajo.

El enfoque metodológico para responder a las preguntas planteadas consistió en el desarrollo de un modelo de simulación numérica, específicamente el método de Diferencias Finitas en el Dominio del Tiempo (DFDT). Debido a los requerimientos de memoria computacional del método, fue necesario obtener una aproximación en dos dimensiones a las ecuaciones de Maxwell, considerando la simetría azimutal del problema. Después de que el modelo numérico fue validado y probado mediante resultados de modelos canónicos, se utilizó para predecir y observar la propagación de ondas electromagnéticas generadas por rayos bajo diferentes escenarios. Además, se modelaron seis perfiles de relieve reales

sobre el territorio Colombiano y se usaron para determinar su efecto sobre la propagación de ondas electromagnéticas de rayo. También se midieron los tiempos de arribo de las ondas a diferentes puntos de observación y se compararon los casos de tiempos obtenidos para propagación sobre terreno plano con los obtenidos para propagación sobre terreno irregular.

Los resultados mostraron que el efecto global de las irregularidades del suelo sobre la propagación de las ondas puede ser de dos tipos: incremento o atenuación del valor pico de la señal. Sin embargo, las derivadas temporales o tiempo de frente de las ondas no se vieron afectados de manera significativa. Esto es, las irregularidades del suelo únicamente, sin el efecto de la conductividad del suelo, pueden modificar únicamente la amplitud de las ondas electromagnéticas. La atenuación del valor pico de la señal se obtiene como resultado de la propagación sobre obstáculos eléctricamente grandes y es debida a la reflexión de la onda. El incremento del valor pico de la señal de campo electromagnético se explica a través del fenómeno de interferencia constructiva de ondas cuando el punto de observación se encuentra a cierta altitud por encima de la fuente. Se pueden dar algunos números; por ejemplo, para una fuente con una longitud de onda alrededor de 5000 m, y un obstáculo con altura de alrededor de 0.8 veces la longitud de onda, el valor pico del campo eléctrico vertical tuvo reducción cercana al 22% del valor obtenido para propagación sobre suelo plano. Para una fuente con longitud de onda alrededor de 790 m, el valor pico del campo eléctrico vertical sufrió una reducción cercana al 43% de su valor cuando se propagaba sobre suelo plano. Los resultados descritos fueron obtenidos para el caso de propagación sobre un obstáculo de igual altura, pero diferentes longitudes de onda de la fuente, lo cual demuestra que la discusión se debe dar en términos de longitudes de onda y su relación con el tamaño de los obstáculos. El punto importante es que el cambio en el valor pico de la señal cuando se propaga sobre zonas montañosas de altura importante —como las que existen en Colombia debido a la Cordillera de los Andes— se deben considerar con el fin de obtener un modelado preciso de la propagación. Los resultados también mostraron que los tiempos de arribo de las señales no se modificaron más allá del 4% con respecto a los tiempos de arribo para propagación sobre suelo plano. De hecho, cinco de los seis

perfiles reales del relieve estudiados mostraron que el error en el cálculo de los tiempos de arribo estaba por debajo del 1% cuando se incluyeron las irregularidades del terreno en el modelo de propagación.

Al inicio de esta investigación, la hipótesis indicaba que el efecto más significativo de las irregularidades del terreno sobre la propagación de ondas electromagnéticas generadas por rayo era sobre la precisión de localización de los sistemas de localización de rayos. Sin embargo, los resultados obtenidos sugieren un cambio de dirección al pensar en estos efectos, puesto que los tiempos de arribo de la señal de campo dependen fuertemente del tiempo de frente de la señal, pero este parámetro no puede ser modificado significativamente por las irregularidades del terreno únicamente. Con respecto a esto, los efectos de la conductividad del terreno son de hecho más importantes porque estos causan atenuación selectiva de ciertas componentes de frecuencia, como ha sido demostrado por varios autores en la literatura científica. Por lo tanto, esta tesis demostró que los efectos de propagación debidos a las irregularidades del terreno tienen su efecto más importante en otros aspectos de la aplicación a sistemas de localización de rayos, como por ejemplo la eficiencia de la detección y principalmente, la estimación de parámetros de rayo a partir de la información contenida en sistemas de localización de rayos.

Palabras clave

Análisis DFDT, efectos de propagación, propagación de ondas de radio, sistemas de localización de rayos, suelo irregular.

Acknowledgements

I am deeply grateful to several people and institutions:

To my advisor, **Professor Camilo Younes**. Your support and guidance in all of these years of joint work have greatly contributed to my academic and personal development. Thank you very much for all your valuable suggestions, patience, and camaraderie.

To my alma mater: the **Universidad Nacional de Colombia**, and in general to the public education system. It would have been impossible for me to get to this point if I had not had access to public education. I firmly believe in education as a means for achieving equity, progress, and well being of society.

To **Professor Vernon Cooray** and **Uppsala Universitet** for the opportunity to work with you at the **Ångströmlaboratoriet** during my internship in Sweden. Your valuable suggestions were key to the development of this work. I also appreciate very much the kindness of all the friends and people that I met in Sweden.

Special thanks to the Colombian Administrative Department of Science, Technology and Innovation - **COLCIENCIAS** for funding this project, and to the Foundation for the Future of Colombia - **COLFUTURO** for the successful management of the resources of the project.

Finally, I thank my family, friends and everyone else that somehow supported me during the development of this project.

Contents

Abstract	v
Resumen	viii
List of Figures	xix
List of Tables	xx
Nomenclature	xxi
List of Acronyms	xxiv
1 Introduction	1
1.1 General Background	1
1.2 Scientific Literature	3
1.2.1 Simplified Equations	4
1.2.2 Integral Equation Method	6
1.2.3 Full-Wave Numerical Analysis	11
1.2.4 Conclusion	16
1.3 Research Question	18
1.4 Hypothesis	18
1.5 Objectives	18
1.5.1 General Objective	18
1.5.2 Specific Objectives	19

1.6	Outline	19
2	Methodology	21
2.1	Mathematical Model of the Problem	22
2.1.1	Problem Geometry and Description	22
2.1.2	Two-Dimensional Maxwell's Equations	24
2.1.3	2D-FDTD Discretization	27
2.1.4	Modelling of the Lightning Channel	29
2.1.5	Modelling of Irregular Terrain	30
2.1.6	Absorbing Boundary Conditions	30
2.2	Simulation Set-Up	31
2.2.1	Numerical Validation of the Model	31
2.2.2	Numerical Experiments for Propagation Effects	32
2.2.3	Numerical Experiments for Location Accuracy	35
3	Results	40
3.1	Numerical Validation of the Model	40
3.1.1	Comparison with Canonical Model	41
3.1.2	Validation of the Obstacle Effect	42
3.2	Numerical Experiments for Propagation Effects	43
3.2.1	Source Wavelength-Obstacle Height Relationship	44
3.2.2	Effect of Ionospheric Reflections	46
3.2.3	Effects of Propagation Over Relief Profiles in Colombia	48
3.3	Evaluation of the Onset Time for the Relief Profiles Examined	52
4	Discussion	60
4.1	Interpretation of Results	60
4.1.1	Numerical Validation of the Model	60
4.1.2	Numerical Experiments for Propagation Effects	62
4.1.3	Evaluation of the Onset Time for the Relief Profiles Examined	65
4.2	Weaknesses	66

4.3	Contribution	67
4.4	Further Studies	68
4.5	Summary and Conclusions	69
A	Classical Electrodynamics	71
A.1	Maxwell's Equations	71
A.2	Integral Form of Maxwell's Equations	72
A.3	Differential Form of Maxwell's Equations	73
B	Basics of the FDTD Method	74
B.1	Finite Difference Schemes	74
B.2	The Yee Algorithm	77
B.3	Discretization of Maxwell's Equations	79
B.4	Accuracy and Stability of the Method	82
B.5	Two-Dimensional FDTD Equations	82
B.6	Numerical Computation	85
	B.6.1 Simulation Region	85
	B.6.2 Grid Size and Simulation Parameters	85
	B.6.3 Definition of the Source	85
	B.6.4 Wave Propagation	86
C	Lightning Return-Stroke Modelling	94
C.1	Engineering-Type Models	94
C.2	Channel Base Current	95
C.3	Examples of Current Distributions	96
	C.3.1 MTLE Model Example	96
	C.3.2 MTL Model Example	96
D	Vectorization of the Trapezoidal Rule	99
D.1	Introduction	99
D.2	Functions of One Independent Variable	100

D.2.1	Intuitive Idea	100
D.2.2	Worked Example	101
D.2.3	Generalization of the Idea	102
D.2.4	Vectorization for MATLAB [®]	102
D.2.5	Numerical Example	104
D.3	Functions of Two Independent Variables	104
D.3.1	Generalization of the Idea for Functions of Two Variables	104
D.3.2	Vectorization for MATLAB [®]	107
D.3.3	Numerical Example	109
D.4	MATLAB [®] Code Listings for the Examples	110

References

113

List of Figures

1.1	Geometry for propagation in a vacuum over perfectly conducting ground.	4
1.2	Geometry for field strength calculation over irregular ground.	8
2.1	Geometry for the propagation of the LEMP in the Earth-Ionosphere waveguide (not to scale).	22
2.2	Positions of the electric and magnetic field components in a unit cell of the Yee's grid in cylindrical coordinates.	27
2.3	Representation of the problem geometry in the FDTD grid (not to scale).	31
2.4	Elevation map of Colombia. Circles represent the chosen lightning striking points, triangles represent the chosen lightning sensors (observation points).	33
2.5	Relief profile for simulation of propagation effects. Case P_1	35
2.6	Relief profile for simulation of propagation effects. Case P_2	36
2.7	Relief profile for simulation of propagation effects. Case P_3	37
2.8	Relief profile for simulation of propagation effects. Case P_4	37
2.9	Relief profile for simulation of propagation effects. Case P_5	38
2.10	Relief profile for simulation of propagation effects. Case P_6	38
2.11	Definition of signal onset time: t_{on}	39
3.1	Magnetic flux density at 1 km from the lightning channel. Black solid line represents the calculation by means of Equation (1.2) and gray solid line represents the calculation by means of the FDTD method.	41

3.2	Electric field intensity at 1 km from the lightning channel. Black solid line represents the calculation by means of Equation (1.3) and gray solid line represents the calculation by means of the FDTD method.	42
3.3	Simulation scenario for testing effect of the obstacle height.	43
3.4	Electric field intensity at 80 km from a lightning discharge and propagation in an empty space with rectangular obstacle of different heights.	44
3.5	Magnetic field intensity at 80 km from a lightning discharge and propagation in an empty space with rectangular obstacle of different heights. . . .	45
3.6	Electric field intensity at 80 km from a lightning discharge and propagation in an empty space with rectangular obstacle of different heights: risetime effect.	46
3.7	Magnetic field intensity at 80 km from a lightning discharge and propagation in an empty space with rectangular obstacle of different heights: risetime effect.	47
3.8	Electric field intensity at 80 km from a lightning discharge. Difference between propagation in Free Space and EIWG.	48
3.9	Magnetic field intensity at 80 km from a lightning discharge. Difference between propagation in Free Space and EIWG.	49
3.10	Electric field intensity at 80 km from a lightning discharge. Ionospheric Effects.	50
3.11	Magnetic field intensity at 80 km from a lightning discharge. Ionospheric Effects.	51
3.12	Electric field intensity at 80 km and 300 km from a lightning discharge. Difference between propagation over flat ground and over relief profile: Case P_1 . Source wavelength $\lambda \approx 5000$ m.	52
3.13	Magnetic field intensity at 80 km and 300 km from a lightning discharge. Difference between propagation over flat ground and over relief profile: Case P_1 . Source wavelength $\lambda \approx 5000$ m.	53

3.14	Electric field intensity at 220 km from a lightning discharge. Difference between propagation over flat ground and over relief profile: Case P_2 . Source wavelength $\lambda \approx 5000$ m.	54
3.15	Magnetic field intensity at 220 km from a lightning discharge. Difference between propagation over flat ground and over relief profile: Case P_2 . Source wavelength $\lambda \approx 5000$ m.	54
3.16	Electric field intensity at 500 km from a lightning discharge. Difference between propagation over flat ground and over relief profile: Case P_3 . Source wavelength $\lambda \approx 5000$ m.	55
3.17	Magnetic field intensity at 500 km from a lightning discharge. Difference between propagation over flat ground and over relief profile: Case P_3 . Source wavelength $\lambda \approx 5000$ m.	55
3.18	Electric field intensity at 280 km from a lightning discharge. Difference between propagation over flat ground and over relief profile: Case P_4 . Source wavelength $\lambda \approx 5000$ m.	56
3.19	Magnetic field intensity at 280 km from a lightning discharge. Difference between propagation over flat ground and over relief profile: Case P_4 . Source wavelength $\lambda \approx 5000$ m.	56
3.20	Electric field intensity at 150 km from a lightning discharge. Difference between propagation over flat ground and over relief profile: Case P_5 . Source wavelength $\lambda \approx 5000$ m.	57
3.21	Magnetic field intensity at 150 km from a lightning discharge. Difference between propagation over flat ground and over relief profile: Case P_5 . Source wavelength $\lambda \approx 5000$ m.	57
3.22	Electric field intensity at 55 km from a lightning discharge. Difference between propagation over flat ground and over relief profile: Case P_6 . Source wavelength $\lambda \approx 5000$ m.	58

3.23	Magnetic field intensity at 55 km from a lightning discharge. Difference between propagation over flat ground and over relief profile: Case P_6 . Source wavelength $\lambda \approx 5000$ m.	58
3.24	Absolute error in the onset time due to propagation effects of different relief profiles.	59
B.1	Positions of the electric and magnetic field components in a unit cell of the Yee's grid in Cartesian coordinates.	79
B.2	Profile of the incident wave used by Yee (1966).	87
B.3	Calculation of \mathcal{E}_z by means of Equation (B.22) for different time steps in the absence of the obstacle.	88
B.4	Calculation of \mathcal{E}_z by means of Equation (B.22) for different time steps in presence of the obstacle. The vertical point of observation is $j = 30$	89
B.5	Calculation of \mathcal{E}_z by means of Equation (B.22) for different time steps in presence of the obstacle. The vertical point of observation is $j = 50$	90
B.6	Calculation of \mathcal{E}_z by means of Equation (B.22) for different time steps in presence of the obstacle. The vertical point of observation is $j = 65$	91
B.7	Three-dimensional view of the wave propagation for time $n = 0$	92
B.8	Three-dimensional view of the wave propagation for time $n = 49$	92
B.9	Three-dimensional view of the wave propagation for time $n = 95$	93
C.1	MTLE model example with Nucci-type channel base current.	97
C.2	MTLL model example with Nucci-type channel base current.	97
D.1	Trapezoidal Rule: Intuitive Idea	100

List of Tables

2.1	Geographical coordinates of three different lightning striking points.	32
2.2	Geographical coordinates of six different lightning sensors.	34
2.3	Location of the end points for six different relief profiles.	34
2.4	Lightning striking points and sensors used for its localization.	36
3.1	Simulation parameters used for FDTD simulation of Figures 3.1 and 3.2. .	41
3.2	Simulation parameters used for FDTD simulation of Figures 3.4 and 3.5. .	43
3.3	Simulation parameters for FDTD simulation of Figures 3.6 and 3.7.	46
4.1	Effect of Obstacle Height on Electric Field in Terms of Source Wavelengths	63
C.1	$P(z')$ and v parameters for engineering-type return-stroke models.	95

Nomenclature

Constants

μ_0	Magnetic permeability of free space	$4\pi \times 10^{-7}$ [H/m]
ϵ_0	Electric permittivity of free space	$8.85418782 \times 10^{-12}$ [F/m]
c	Speed of light in free space	299792458 [m/s]

Notation Symbols

$\hat{()}$	Unit vector
$\overline{()}$	Vector field
$\underline{()}$	Vector quantity
$\underline{\underline{()}}$	Matrix quantity

Parameters

α	Current decay constant in the MTLL return-stroke model
ϵ	Electric permittivity of a medium
λ	Wavelength
μ	Magnetic permeability of a medium
σ	Electric conductivity of a medium
f	Frequency

H	Total height or length of a lightning channel
v	Speed of a lightning return stroke front
Z	Intrinsic impedance of a medium

Superscripts

'	First derivative
"	Second derivative
'''	Third derivative
(m)	m-th derivative
n	Index of time iteration in a time-marching algorithm

Subscripts

i, j, k	Indexes of a grid point in three-dimensional space
r, ϕ, z	Vector components of a quantity along the respective cylindrical coordinates
x, y, z	Vector components of a quantity along the respective Cartesian coordinates

Variables

(r, ϕ, z)	Cylindrical coordinates: radial distance, azimuthal angle and vertical distance
$\overline{\mathcal{B}}(\bar{r}, t)$	Magnetic flux density in time domain
$\overline{\mathcal{D}}(\bar{r}, t)$	Electric displacement in time domain
$\overline{\mathcal{E}}(\bar{r}, t)$	Electric field strength in time domain
$\overline{\mathcal{H}}(\bar{r}, t)$	Magnetic flux strength in time domain

$\vec{\mathcal{J}}(\vec{r}, t)$	Electric current density in time domain
\vec{r}	General position vector in arbitrary coordinates system
$\rho(\vec{r}, t)$	Electric charge density in time domain
$i(0, t)$	Lightning return stroke current at channel base and time t
$i(z', t)$	Lightning return stroke current at height z' and time t
t	Time
$u(t)$	Heaviside's unit step function
z'	Height along a lightning channel

List of Acronyms

ABC Absorbing Boundary Conditions. 29

CFL Courant-Friedrichs-Lewy Condition. 81

DE Detection Efficiency. 16

EIWG Earth-Ionosphere Waveguide. 11, 13, 22, 45

ELF Extremely Low Frequency. 12

FDTD Finite Difference Time-Domain. 9, 11–14, 16, 18, 20, 21, 23, 26, 28, 29, 39–41, 44–47, 59, 60, 65, 68, 73, 76, 81, 82

LA Location Accuracy. 2, 16, 17

LEMP Lightning Electromagnetic Pulse. 1–3, 5, 7, 11–14, 17–19, 22, 30, 31, 33, 43, 45

LF Low Frequency. 2, 10, 62, 64

LLS Lightning Locating Systems. 2, 16, 17, 39, 64, 66, 68, 69

MTLE Modified Transmission Line Model with Exponential Decay. 22, 23, 28, 93–95

MTLL Modified Transmission Line Model with Linear Decay. 13, 22, 23, 28, 41, 44, 47, 93–95

PEC Perfect Electric Conductor. 46, 50, 84

RAM Random Access Memory. 20, 23, 46, 47, 60, 61, 66

SCA Staircase Approximation. 29

ToA Time of Arrival. 15, 66

VLF Very Low Frequency. 2, 12, 22, 62, 64

Chapter 1

Introduction

1.1 General Background

The subject of this thesis is the propagation of the Lightning Electromagnetic Pulse (LEMP) over *irregular ground*, i.e., over a ground surface that has variations in height. It is part of the more general problem of *Radiowave Propagation Over Ground*; a very difficult problem in mathematical physics, which has been subject of interest for more than one century. Just for the purpose of having an idea of the complexity of this problem, let us consider a little bit of its history: on December 12, 1901, engineer Guglielmo Marconi was able to transmit the first wireless signal across the Atlantic between Poldhu, Cornwall, and St. John's, Newfoundland, a distance of more than 3200 km (Carassa, 1982). That experiment—which gave rise to the development of wireless telegraphy—arose a question among the scientists of that time. They wondered about the mechanism by which waves could propagate over such great distances (beyond the line-of-sight to the horizon). Since then, many theoretical and experimental researches have been carried out around this problem (the main ones are concisely reviewed in Section 1.2). For instance, the work of Arnold Sommerfeld (Sommerfeld, 1909) may be said to be the first study around this problem.

In regard to the subject of this thesis, some aspects of the lightning physics have to be considered before the purpose of the work is stated. First, experimental measurements

have shown that the electromagnetic waves generated during the return-stroke phase of a lightning discharge are composed by frequencies belonging to the radio spectrum, specifically by values within the Low Frequency (LF 30–300 kHz, with wavelengths from 10 to 1 kilometres) and the Very Low Frequency (VLF 3–30 kHz, with wavelengths from 100 to 10 kilometres) bands (Uman, 1987). Because of their long wavelengths, lightning electromagnetic waves can *diffract* over *obstacles* and travel beyond the horizon following the curvature of the Earth. This mode of propagation, called *ground wave*, is the main mode in the LF/VLF bands. However, at the VLF band, long distance propagation occurs mainly as an Earth–Ionosphere *waveguide* mechanism (Hunsucker & Hargreaves, 2003, p. 419). Additionally, these kind of waves present a very low path attenuation (2–3 dB/1000 km) (Hunsucker & Hargreaves, 2003, p. 419).

The characteristics mentioned above make possible to model the lightning discharge channel as a transmitting antenna whose radiated energy can propagate long distances. This allows the detection of lightning at a global scale and makes possible to have Lightning Locating Systems (LLS) that are constantly detecting and localizing lightning discharges over the surface of the earth. However, the diffraction mechanism of radio waves over obstacles depends on the size of them and on the length of the wave. More precisely, the obstacles formed by the irregularities of the ground surface are “seen” by the wave like small or large, depending on the wavelengths involved. This means: if the obstacle is of small height–relative to the wave’s wavelength–, its effect will also be small because the electromagnetic wave will not see an important difference when compared to the absence of the obstacle. On the other hand; if the height of the obstacle is large, it will affect the predictions of the propagation model and then, these irregularities will have to be taken into account.

With all of the above in mind, one could ask questions like: What is the maximum height of a mountain range such that it can be considered to have no effect on the propagation of LEMP? When do the ground irregularities introduced by mountains are worth to be included in a propagation model for lightning localization? How is the Location Accuracy (LA) of LLS affected by propagation over mountainous terrain? These questions

point in the direction of the purpose of the thesis. The next section is a concise review of the related scientific literature around this subject.

1.2 Scientific Literature

The scientific literature on the subject of this thesis is very vast. It dates back to the pioneering work of Arnold Sommerfeld (Sommerfeld, 1909); continues with many fruitful approximations derived from it, like for example the very well known works of Norton (1937), Hufford (1952), Ott (1971a), Bannister (1984); passes through different works that took advantage of the advent of computers (and combine it with analytical deductions) (Monteath, 1978), (Ott, Vogler, & Hufford, 1979); and comes to contemporary days where the majority of the methodologies seem to be entirely based on numerical simulation. See for example (Li, Azadifar, Rachidi, Rubinstein, Diendorfer, et al., 2016), (Aoki, Baba, & Rakov, 2015). Therefore, this section focuses on presenting the most important works according to the purpose of the thesis. It is a very concise compilation with two objectives in mind: i) to identify “the gap” in the literature to which this thesis is aimed to contribute, and ii) to present specific details that will be useful in the development of the methodology.

For this purpose, the most important works were categorized in three different groups according to the methodological approach and approximations that their authors have followed. The categorization also takes into account other aspects: the interest of the scientific community that addresses the problem, the method of solution for the equations, and the advantages and disadvantages of the models for particular applications. The three categories were identified according to these criteria, with the following names: simplified equations, integral equation method, and full-wave numerical analysis. A concise description of these three categories is to follow. At the end, the section is concluded with a synthesis where the gap in the literature is stated.

1.2.1 Simplified Equations

The equations presented here were formulated to model the propagation of LEMP (radiowaves) over a perfectly conducting planar surface. This is an idealized model that is not useful for many engineering applications; however, for the purpose of practical calculations, which are mainly used by lightning research engineers, the equations are enough. Some applications of this idealized model include the calculation of lightning induced overvoltages on power lines, design of lightning protection systems, lightning modelling, and the estimation of lightning parameters.

The geometry for the solution of this problem is shown in Figure 1.1. The fields are obtained from the scalar and vector retarded potentials, together with the Lorenz condition:

$$\nabla \cdot \vec{A} + \frac{1}{c^2} \frac{\partial \phi}{\partial t} = 0. \quad (1.1)$$

The boundary conditions at the plane are satisfied by means of the images method. The current at any height is assumed to be any continuous function $i(z, t)$ that propagates along the antenna with a finite speed v . The final result for the fields is given by Equations (1.2) and (1.3). The detailed derivation of these equations can be found in (Uman, McLain, & Krider, 1975).

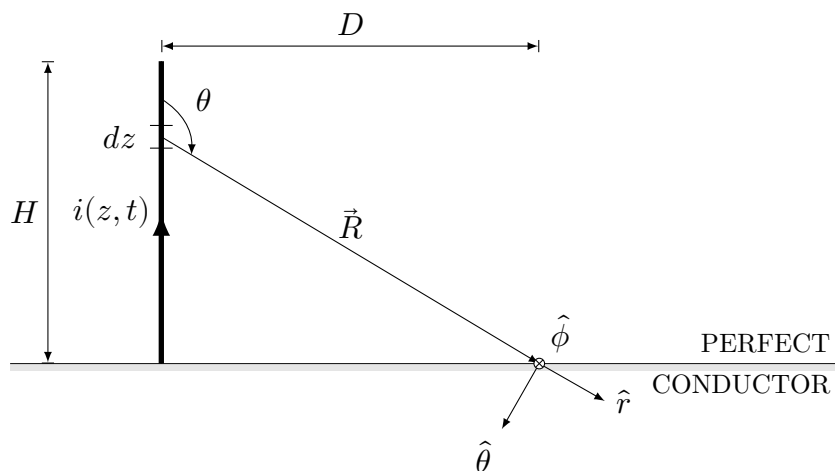


Figure 1.1: Geometry for propagation in a vacuum over perfectly conducting ground.

$$B_\phi(D, t) = \frac{\mu_0}{2\pi} \int_0^H \frac{\sin \theta}{R^2} i\left(z, t - \frac{R}{c} - \frac{z}{v}\right) dz + \frac{\mu_0}{2\pi} \int_0^H \frac{\sin \theta}{cR} \frac{\partial}{\partial t} i\left(z, t - \frac{R}{c} - \frac{z}{v}\right) dz, \quad (1.2)$$

$$\begin{aligned} E_z(D, t) = \frac{1}{2\pi\epsilon_0} & \left[\int_0^H \int_0^t \frac{(2 - 3 \sin^2 \theta)}{R^3} i\left(z, \tau - \frac{R}{c} - \frac{z}{v}\right) d\tau dz \right. \\ & + \int_0^H \frac{(2 - 3 \sin^2 \theta)}{cR^2} i\left(z, t - \frac{R}{c} - \frac{z}{v}\right) dz \\ & \left. - \int_0^H \frac{\sin^2 \theta}{c^2 R} \frac{\partial}{\partial t} i\left(z, t - \frac{R}{c} - \frac{z}{v}\right) dz \right]. \end{aligned} \quad (1.3)$$

Where

D is the distance from the antenna base to the observation point;

H is the height of the antenna;

$i(z, t) = i(t - z/v)$ is the current pulse that propagates up the antenna; and

v is the speed of propagation of the current pulse.

The numerical solution of the equations for this model is easily obtained by computer. This is a simplified model that is not difficult to implement, but it is restricted to the very idealized case of propagation over perfectly conducting planar ground. This model is not able to include ground irregularities and its effect on the propagation of LEMP. It is neither able to account for propagation effects due to ground conductivity. This model, as mentioned at the beginning, has reduced application. For the purpose of this thesis, this model will be useful only as a canonical model that will serve for validation.

Further discussion of this model was carried out by Rubinstein and Uman (1989). The authors focused on comparing two equivalent approaches used to obtain the equations—the dipole technique, and the monopole technique. No further contributions were made in that paper as for the purpose of this thesis.

1.2.2 Integral Equation Method

The integral equation method has been historically developed by physicists and mathematicians; see for instance (Sommerfeld, 1909) and (Hufford, 1952). However, there were some engineers that made contributions to the solution of the radiowave propagation problem by means of this method; see for instance (Norton, 1937) and (Bannister, 1984). The application of this methodology is closely related to the work of radio engineers (broadcasting, wireless communications, etcetera). Because of this, the integral equation method mainly provides the *field strength* as a function of the propagation distance, and for the boundary conditions imposed by ground inhomogeneities and irregularities in the propagation path.

In the integral equation method, the electromagnetic field strength is put in form of an integral equation. This integral equation can be derived using either the Green's theorem (Green's second identity) or the compensation theorem. Once the integral equation has been derived, it can be solved numerically provided that the ground inhomogeneities and irregularities are known. One problem of this method is that the numerical solution of the integral equation becomes increasingly inaccurate as the frequency raises. In order to avoid this problem, the authors in (Maclean & Wu, 1993) present an alternative approach in which the integral equation is approximated by an integral. A detailed review of this method, which cites the most valuable works, goes in very deep detail, and focuses on contemporary applications, is provided in (Maclean & Wu, 1993). Coming up next, we will dig deeper in the main models that use this methodology. The division is made according to the scope of the models.

Propagation over Homogeneous Flat Ground

The propagation of radiowaves over a homogeneous flat ground with finite conductivity and dielectric constant is a much more realistic model to the problem of radiowave propagation than the approximation given by Equations (1.2) and (1.3). This is the classical Sommerfeld problem (Sommerfeld, 1909). There is only one change in the conditions of the problem represented by Figure 1.1: the ground constants in the lower half-space are

now $\mu = \mu_0$, $\epsilon = \epsilon_1$, and $\sigma = \sigma_1$. The parameters of the upper half-space remain as the ones for free space $\mu = \mu_0$, $\epsilon = \epsilon_0$, and $\sigma = 0$. Even so, the problem becomes extremely complex. The exact solution given by Sommerfeld was formulated as a set of integrals. This solution is difficult to evaluate, even numerically, because the equations are time consuming and also because of numerical instability for high frequencies. Due to this fact, several simplifications have been made.

Two of the most widely used approximations to Sommerfeld's integrals are the ones derived by Norton (1937) and Bannister (1984). These works formulated an approximation that gives an attenuation function of the field in terms of the homogeneous ground parameters. This is the case because the application was thought mainly for wireless communications. However, these approximations were used by Cooray (2008) to calculate the propagation effects of finite ground conductivity on the propagation of LEMP. The author also provided validation to the Norton's and Bannister's approximations by comparing the results with the exact solution of Sommerfeld's equations. The results showed agreement with a precision better than 10% for distances of propagation between 10 m and 1 km from the lightning channel.

There are several other works that were developed in the light of the integral equation method, but all of them were aimed to derive simpler, more accurate expressions for the field strength as the electromagnetic wave propagates over finitely conducting ground. Therefore, those results are not of interest to the scope of this thesis, which focuses on the propagation effects of ground irregularities. Thus, the following section concerning the main works on propagation over irregular ground will describe them in more detail.

Propagation over Irregular Ground

One of the most important works aimed to find an attenuation function for harmonic electromagnetic waves that propagate over irregular ground, is the one presented in (Hufford, 1952). In this work, the author makes use of the Green's theorem to derive an integral equation for the field strength. It is further reduced to another one for the one-dimensional case. The final result is given by Equation (1.4), and the geometry of the problem is de-

scribed in Figure 1.2. Here, P is the point of the receiving antenna (observation point), O is the point of the transmitting antenna, and Q is an integration point.

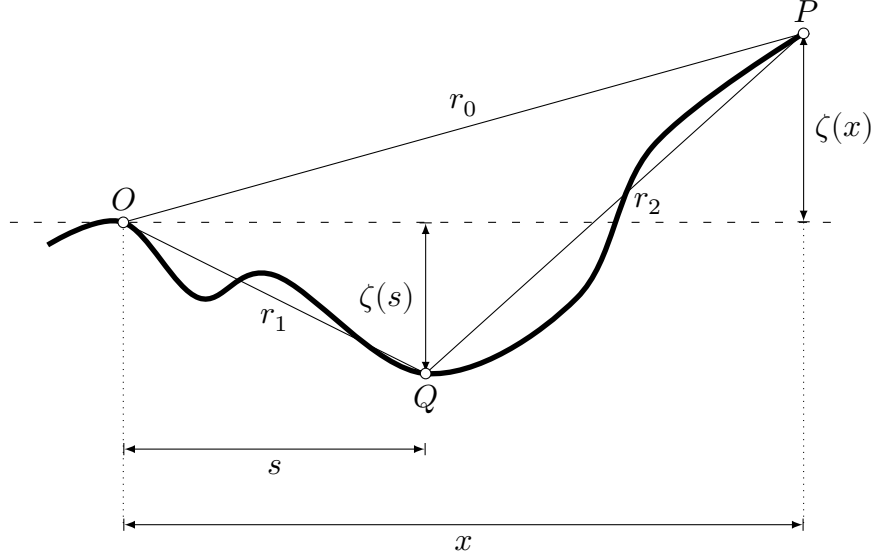


Figure 1.2: Geometry for field strength calculation over irregular ground.

$$W(x) = g(x) - e^{-j\pi/4} \sqrt{\left(\frac{k}{2\pi}\right)} \int_0^x W(s) \left(\delta + \frac{\partial r_2}{\partial n}\right) e^{jk(r_1+r_2-r_0)} \sqrt{\frac{x}{s(x-s)}} ds \quad (1.4)$$

where

$\zeta(x)$ is a function that represents the ground irregularities (terrain elevation);

$g(x)$ is a function that represents the antenna pattern or the gain of the antenna over an isotropic radiator at O ; and

$W(x)$ is the field strength.

Given a particular ground geometry, Equation (1.4) can be solved for $W(x)$. However; the model can only include irregularities along the radial direction, and is only valid for homogeneous ground. An inconvenient is that the model is not useful for high frequencies due to the rapid accumulation of round-off errors in the numerical solution.

After Hufford's work, several others derived similar integral equations, included numerical solutions for them, and provided experimental measurements that further validated their, and Hufford's theoretical work. The most important ones will be mentioned next. In (Ott & Berry, 1970) and (Ott, 1971a), the authors derived an alternative integral equation. It was made by means of the parabolic equation method. This equation was seen like an improvement of the Hufford's work because it was able to include large-slope terrain profiles, spherical earth, and was used to analyse the propagation over a Gaussian-shaped ridge. This last example confirmed again the hypothesis that the field strength is increased when it encounters a terrain anomaly, such as a high conducting ridge. It is important to notice that the frequency of the electromagnetic wave used was 1 MHz ($\lambda \approx 3$ km), and the height of the obstacle was 1 km. This gives a relationship of $\lambda = 3h$. A physical explanation of this observation is made by Ott (1971a):

The physical characteristics of the results in Figure 1 are interpreted most easily using the ray picture. The attenuation function decreases at the flat earth rate for the first 2 km. Then, as the observation point moves up the crest of the hill, the attenuation function increases, owing to constructive interference of the direct ray and the surface ray on the lit side of the crest. The attenuation function reaches its maximum value very close to the point on the terrain where there is an inflection point.

This is a physical fact that has been observed by several authors. Even nowadays, numerical simulations that use the FDTD method confirm this fact. See (Aoki et al., 2015), (Li, Azadifar, Rachidi, Rubinstein, Diendorfer, et al., 2016).

Several works followed by the time, mainly interested in developing numerical computer codes for the solution of previously proposed integral equations. There was also an interest in validating such results with experimental measurements. Thus, the authors in (Ott, 1971b) presented the same integral equation as in (Ott, 1971a), a Fortran code listing, and several examples. The examples showed the suitability of the model for the propagation of high frequency waves. Further, in (Ott et al., 1979) the authors made improvements to the numerical code presented in (Ott, 1971a); it allowed to include re-

alistic terrain profiles, and then the authors were able to compare the numerical results with real experimental observations for waves with frequencies up to the VHF band. Two real terrain profiles were compared with the integral equation numerical results, showing general good agreement except for large path distances. The authors suggested full-wave and three dimensional approximation to the problem in order to obtain better results. More experimental measurements were provided in (Kissick, Haakinson, & Stonehocker, 1978) where the authors included transmitters in the 100 to 2000 kHz band. The path lengths observed were up to 50 km, and a two-dimensional terrain profile was used for the simulations. Finally, in (Monteath, 1978) the authors provided a Fortran code to solve Hufford's integral equation. A real two-dimensional terrain profile was used to test the validity of the Hufford's model predictions, including LF and MF waves propagating up to 300 km range. The results showed a 3 dB gain in the signal strength when it encountered an obstacle 200 m height (using a 950 m wavelength wave, $\lambda \approx 4.75h$).

The latest theoretical works on the propagation over irregular ground include (Furutsu, 1982) where the authors give explicit formulas (closed-form solutions) for signal attenuation but considering only certain types of idealized terrain shapes. In (Wu, Maclean, Bagwell, & Mehler, 1988), a new integral equation generalises previous work to treat arbitrary terrain, so that both gradual and sharp changes of terrain height, such as a cliff and a knife edge are considered. With this approximation, arbitrary terrain slopes can be considered, but transverse irregularities are not possible. Finally, Gong, Maclean, and Wu (1989) present an integral equation for the propagation over a rectangular plateau; the integral equation is further reduced to an integral expression by means of the analytical results of Wu et al. (1988). This allows the integral to be solved numerically by computer. This last technique of reducing the integral equation to an integral expression, as stated at the beginning of this section, was developed in order to avoid the numerical instability that arises when solving the typical integral equations that appear in this kind of problems. This new methodology has shown to be very satisfactory, and so the reader is referred again to reference (Maclean & Wu, 1993) where a very deep treatment of this method is presented.

1.2.3 Full-Wave Numerical Analysis

Contemporary research on the problem of radiowave propagation over ground is almost exclusively based on numerical simulation. The reason for this is that modern digital computers are capable to provide sufficient computing power for the solution of many electromagnetic problems. Moreover, numerical simulation has many advantages as compared to analytical solutions: it is much easier to implement, more realistic models can be formulated, and much more output variables for a problem can be calculated. With numerical simulation, the implementation of a full-wave numerical analysis can be easily done. In this kind of analysis, the Maxwell's equations are solved completely and all components of the fields are known. However; depending on the particular application, the simulating times and memory requirements could be impractical. Another disadvantage is that the physical interpretation of the phenomena is obscured by the simulation. Therefore, the large amount of information given by numerical analyses has to be complemented with careful theoretical analysis.

There are several numerical techniques that are of interest to the purpose of this thesis. There is for example the Method of Moments, the Finite Elements Method, Finite Difference in Time Domain Methods, and Spectral methods. The objective of this thesis is not to make a review of each of them, or to study their adequacy for the problem of radiowave propagation. Instead, the choice of the Finite Difference Time Domain (FDTD) method is supported by several of its characteristics. First, the FDTD method is very simple to understand and to implement; second, a realistic simulation scenario can be developed easily due to the simple discretization process; and finally, the Maxwell's equations are solved in time domain, which makes the method particularly useful for transient problems like the one of this thesis. All of these advantages are confirmed by the number of works published in recent years that use the FDTD method, see for instance (Aoki et al., 2015), (Arzag, Azzouz, & Ghemri, 2016), (Bérenger, 2002), (Thang, Rakov, Baba, & Somu, 2016), (Thèvenot, Bérenger, Monédière, & Jecko, 1999), (Thang, Baba, Somu, & Rakov, 2017). So this section finalizes the review of the three main methods identified in this thesis for addressing the problem of radiowave propagation.

The iconic paper that presented the application of a finite difference scheme to the solution of Maxwell’s equations was presented in the year 1966 (Yee, 1966). However, the method popularized only after the 1990s with the growth of computer power (Inan & Marshall, 2011). The method has been successfully applied to a diverse number of electromagnetic problems, including the propagation of radiowaves over the ground and in the cavity formed by the Earth-Ionosphere Waveguide (EIWG). This section will present only the published works that are strictly related to the purpose of this thesis. As mentioned before, it is straightforward to include homogeneous or inhomogeneous ground in a FDTD simulation model. It is also straightforward to include ideal or realistic ground irregularities. Thus, the works presented here have focused their attention on evaluating the propagation effects of these two factors on LEMP. Therefore, the results obtained by means of the integral equation method presented in the last section have become *canonical models* that can be used as a means of validation.

FDTD Earth-Ionosphere Waveguide Propagation Models

The works of Thèvenot et al. (1999), Cummer (2000) and Bérenger (2002) are among the first ones that applied the FDTD method for modelling ELF/VLF propagation in the earth-ionosphere waveguide. Whereas these works are not strictly related to the problem of LEMP propagation over irregular ground, they are important for being pioneering works in the development of a model that allows such investigations. A concise description of these works is presented:

- In (Thèvenot et al., 1999) the authors focused their model on the inclusion of variations of the radiopath parameters, such as ground conductivity and the electronic density of the ionosphere. The model was developed based on the solution of Maxwell’s equations along with the differential equation that governs the current density in the ionosphere. Even though the authors presented examples for a 20 kHz vertical transmitter, the model is perfectly applicable to the propagation of lightning pulses, as the authors suggested.
- In (Cummer, 2000) the author investigated mainly the validity of the different ap-

proximations for modelling the ionospheric upper boundary.

- In (Bérenger, 2002) the author further improved the computation times of the FDTD method, but the applicability of this approach is restricted only to single frequency radiators.

The FDTD method has been further applied to the specific problem of LEMP propagation in the earth-ionosphere waveguide (Thang et al., 2016). In this work, the authors built a simulation scenario consisting of a planar perfectly conducting ground, a conducting atmosphere, and a lightning channel along which a return-stroke current propagates. The conducting atmosphere was included up to 110 km height, and one-hop and two-hop skywaves (reflections from the ionosphere) were identified in the computed waveforms. The observation point was taken over the surface of the ground, with distances to the lightning channel from 50 km to 500 km. In this study, the authors used a simplified model for the conductive atmosphere, which is presented below:

$$\sigma(h) = \sigma_0 e^{\beta(h-h')} \quad (1.5)$$

where $\sigma_0 = 2.22 \mu\text{S/m}$, $\beta = 0.67 \text{ km}^{-1}$, and $h' = 84 \text{ km}$. By means of this model the authors estimated that reflection heights are not farther than 84 km. Another important result is that first and second skywaves present important peaks (as compared to the peak value of the ground wave) for distances of propagation greater than 100 km.

Finally, Thang et al. (2016) presented another work in which they further validated and improved their FDTD model (Thang et al., 2017). In this last work, the same two-dimensional model for propagation of LEMP in the EIWG was used. Emphasis was in a more realistic return-stroke modelling. For that purpose, the authors used a Modified Transmission Line Model with Linear decay (MTLL). The complete model was developed considering planar ground surface, which is adequate for propagating distances of up to 500 km. After this value, the curvature of the earth would affect the propagation model. The conductivity of the atmosphere was assumed to increase exponentially with height and the model was simplified to consider it to be isotropic and linear. The authors

found good agreement of their model with experimental results—measured with a lightning detection network in China—presented in (Qin, Chen, Zhu, & Du, 2017). This time, the authors also included different parameters for the model given by Equation (1.5). For daytime conditions, the parameters used were $\beta = 0.3 \text{ km}^{-1}$, $h' = 70 \text{ km}$. For night-time conditions, they were $\beta = 0.8 \text{ km}^{-1}$, $h' = 84 \text{ km}$.

FDTD Ground Wave Propagation Models

The following works are in the same line of the numerical simulation approach; they are intended to calculate propagation effects on LEMP. However, they do not include ionospheric reflections. These models are for relatively short distances of propagation and their main interest is on the propagation effects of lossy ground. There are also a couple of them that consider the propagation effects due to ground irregularities at some extent.

The works (Aoki et al., 2015) and (Li, Azadifar, Rachidi, Rubinstein, Paolone, et al., 2016) are both based on two-dimensional FDTD simulation. Their main characteristics are as follows:

- In (Aoki et al., 2015) the LEMP propagation is modelled considering lossy ground. The authors claim to be the first ones to present a full-wave study of LEMP propagation effects. The calculations were made for propagation distances between 5 – 200 km from the lightning channel. An important characteristic is that the return-stroke model used accounts for the complete frequency range of the currents in lightning discharges. The main interest was to find the effect of current rise-time, current propagation speed, and ground conductivity on three components of the electromagnetic fields: azimuthal magnetic field H_ϕ , vertical electric field E_z , and horizontal electric field E_h . The authors validated their model with the simplified equations of Uman et al. (1975) for an idealized case. The model presented in (Thang et al., 2017) could be seen as an extension to this one since the latter includes ionospheric reflections and considers a similar approach.
- In (Li, Azadifar, Rachidi, Rubinstein, Paolone, et al., 2016) the authors presented an example of calculation using a two-dimensional FDTD simulation with a real terrain

profile. The results were compared with experimental measurements obtained close to the Säntis instrumented tower in Switzerland. The propagation distance of this example was about 15 km. The results confirmed again the predictions about the increase in the field strength over a hilly terrain, which can be predicted with a model like the one given by Equation (1.4), derived in (Hufford, 1952).

The last work considered to be important as for the purpose of this thesis is (Li, Azadifar, Rachidi, Rubinstein, Diendorfer, et al., 2016). This is also the work that is closest to the objectives of the present work because it considers the propagation effects caused by ground irregularity and also makes some calculations related to the location accuracy of lightning locating systems over mountainous terrain. This work does not consider ionospheric reflections in the FDTD model used to account for LEMP propagation, and the propagation distances are relatively short (from 1 to 100 km). An interesting feature of this study is that it includes a mountainous-like obstacle in the radiopath; specifically, a pyramidal object with a squared base of 1 x 1 km and different heights: 290, 500 and 870 m. Given that this study was made with a three-dimensional FDTD approach, the simulation time would be impractical for the propagation distances under observation. In order to solve this problem, the authors make this observation: “it is worth noting that beyond 50 km or so, the electromagnetic field generated by a lightning channel is dominated by its radiation component; and therefore, it can be represented by a plane wave.” The authors then used the results obtained by means of the simplified Equations (1.2) and (1.3) (given in (Uman et al., 1975)) to calculate incident plane waves, which are injected into the simulation domain for propagation distances greater than 50 km. This approach is detailed in (Watts, 2003). The authors present the main results in the following paragraph (Li, Azadifar, Rachidi, Rubinstein, Diendorfer, et al., 2016):

(1) the time delays and amplitudes of the lightning-radiated electromagnetic fields can be significantly affected by the presence of a mountainous terrain and associated diffraction phenomena; (2) for a finitely conducting ground, the time delay shows a slight increase with the increase of the observation distance, but the time delay resulting from the finite ground conductivity appears to be

smaller than that caused by the mountainous terrain; and (3) the timing error associated with the ToA technique depends on the threshold times.

To conclude, a final comment about these results is useful: the time delays found are to be expected in a certain way because of the elongation of the propagation path. For example, Schulz and Diendorfer (2000) found that the location accuracy of lightning locating systems could be improved only by including an elevation model of the earth in the localization algorithm. The authors in (Li, Azadifar, Rachidi, Rubinstein, Diendorfer, et al., 2016), however, did not calculate any location accuracy errors due to the error in time delays; they calculated only the errors in the onset time. On the other hand, the result concerning the changes in the amplitude of the signal due to mountains, further validates the prediction of Equation (1.4), derived by (Hufford, 1952).

1.2.4 Conclusion

For the purpose of this thesis, the contribution of the scientific literature to the field of radiowave propagation could be summarized in the following points:

- There are simplified equations that were formulated for very idealized models, which are not able to account for ground irregularities or finite conductivity. However, those models fulfil the purpose for which they were conceived. They are also useful as canonical models for the validation of others more precise.
- There are also mathematical formulations that are useful for the calculation of signal attenuation when the radiowave propagates over lossy ground and/or over irregular ground. However, those formulations are only valid for specific idealized shapes of ground irregularity; they are not useful either for calculating the effect of ground irregularity on other signal parameters. This approach is mainly used for the planning of wireless communication systems, where the signal power is a critical factor to be determined.
- On the other hand, the last research works tend to focus on a numerical simulation approach, which permits to develop much more realistic models. Specifically, the

FDTD method for solving Maxwell's equations seems to be promising. This is a full-wave approach that allows to include variables like ground irregularities, ground conductivity, and ionospheric reflections. However, the physical description of the phenomenon is obscured by the lack of interpretation of the numerical results.

Now, with regards to the research question of this thesis, there is not a determining answer yet, and it will not possibly be available within a few years. However, the scientific literature demonstrates that there are some critical and well understood factors. First, the field strength from a radiowave signal is affected by both ground irregularities and ground conductivity. Ground conductivity causes selective attenuation of different frequency components, and ground irregularity can cause an increase or attenuation of the signal strength, depending on the type of irregularity and on the observation point. Second, the ionosphere plays an important role in the propagation of low-frequency signals: it allows the waveguide mode of propagation.

With this in mind, the objective of this thesis was conceived. This work is an effort aimed to contribute to the field of radiowave propagation. The applications of this formulation are aimed to be used in the planning of lightning locating systems that operate over mountainous regions. There are two main performance parameters of LLS: the Location Accuracy (LA) and the Detection Efficiency (DE). At the moment of writing this document, the LA of major LLS in the United States of America and in Europe are in the order of hundreds of metres, with values of up to 500 m (Cummins & Murphy, 2009). However, smaller LLS present LA errors in the order of several kilometres (Pérez-Pérez, 2014). This is the case of Colombia; a country that is traversed by the Cordillera of the Andes, which is a mountain range with heights of about 5000 m. With the results presented in the literature review, there is support to the hypothesis that the LA errors of LLS over mountainous regions could be reduced by a factor of two if ground propagation effects are properly taken into account (Cummins & Murphy, 2009), (Schulz & Diendorfer, 2000).

1.3 Research Question

Consequently, the research question is stated like: given points A and B over the surface of the Earth, with a transmitter at A (a lightning discharge that produces a LEMP signal) and an observer at B , how is the LEMP signal affected (changed) by the ground irregularities as it propagates (travels) from A to B ? These changes in the character of electromagnetic waves as they propagate over the ground surface are known in the scientific literature as *propagation effects*. It is known that they are mainly due to two factors: selective attenuation of the high frequency components of the signal by finitely conducting ground, and to the presence of ground irregularities (Cooray, 2008). This thesis focuses on the propagation effects due to irregular ground because it is the effect that is less understood nowadays and because of its *apparent* importance in the Location Accuracy (LA) of LLS (Cummins & Murphy, 2009).

1.4 Hypothesis

The ground irregularities have a significant effect on the propagation of radio frequency electromagnetic waves. The special case of the lightning electromagnetic pulse propagation modelling for its application to lightning locating systems, needs to take these effects into account. Furthermore, lightning locating systems operating over mountainous regions of important altitude could reduce the location accuracy errors by a factor of two when the propagation effects due to mountains are included.

1.5 Objectives

1.5.1 General Objective

To determine the effect of irregular ground on the propagation of the lightning electromagnetic pulse, for its application to lightning locating systems.

1.5.2 Specific Objectives

- To formulate a numerical simulation model for the propagation of electromagnetic waves over irregular ground.
- To describe the changes undergone by lightning electromagnetic pulse due to different types of ground irregularities in the propagation path.
- To evaluate the difference between the onset times of lightning electromagnetic waves that propagate over flat ground and over irregular ground.

1.6 Outline

This document is divided into four main chapters which follow the canonical IMR&D (Introduction, Methodology, Results and Discussion) format. Consequently, the different chapters are grouped as follows:

In Chapter 1, the subject of the thesis is put in context, the research question is defined, a concise literature review is given, and the main hypothesis and objectives of the work are stated.

Subsequently, the research methodology is presented in Chapter 2, which describes the development of a Finite Difference Time Domain (FDTD) simulation scheme for LEMP propagation; also, it describes the simulation set-up to determine the effects of ground irregularities on the propagation of LEMP and on the onset times used by the time-of-arrival technique.

Then, the results for all the simulations are presented in Chapter 3. It summarizes the main results by means of tables and figures.

Finally, the results are discussed in Chapter 4 and conclusions are given. The propagation effects due to ground irregularities on LEMP propagation, and on the time-of-arrival technique are examined. In brief, this chapter responds to the research question, and gives suggestions for future research.

Also, at the end of the document, there are several appendixes which give concise

introduction to the main concepts used in the thesis. These appendixes also serve the purpose of being a literature review about the specific subject of the thesis, i.e., a useful summary of the concepts needed.

Chapter 2

Methodology

This chapter describes the methodology that was followed during the development of the study. The chapter is divided into two main sections; the first one presents the mathematical model of the problem and the second one presents the simulation set-up.

In particular, the section of modelling starts presenting the geometry and description of the problem and stating the assumptions used for its abstraction. It then continues with a two-dimensional approximation to Maxwell's equations, which was necessary due to the limitations in speed and RAM of today's computers. The equations of the transverse magnetic and transverse electric modes of propagation are presented and stated in its discrete version according to the application of the FDTD algorithm in cylindrical coordinates. The section concludes by presenting aspects of the boundary conditions and representation of the lightning discharge and irregular terrain.

The second section of the chapter explains the simulation scenarios that were used to obtain the results. In the first place, it describes the simulations that were used to test the validity of the mathematical model described before. Then, it continues to present the numerical experiments created to observe the propagation effects caused by the terrain irregularities. And finally, the section presents the numerical experiments created to observe the influence of the terrain irregularities on the location accuracy of lightning discharges.

2.1 Mathematical Model of the Problem

The problem of this work is electromagnetic in nature; as such, it is completely described by Maxwell's equations. These equations model the problem completely, but given the specific boundary conditions and source of the fields its solution comes to be very complex and in some cases of no practical interest. Because of these reasons and the ones given in Chapter 1, the analytical solution of the problem is left in benefit of the numerical solution: the FDTD method (see Appendix B). This section will then elaborate on the description of the equations used for finding the numerical solution to Maxwell's equations when applied to the problem of the work.

2.1.1 Problem Geometry and Description

The propagation problem solved can be summarized in Figure 2.1. It is a schematic of the main components used in the abstraction (modelling).

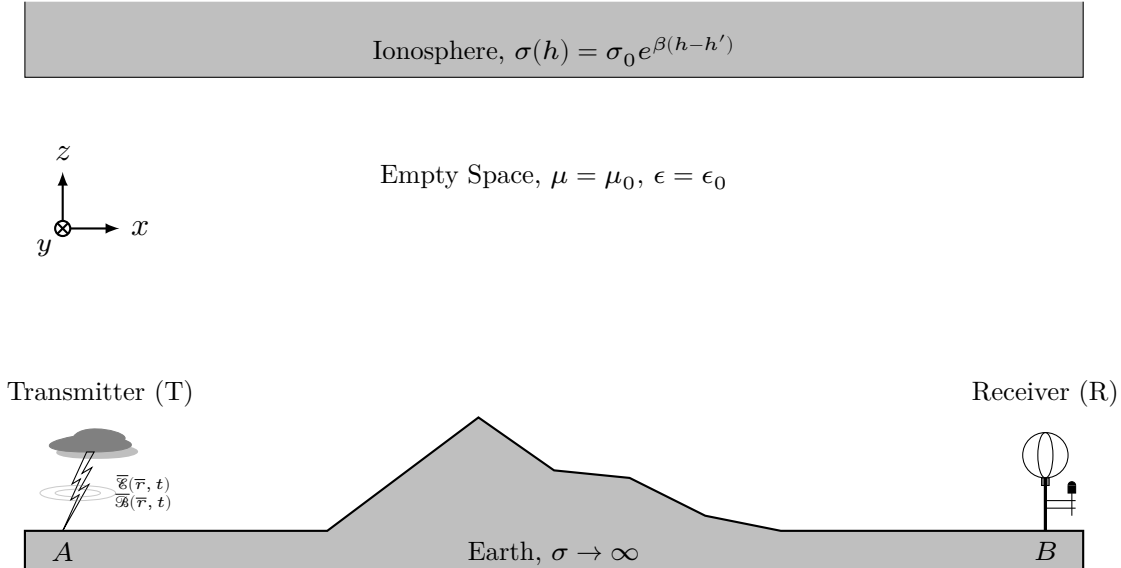


Figure 2.1: Geometry for the propagation of the LEMP in the Earth-Ionosphere waveguide (not to scale).

The following components are the most important ones for the process of modelling the phenomenon:

- a) The Transmitter (T). Evidently, this is the source of the electromagnetic waves; the lightning discharge producing the LEMP. The transmitter is located at position A .
- b) The Receiver (R). For the purpose of simulation, it is just an observation point located at position B . However, in the real world it is a VLF loop antenna, which is commonly used by lightning locating systems.
- c) The Earth-Ionosphere Waveguide (EIWG). For this model, the Earth is not modelled as a flat surface, but as an irregular one, i.e., as a surface which has variations in height. The importance of this is that the model allows to include mountain ranges of important altitude and length, between the transmitter and the receiver. The second important component of the waveguide is the ionized part of the upper atmosphere: the Ionosphere. As explained in the review of scientific literature given in Chapter 1, it can be precisely modelled as a region of varying conductivity.
- d) The Propagation Medium (PM). This is the space between the Ionosphere and the Earth.

After this description of the model components, the assumptions made in order to develop equations for the propagation problem are presented:

- a) The transmitter was modelled as a straight vertical wire. This wire carries a current modelled by a typical return stroke current, as the MTLL or MTLE models. For a concise description of these models, see Appendix C.
- b) The receiver needs no assumptions to be made, as it is simply an observation point. The only one would be to assume that this observation point is at a particular location, which could be at zero height or above a mountain of any altitude over the sea level.
- c) The waveguide was modelled under two important assumptions. Firstly, the Earth's surface was assumed to have an infinite electric conductivity ($\sigma \rightarrow \infty$). Secondly, the Ionosphere was assumed to have an electric conductivity that varies with height ($\sigma(h)$). And finally, the Ionosphere was assumed to begin at a height of 60 km.

d) The propagation medium was assumed to be empty space, i.e., $\mu = \mu_0$, and $\epsilon = \epsilon_0$.

Finally, a justification of these assumptions is needed. It is accepted by the scientific community that the MTLE and MTL models can be used for representing the lightning return stroke current with sufficient accuracy (Rakov & Uman, 1998). As to the purpose of this work, any mathematical function with a shape similar to those produced by real lightning would be adequate, because the focus is on the propagation effects. In addition, if desired, the return stroke model can be easily changed in the propagation model developed. Consequently, assumption a) is reasonable. For assumption b): the location of the observation point (receiver) can be placed at any specific position in the simulation space. It would depend only on what one wants to explain. This assumption does not need any further justification. As for the waveguide, the reasons given in the review of scientific literature of Chapter 1 explain very well the assumptions made in terms of the the height and electric conductivity of the Ionosphere. For the Earth's surface, the assumption of infinite electric conductivity does need some explanation. There are several studies that show the influence of the finite electric conductivity of the Earth on the propagation of lightning electromagnetic waves (described in Chapter 1). However, the reason for choosing an infinite conductivity in the present model was the fact that the only propagation effect of interest is the one caused by terrain irregularities. Thus, if a finite conductivity had been chosen, it would have influenced (and maybe obscured) the effects of the terrain irregularities. This completes the justification of assumption c). To conclude, the air has relative permeability and relative permittivity values very close to unity; that means that assuming the propagation medium as empty space is completely justified.

2.1.2 Two-Dimensional Maxwell's Equations

The use of Maxwell's equations in two dimensions for the solution of the problem is justified by two reasons: i) a numerical solution was the objective of the model, and ii) a three-dimensional solution of Maxwell's equations by means of the FDTD method would require a prohibitive amount of computational resources due to the speed and RAM of today's computers. In addition, the two-dimensional approximation is valid considering

that azimuthal symmetry can be assumed in the solution of the present problem. This is: considering the lighting channel as a straight wire antenna, the electromagnetic waves generated by this channel will be the same for different points around it—this implies that in a cylindrical coordinates system the variation of the fields with respect to ϕ have to be zero $\frac{\partial}{\partial\phi} = 0$. There is one downside to this assumption, namely, the fact that the terrain irregularities will have to be assumed as having cylindrical symmetry as well.

Maxwell's curl equations in three dimensional cylindrical coordinates are as follow:

$$\frac{\partial \mathcal{B}_r}{\partial t} = \frac{\partial \mathcal{E}_\phi}{\partial z} - \frac{1}{r} \frac{\partial \mathcal{E}_z}{\partial \phi}, \quad (2.1a)$$

$$\frac{\partial \mathcal{B}_\phi}{\partial t} = \frac{\partial \mathcal{E}_z}{\partial r} - \frac{\partial \mathcal{E}_r}{\partial z}, \quad (2.1b)$$

$$\frac{\partial \mathcal{B}_z}{\partial t} = \frac{1}{r} \left[\frac{\partial \mathcal{E}_r}{\partial \phi} - \frac{\partial (r \mathcal{E}_\phi)}{\partial r} \right], \quad (2.1c)$$

$$\frac{\partial \mathcal{D}_r}{\partial t} = \frac{1}{r} \frac{\partial \mathcal{H}_z}{\partial \phi} - \frac{\partial \mathcal{H}_\phi}{\partial z} - \mathcal{J}_r, \quad (2.1d)$$

$$\frac{\partial \mathcal{D}_\phi}{\partial t} = \frac{\partial \mathcal{H}_r}{\partial z} - \frac{\partial \mathcal{H}_z}{\partial r} - \mathcal{J}_\phi, \quad (2.1e)$$

$$\frac{\partial \mathcal{D}_z}{\partial t} = \frac{1}{r} \left[\frac{\partial (r \mathcal{H}_\phi)}{\partial r} - \frac{\partial \mathcal{H}_r}{\partial \phi} \right] - \mathcal{J}_z. \quad (2.1f)$$

These equations are obtained after expressing (A.5) and (A.6) in cylindrical coordinates, and separating their field components.

Now, under the assumption of no external sources and of an isotropic medium, the equations can be transformed into:

$$\frac{\partial \mathcal{H}_r}{\partial t} = \frac{1}{\mu} \left[\frac{\partial \mathcal{E}_\phi}{\partial z} - \frac{1}{r} \frac{\partial \mathcal{E}_z}{\partial \phi} \right], \quad (2.2a)$$

$$\frac{\partial \mathcal{H}_\phi}{\partial t} = \frac{1}{\mu} \left[\frac{\partial \mathcal{E}_z}{\partial r} - \frac{\partial \mathcal{E}_r}{\partial z} \right], \quad (2.2b)$$

$$\frac{\partial \mathcal{H}_z}{\partial t} = \frac{1}{\mu} \frac{1}{r} \left[\frac{\partial \mathcal{E}_r}{\partial \phi} - \frac{\partial}{\partial r} (r \mathcal{E}_\phi) \right], \quad (2.2c)$$

$$\frac{\partial \mathcal{E}_r}{\partial t} = \frac{1}{\epsilon} \left[\frac{1}{r} \frac{\partial \mathcal{H}_z}{\partial \phi} - \frac{\partial \mathcal{H}_\phi}{\partial z} \right], \quad (2.2d)$$

$$\frac{\partial \mathcal{E}_\phi}{\partial t} = \frac{1}{\epsilon} \left[\frac{\partial \mathcal{H}_r}{\partial z} - \frac{\partial \mathcal{H}_z}{\partial r} \right], \quad (2.2e)$$

$$\frac{\partial \mathcal{E}_z}{\partial t} = \frac{1}{\epsilon} \frac{1}{r} \left[\frac{\partial}{\partial r} (r \mathcal{H}_\phi) - \frac{\partial \mathcal{H}_r}{\partial \phi} \right]. \quad (2.2f)$$

The next step is to make all the azimuthal derivatives equal to zero and separate the resulting equations in two groups that are *decoupled* from each other. Each group contains the following set of three equations.

- **Transverse Magnetic Mode TM_ϕ .** This is called the transverse to ϕ magnetic mode because the two components of the magnetic field are those transversal to the ϕ coordinate.

$$\frac{\partial \mathcal{H}_r}{\partial t} = \frac{1}{\mu} \frac{\partial \mathcal{E}_\phi}{\partial z}, \quad (2.3a)$$

$$\frac{\partial \mathcal{H}_z}{\partial t} = -\frac{1}{\mu} \frac{1}{r} \frac{\partial}{\partial r} (r \mathcal{E}_\phi), \quad (2.3b)$$

$$\frac{\partial \mathcal{E}_\phi}{\partial t} = \frac{1}{\epsilon} \left[\frac{\partial \mathcal{H}_r}{\partial z} - \frac{\partial \mathcal{H}_z}{\partial r} \right]. \quad (2.3c)$$

- **Transverse Electric Mode TE_ϕ .** This is called the transverse to ϕ electric mode because the two components of the electric field are those transversal to the ϕ coordinate.

$$\frac{\partial \mathcal{E}_r}{\partial t} = -\frac{1}{\epsilon} \frac{\partial \mathcal{H}_\phi}{\partial z}, \quad (2.4a)$$

$$\frac{\partial \mathcal{E}_z}{\partial t} = \frac{1}{\epsilon} \frac{1}{r} \frac{\partial}{\partial r} (r \mathcal{H}_\phi), \quad (2.4b)$$

$$\frac{\partial \mathcal{H}_\phi}{\partial t} = \frac{1}{\mu} \left[\frac{\partial \mathcal{E}_z}{\partial r} - \frac{\partial \mathcal{E}_r}{\partial z} \right]. \quad (2.4c)$$

2.1.3 2D-FDTD Discretization

The next step in the development of the model is the discretization of Equations (2.3) and (2.4). By starting with these two equations, a set of finite difference equations were obtained, which can be implemented in a computer program through a time-marching algorithm. The two equations are (2.5) and (2.6). Additional considerations needed to arrive to the mentioned equations are presented below.

For the case of cylindrical coordinates, a Yee cell¹ in that coordinate system was used (shown in Figure 2.2). The importance of this figure lies in the fact that it contains the positions of the electric and magnetic field components in a typical cell of the space after its discretization. As shown, the magnetic field components were located in the centre of the faces of the cell, and the electric field components were located in the centre of the edges. This is fundamental for arriving to the algebraic version of the partial differential equations.

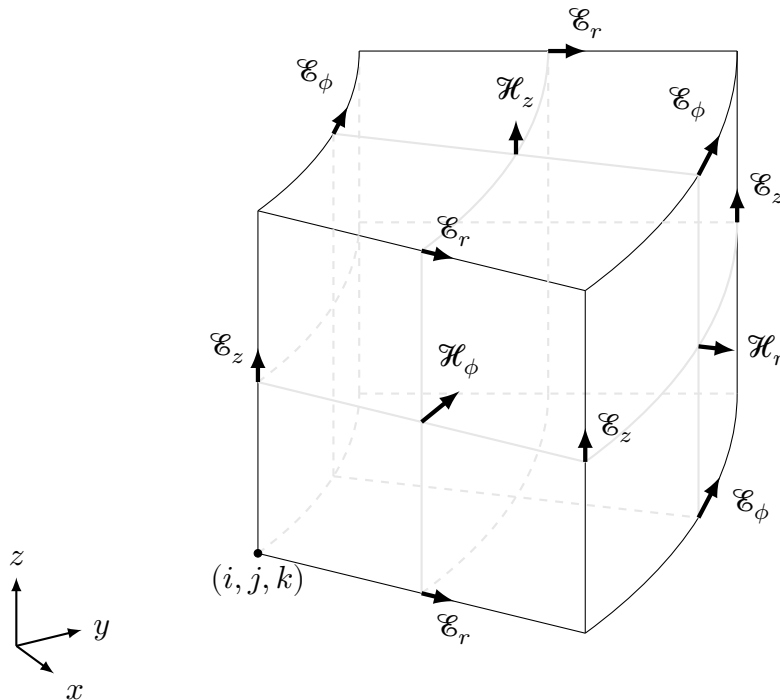


Figure 2.2: Positions of the electric and magnetic field components in a unit cell of the Yee's grid in cylindrical coordinates.

¹For a concise introduction to the FDTD method and related terms, see Appendix B.

Finally, with support of Figure 2.2 and with Equations (2.3) and (2.4), the following two sets of algebraic equations were obtained:

Discretization of the Transverse Magnetic Mode TM_ϕ

$$\mathcal{H}_r \Big|_{i,k+\frac{1}{2}}^{n+\frac{1}{2}} = \mathcal{H}_r \Big|_{i,k+\frac{1}{2}}^{n-\frac{1}{2}} + \frac{\Delta t}{\mu \Big|_{i,k+\frac{1}{2}}} \left[\frac{\mathcal{E}_\phi \Big|_{i,k+1}^n - \mathcal{E}_\phi \Big|_{i,k}^n}{\Delta z} \right], \quad (2.5a)$$

$$\mathcal{H}_z \Big|_{i+\frac{1}{2},k}^{n+\frac{1}{2}} = \mathcal{H}_z \Big|_{i+\frac{1}{2},k}^{n-\frac{1}{2}} - \frac{\Delta t}{\mu \Big|_{i+\frac{1}{2},k}} \left[\frac{r \Big|_{i+1} \mathcal{E}_\phi \Big|_{i+1,k}^n - r \Big|_i \mathcal{E}_\phi \Big|_{i,k}^n}{r \Big|_{i+\frac{1}{2}} \Delta r} \right], \quad (2.5b)$$

$$\mathcal{E}_\phi \Big|_{i,k}^{n+1} = \mathcal{E}_\phi \Big|_{i,k}^n + \frac{\Delta t}{\epsilon \Big|_{i,k}} \left[\frac{\mathcal{H}_r \Big|_{i,k+\frac{1}{2}}^{n+\frac{1}{2}} - \mathcal{H}_r \Big|_{i,k-\frac{1}{2}}^{n+\frac{1}{2}}}{\Delta z} - \frac{\mathcal{H}_z \Big|_{i+\frac{1}{2},k}^{n+\frac{1}{2}} - \mathcal{H}_z \Big|_{i-\frac{1}{2},k}^{n+\frac{1}{2}}}{\Delta r} \right]. \quad (2.5c)$$

Discretization of the Transverse Electric Mode TE_ϕ

$$\mathcal{E}_r \Big|_{i+\frac{1}{2},k}^{n+1} = \mathcal{E}_r \Big|_{i+\frac{1}{2},k}^n - \frac{\Delta t}{\epsilon \Big|_{i+\frac{1}{2},k}} \left[\frac{\mathcal{H}_\phi \Big|_{i+\frac{1}{2},k+\frac{1}{2}}^{n+\frac{1}{2}} - \mathcal{H}_\phi \Big|_{i+\frac{1}{2},k-\frac{1}{2}}^{n+\frac{1}{2}}}{\Delta z} \right], \quad (2.6a)$$

$$\mathcal{E}_z \Big|_{i,k+\frac{1}{2}}^{n+1} = \mathcal{E}_z \Big|_{i,k+\frac{1}{2}}^n + \frac{\Delta t}{\epsilon \Big|_{i,k+\frac{1}{2}}} \left[\frac{r \Big|_{i+\frac{1}{2}} \mathcal{H}_\phi \Big|_{i+\frac{1}{2},k+\frac{1}{2}}^{n+\frac{1}{2}} - r \Big|_{i-\frac{1}{2}} \mathcal{H}_\phi \Big|_{i-\frac{1}{2},k+\frac{1}{2}}^{n+\frac{1}{2}}}{r \Big|_i \Delta r} \right], \quad (2.6b)$$

$$\begin{aligned} \mathcal{H}_\phi \Big|_{i+\frac{1}{2},k+\frac{1}{2}}^{n+\frac{1}{2}} &= \mathcal{H}_\phi \Big|_{i+\frac{1}{2},k+\frac{1}{2}}^{n-\frac{1}{2}} + \frac{\Delta t}{\mu \Big|_{i+\frac{1}{2},k+\frac{1}{2}}} \left[\frac{\mathcal{E}_z \Big|_{i+1,k+\frac{1}{2}}^n - \mathcal{E}_z \Big|_{i,k+\frac{1}{2}}^n}{\Delta r} \right. \\ &\quad \left. - \frac{\mathcal{E}_r \Big|_{i+\frac{1}{2},k+1}^n - \mathcal{E}_r \Big|_{i+\frac{1}{2},k}^n}{\Delta z} \right]. \end{aligned} \quad (2.6c)$$

These equations constitute the heart of this thesis. They can be applied also to more

general problems with no homogeneous medium. However, given that for the problem of the thesis the propagation medium inside the waveguide was assumed as empty space, the parameters μ and ϵ can be replaced by μ_0 and ϵ_0 , respectively, at any position in the simulation space.

For the sake of clarity, the complete deduction of these equations is not given in this chapter. The interested reader is referred to Appendix B, where the basic procedure of discretization is explained and some detailed examples are given. In particular, Section B.3 presents the discretization process in complete detail. With that in mind, and by means of Figure 2.2, the path for arriving to (2.5) and (2.6) is complete.

2.1.4 Modelling of the Lightning Channel

Deduction of Equations (2.5) and (2.6) was made under the assumptions of no external sources and of an isotropic medium. These assumptions would be valid for the model being developed if the lightning channel was not included. The inclusion of the lightning channel as an external source of fields can be easily implemented as a specified current source at any location in the simulation space and time. This current source was specified by the MTL or MTLE return-stroke models, as described at the beginning of this section. But there is one last question: how to include a straight vertical antenna with specified current distribution in the FDTD simulation space? The answer to this question is given below.

If the lightning channel is placed at the leftmost part of the simulation space, where its radial coordinate equals zero, it would produce an indetermination on the equation of \mathcal{E}_z for the transverse electric mode of propagation. This issue and the inclusion of the lightning channel as a straight vertical antenna can be solved if one considers the application of Equation A.2 to a circular path of radius $\frac{\Delta r}{2}$. The circular path is coaxial with the z axis and then the electric current density of the lightning channel flows perpendicular to the surface of the circular path. After making the simplifications allowed by the symmetry of the problem, a new equation for the \mathcal{E}_z field in the transverse electric mode is obtained. This equation can be applied to the points of the simulation space where the

electric current exists. The result is shown by Equation (2.7).

$$\mathcal{E}_z \Big|_{i_0, k+\frac{1}{2}}^{n+1} = \mathcal{E}_z \Big|_{i_0, k+\frac{1}{2}}^n + \frac{4\Delta t}{\epsilon\Delta r} \mathcal{H}_\phi \Big|_{i_0+\frac{1}{2}, k+\frac{1}{2}}^{n+\frac{1}{2}} - \frac{4\Delta t}{\epsilon\pi(\Delta r)^2} I \Big|_{i_s, k_s+\frac{1}{2}}^{n+\frac{1}{2}}. \quad (2.7)$$

2.1.5 Modelling of Irregular Terrain

Given that the Earth path between points A and B of Figure 2.1 is not a straight one, it is necessary to include a methodology for the representation of irregular terrain in the simulation model. The technique followed was the so called Staircase Approximation (SCA), which is described in (Noda, Yonezawa, Yokoyama, & Takahashi, 2004). The technique is very simple: given a straight line between two points α and β , choose the zigzag path along the FDTD grid that minimizes the distance between itself and the straight line.

The above is necessary because the electric field components in the FDTD grid cells are located in the centre of the edges, as shown by Figure 2.2. As a consequence, any “object” in the grid has to be approximated according to its geometry. It is then evident that the smaller the size of the grid cells, the better the approximation to the real terrain profile. However, this is limited by the computational resources. A schematic of this situation can be seen in Figure 2.3, where the original problem geometry has been replaced for its discrete version in the FDTD grid.

2.1.6 Absorbing Boundary Conditions

The Absorbing Boundary Conditions (ABC) used for this thesis were the ones first proposed by Liao, Huang, Yang, and Yuan (1984) and then modified and adapted to the cylindrical coordinate system by Yu, Zhou, and Liu (2006). A discussion on the effects of different ABC is out of the scope of the work. However, the Liao’s ABC were chosen because of its simplicity and its effectiveness for lightning-related phenomena.

Finally, by considering the whole aspects of the model, it is worth showing how the complete simulation space of the geometry shown in Figure 2.1 would look like after its discretization in the FDTD grid. This is shown in Figure 2.3, where the effect of SCA is

clearly visible in the representation of the relief profile from A to B .

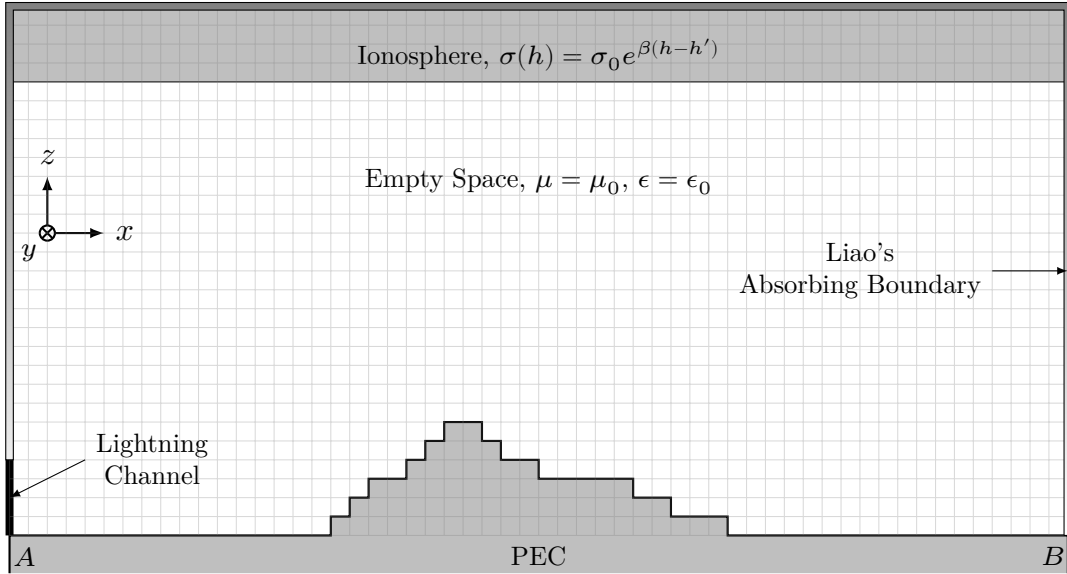


Figure 2.3: Representation of the problem geometry in the FDTD grid (not to scale).

2.2 Simulation Set-Up

As stated at the beginning of the chapter, there are two main sections in it. This is the section that describes the simulation set-up that was developed in order to obtain the results presented in the next chapter. The first stage of the simulation set-up was to validate the mathematical model previously presented, thus accomplishing the first specific objective of the work. The second stage consisted in the simulation of different scenarios of propagation of LEMP along real terrains with variations in elevation over the sea level; this is part of the second specific objective of the thesis. The third and final stage of the simulation set-up was for evaluating the location accuracy of the time-of-arrival technique under the presence of irregular terrain; this being part of the third specific objective.

2.2.1 Numerical Validation of the Model

The validation of the model was carried out by using two strategies. The first one consisted in the comparison of the electromagnetic fields predicted by the model of this thesis with

those predicted by canonical models that are available in the scientific literature. The second strategy consisted in the comparison of the fields predicted by the flat-terrain model against the fields calculated in the presence of an ideally-shaped mountain. The height of this mountain was then varied to different degrees in order to show its effect on the fields predicted by the model.

For the particular case of this work, the model used for comparison in the first strategy was the one developed by Uman et al. (1975). It is a model for the calculation of electromagnetic fields at a distance from a lightning channel and over flat terrain. The ground conductivity in this model is assumed to be infinite and no ionospheric reflections are considered. The equations for the calculation of the fields are (1.2) and (1.3).

These are integral equations that have to be solved numerically, which are very costly in computational terms if they are solved using for cycles. The approach followed in this work, then, was to implement a vectorized version of the trapezoidal rule. This version is explained in Appendix D. The codes developed in this work for solving these integrals are available at the following GitHub repository: [MATLAB® Codes for Numerical Integration](#).

2.2.2 Numerical Experiments for Propagation Effects

In order to describe the changes undergone by LEMP due to different types of ground irregularities in the propagation path, three different lightning striking points over the Colombian territory were chosen, as well as six different observation points (lightning sensors). Both the lightning striking points and the observation points can be seen in Figure 2.4, which also includes an elevation map of the Colombian territory. The geographical coordinates of the lightning striking points and the lightning sensors are presented in Tables 2.1 and 2.2, respectively.

Table 2.1: Geographical coordinates of three different lightning striking points.

Lightning	Latitude [°]	Longitude [°]
L_A	6.095965	-71.369225
L_B	6.404283	-76.822284
L_C	4.891667	-75.323640

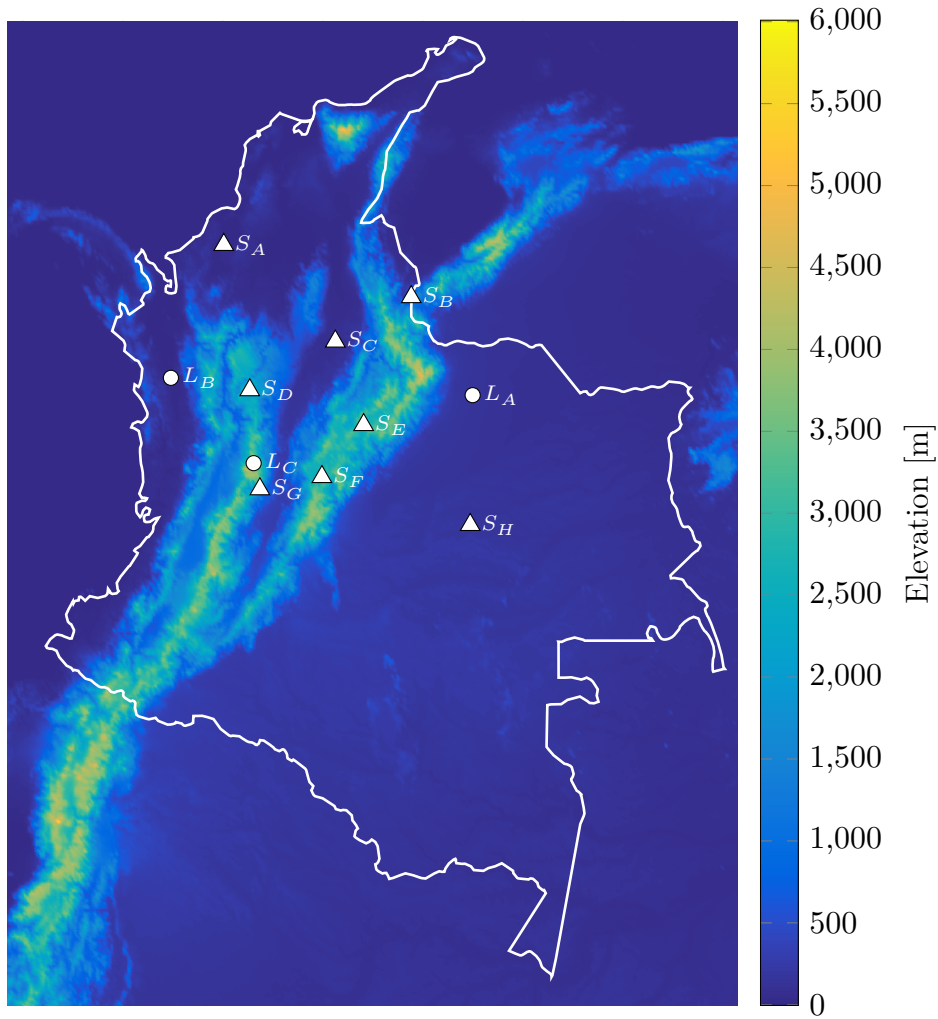


Figure 2.4: Elevation map of Colombia. Circles represent the chosen lightning striking points, triangles represent the chosen lightning sensors (observation points).

Given the lightning striking points and the observation points defined above, six relief profiles were defined for the analysis of its effects on the propagation of LEMP. These six profiles were used to carry out the simulations shown in the next chapter. It is important to remark that they were chosen for being representative in terms of their interest for lightning localization in Colombia, which is a country traversed by the Cordillera of the Andes, with mountain ranges of important altitude (see Figure 2.4). The chosen reliefs are shown in Figures 2.5 to 2.10 and correspond to the direct line of propagation between the end points defined in Table 2.3. For all these figures, the lightning discharge point (identified by letter A in the geometry of Figure 2.1) is the leftmost point of the profile,

Table 2.2: Geographical coordinates of six different lightning sensors.

Sensor	Latitude [°]	Longitude [°]
S_A	8.775286	-75.876638
S_B	7.847637	-72.472629
S_C	7.060000	-73.850000
S_D	6.192189	-75.396762
S_E	5.573621	-73.338913
S_F	4.648610	-74.092374
S_G	4.430331	-75.210687
S_H	3.791452	-71.422942

and the observation point (identified by letter B in the geometry of Figure 2.1) is the rightmost point of the profile. All the profiles were extracted using Google Earth Pro computer software (Google, 2020).

Table 2.3: Location of the end points for six different relief profiles.

Relief Profile	Transmitter	Receiver
P_1	L_A	S_C
P_2	L_A	S_E
P_3	L_B	S_B
P_4	L_C	S_C
P_5	L_C	S_F
P_6	L_C	S_G

The six cases presented were chosen because they represent real situations of propagation effects that can arise in practice. Specifically, the case P_1 represents the typical problem of a hill between the transmitter and receiver. It is important to notice that this mountain has an altitude of about 5000 meters, which is an important altitude when compared to the wavelength of a typical LEMP. Case P_2 is also a mountain, but this time the observation point (lightning sensor) is located at an important altitude (top of the mountain). Case P_3 represents the problem of a wave that has to cross a valley. Finally, cases P_4 , P_5 and P_6 represent the problem of propagation when the transmitter is located itself at the very top of a mountain, and the wave has to descend to the observation point at almost the sea level, or has to descend and then climb again to the observation point,

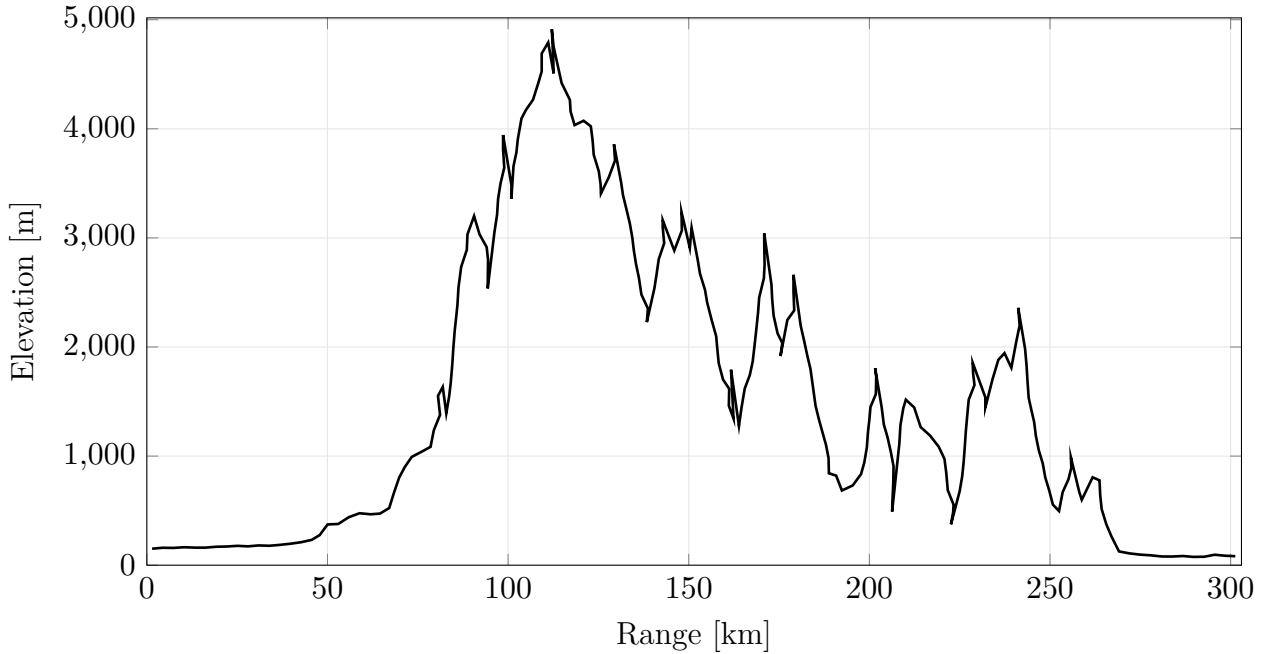


Figure 2.5: Relief profile for simulation of propagation effects. Case P_1 . Adapted from Google Earth Pro (Google, 2020).

or the observation point is covered (hidden) by the mountain itself.

2.2.3 Numerical Experiments for Location Accuracy

For the analysis of the location accuracy of the time-of-arrival technique in the presence of irregular terrain, the same lightning striking points of Table 2.1 were used. The lightning sensors used for its localization were chosen to be at least four, and taking into account that the sensors were the closest ones and covered a region that included the lightning discharge. This strategy allowed to use the results of the previous propagation analysis to calculate the localization accuracy of the time-of-arrival and compare them with the localization obtained when the terrain irregularities were eliminated. Table 2.4 specifies the sensors used for the localization of each individual discharge.

Given that the location accuracy of the time-of-arrival technique is directly related to the onset time of the waves, it was calculated for each of the six sensors that were supposed to receive the signals of the individual lightning discharges. The onset times

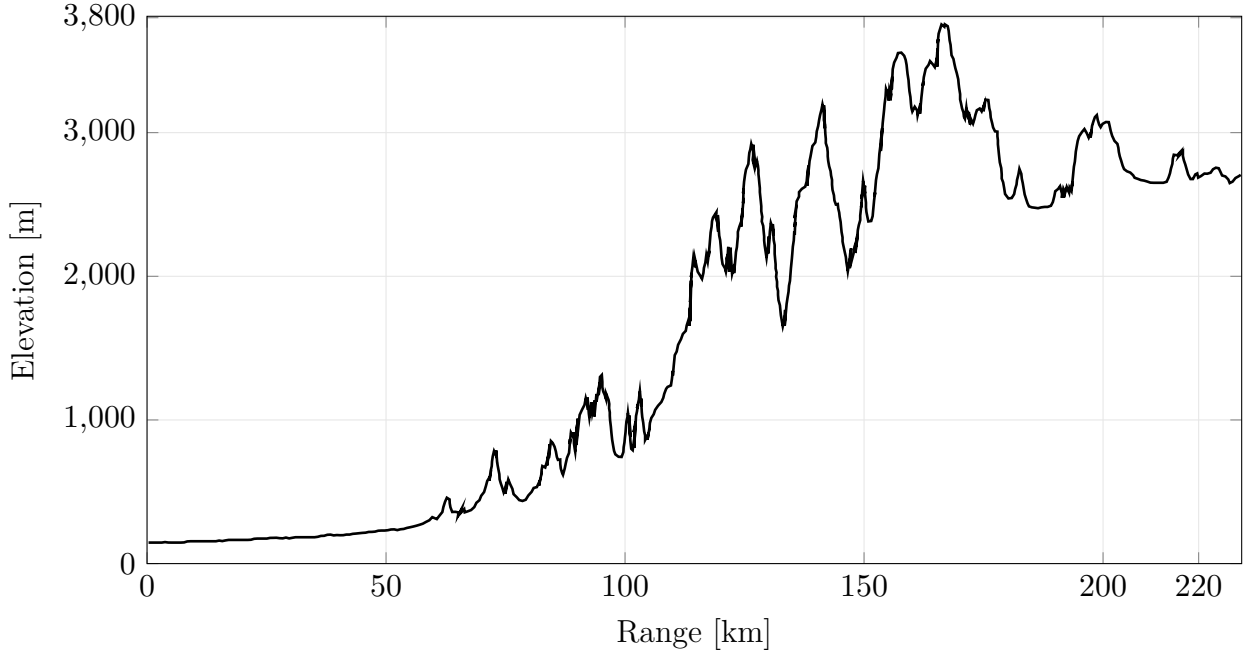


Figure 2.6: Relief profile for simulation of propagation effects. Case P_2 . Adapted from Google Earth Pro (Google, 2020).

Table 2.4: Lightning striking points and sensors used for its localization.

Lightning	Sensors
L_A	S_B, S_C, S_E, S_H
L_B	S_A, S_B, S_C, S_D
L_C	S_D, S_E, S_F, S_G

were calculated by means of the following formula, and considering a threshold value of 10% of the signal peak:

$$t_{on} = t_p - \frac{t_p - t_t}{u_p - u_t} u_p \quad (2.8)$$

Where t_{on} is the onset time, t_p is the time to the signal peak, t_t is the time to the signal threshold considered, u_p is the value of the field peak, and u_t is the threshold value of the field. This definition of the onset times is depicted in Figure 2.11.

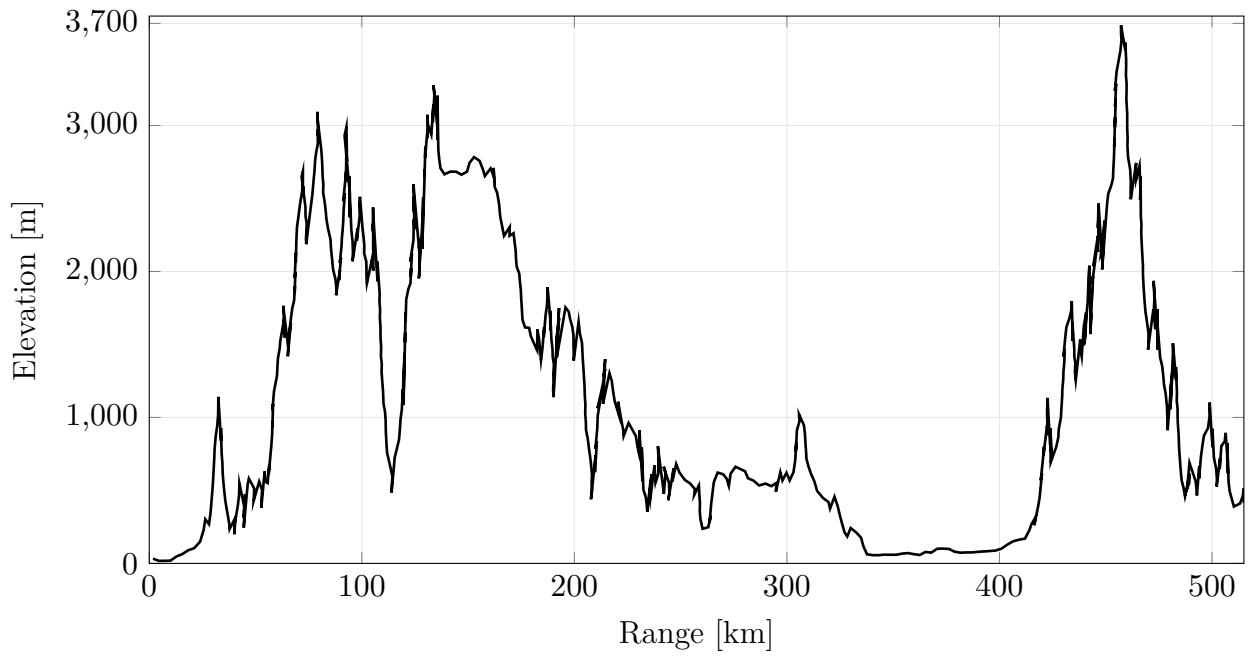


Figure 2.7: Relief profile for simulation of propagation effects. Case P_3 . Adapted from Google Earth Pro (Google, 2020).

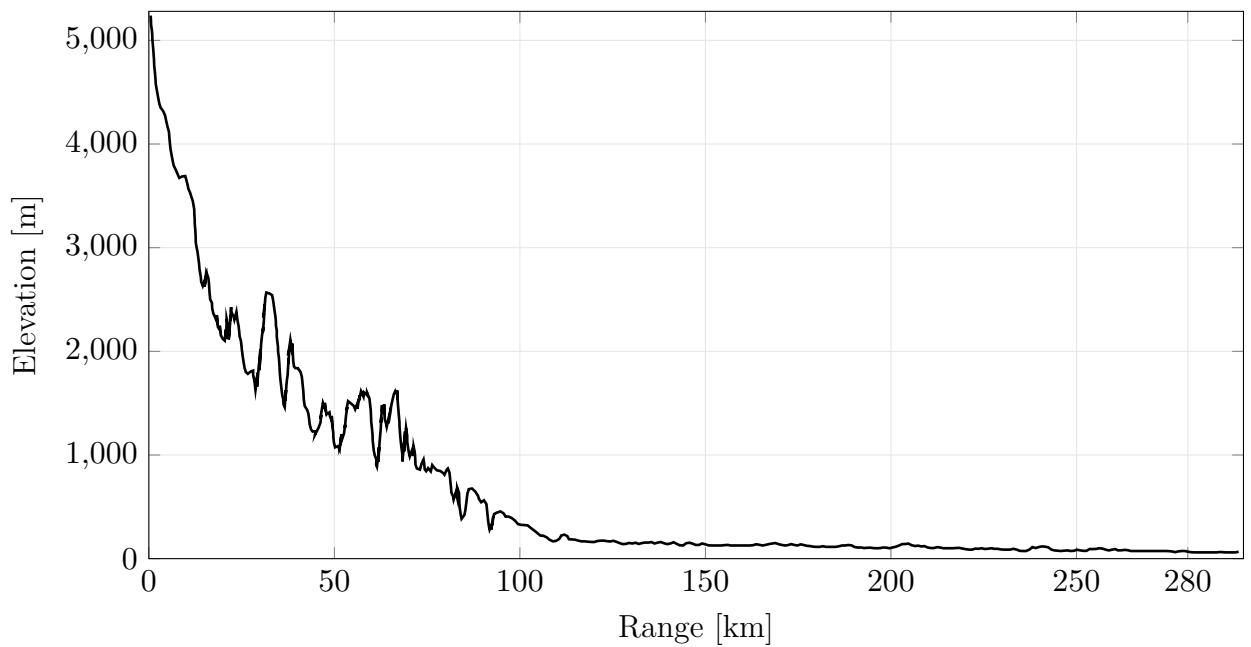


Figure 2.8: Relief profile for simulation of propagation effects. Case P_4 . Adapted from Google Earth Pro (Google, 2020).

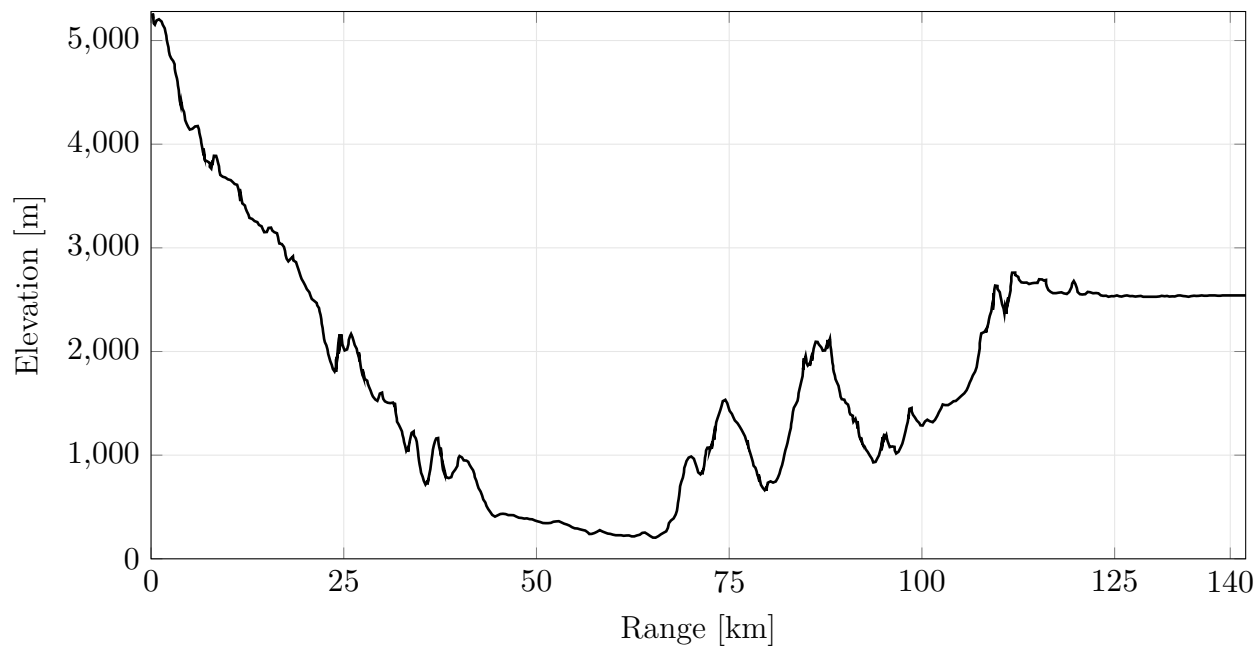


Figure 2.9: Relief profile for simulation of propagation effects. Case P_5 . Adapted from Google Earth Pro (Google, 2020).

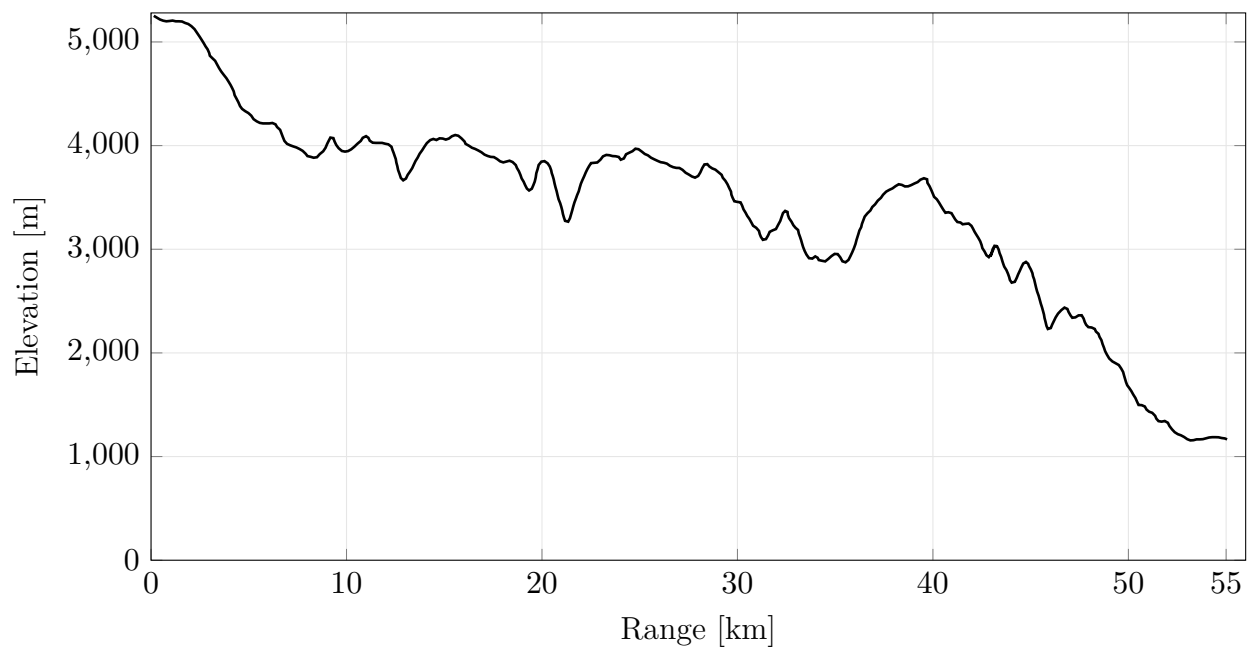


Figure 2.10: Relief profile for simulation of propagation effects. Case P_6 . Adapted from Google Earth Pro (Google, 2020).

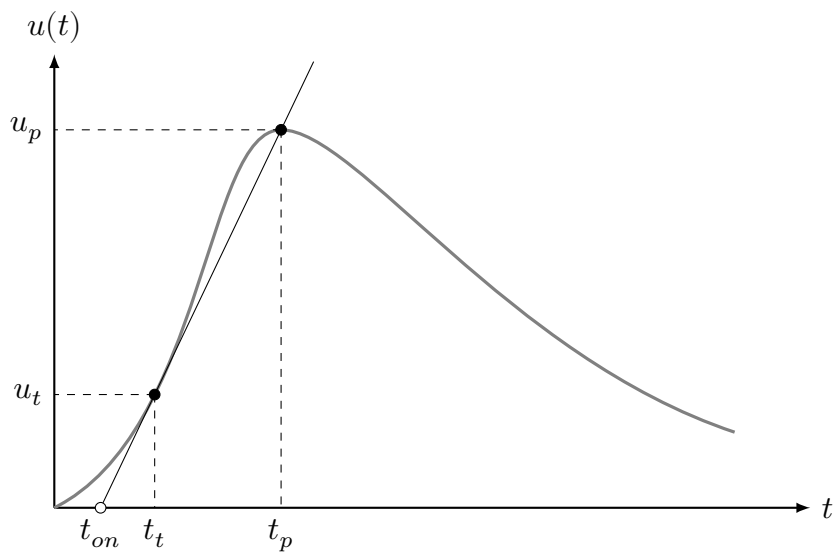


Figure 2.11: Definition of signal onset time: t_{on} .

Chapter 3

Results

This chapter presents the numerical results obtained for different simulation scenarios, according to the description given in Chapter 2. Therefore, the chapter is divided into three main sections; the first one includes the simulations carried out in order to test the validity of the model; the second one presents the simulations carried out in order to examine propagation effects of terrain on the wave propagation; and the third section presents the results of examining the effects of the wave propagation on the location accuracy of LLS. The MATLAB[®] codes implemented for the results shown in this chapter can be found at the following GitHub repository: [EIWGSimulation](#).

3.1 Numerical Validation of the Model

Two strategies were used for the validation of the model. The first one consisted in calculating the electric and magnetic fields from a lightning discharge by means of canonical models, in particular, the model represented by Equations (1.3) and (1.2), which were developed by Uman et al. (1975). Then, the results were compared with those obtained by means of the FDTD model developed in this work. The second strategy consisted in simulating another lightning discharge and evaluating the effect of an obstacle on the propagation of the fields. The height of the obstacle was changed to different multiples of the wavelength.

3.1.1 Comparison with Canonical Model

The comparison results are shown in Figures 3.1 and 3.2. The plots are in good agreement, except for the high frequency components that are seen from the FDTD solution. This will be explained in Chapter 4. Finally, the parameters used for the simulation are the

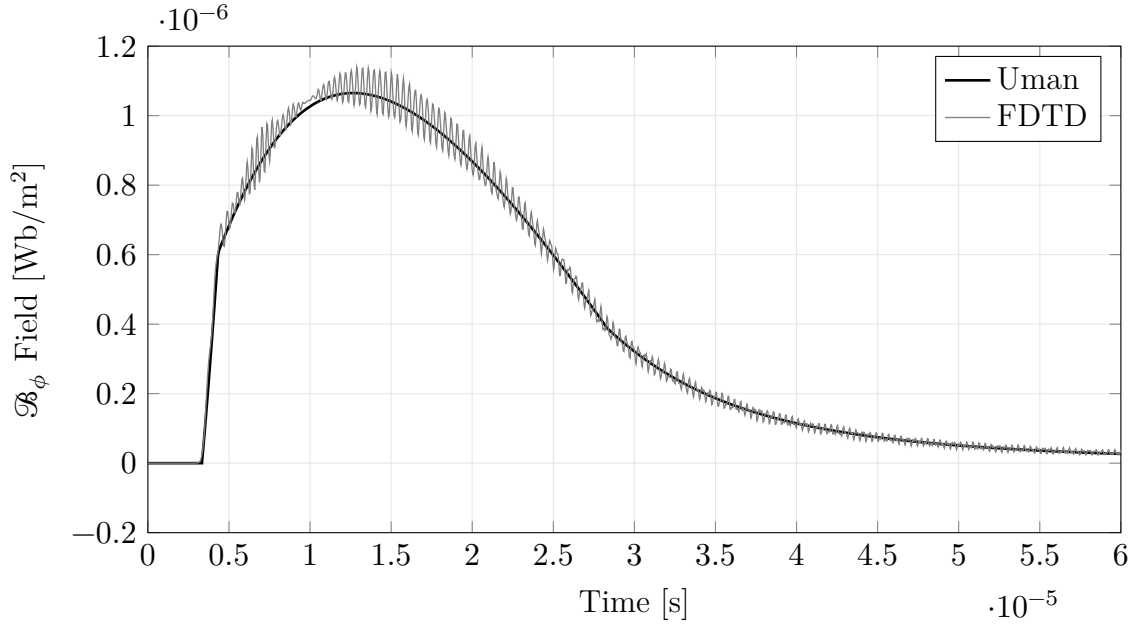


Figure 3.1: Magnetic flux density at 1 km from the lightning channel. Black solid line represents the calculation by means of Equation (1.2) and gray solid line represents the calculation by means of the FDTD method.

same ones presented in the paper (Uman et al., 1975). For the FDTD simulation, it was necessary to find the shortest wavelength of the return-stroke signal used. In order to do this, the signal was analysed to find the smallest frequency containing the 99% of its energy. The wavelength found with this methodology was around $\lambda = 1000$ m. This value was used to define the parameters of Table 3.1 for the FDTD simulation.

Table 3.1: Simulation parameters used for FDTD simulation of Figures 3.1 and 3.2.

Source Wavelength λ [m]	Δr [m]	Δz [m]	Δt [s]
500	$\frac{\lambda}{20}$	$\frac{\lambda}{20}$	$\frac{\Delta r}{2c}$

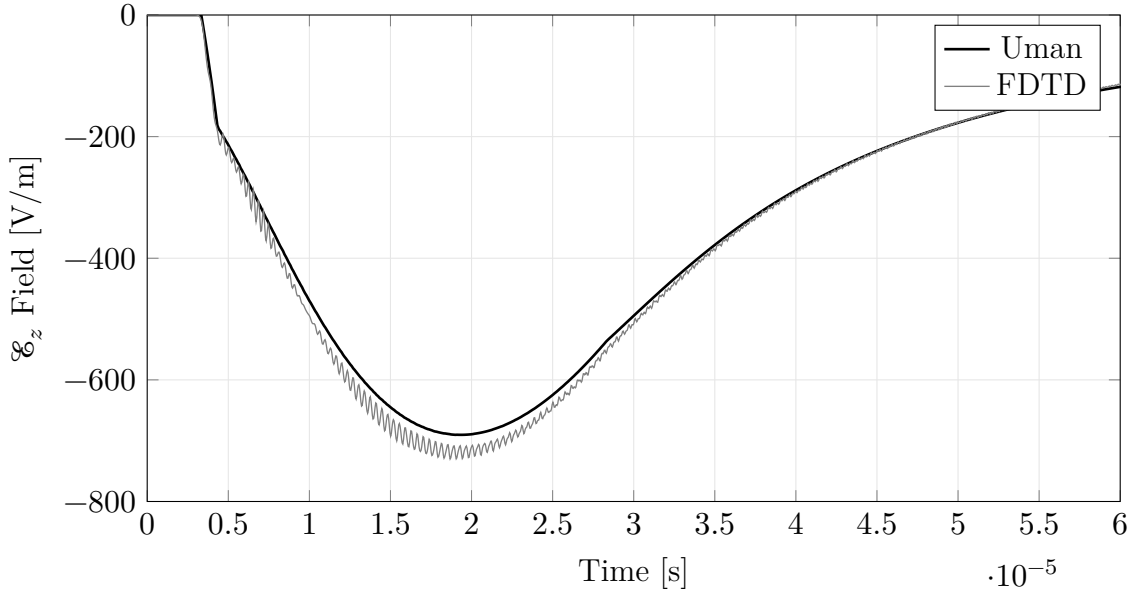


Figure 3.2: Electric field intensity at 1 km from the lightning channel. Black solid line represents the calculation by means of Equation (1.3) and gray solid line represents the calculation by means of the FDTD method.

3.1.2 Validation of the Obstacle Effect

These are the results for the second validation strategy. The important thing here is that the FDTD model developed has been tested for propagation in empty space, and now, the effect of obstacles can be considered. The objective of this part is to show that the results actually depend on the presence of the obstacles.

The simulation space used is represented in Figure 3.3, without the presence of the ionosphere, and with a rectangular obstacle located in the region $30 \text{ km} \leq r \leq 60 \text{ km}$, $0 \text{ km} \leq z \leq H_O$. The observation point is beyond the obstacle, at $r = 80 \text{ km}$. The return-stroke current model used was the MTL with the Nucci channel-base current of Equation (C.2). The parameters used for the lightning current at the channel base are: $I_1 = 46300 \text{ A}$, $I_2 = 35000 \text{ A}$, $\tau_1 = 7.2 \times 10^{-6} \text{ s}$, $\tau_2 = 5 \times 10^{-6} \text{ s}$, $\tau_3 = 100 \times 10^{-6} \text{ s}$, $\tau_4 = 6 \times 10^{-6} \text{ s}$, $\eta = 0.845$, and a channel height of $H = 7 \text{ km}$. This signal has a peak of 30 kA, risetime of $10 \mu\text{s}$, and a fall-time of $100 \mu\text{s}$. The analysis of its frequency content showed that the signal has the shortest wavelength in the order of $\lambda \approx 5000 \text{ m}$. Then, the parameters of Table 3.2 were used to run the FDTD simulation.

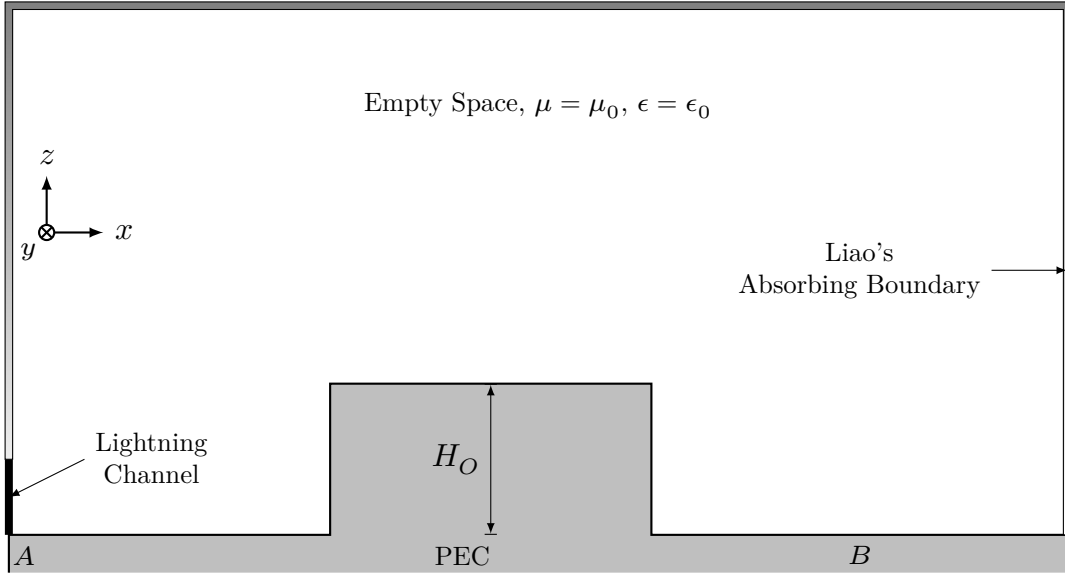


Figure 3.3: Simulation scenario for testing effect of the obstacle height.

Table 3.2: Simulation parameters used for FDTD simulation of Figures 3.4 and 3.5.

Source Wavelength λ [m]	Δr [m]	Δz [m]	Δt [s]
4000	$\frac{\lambda}{20}$	$\frac{\lambda}{20}$	$\frac{\Delta r}{2c}$

Figures 3.4 and 3.5 show the electric and magnetic field, respectively, for different heights of the obstacle.

3.2 Numerical Experiments for Propagation Effects

This section deals with the effects that the terrain irregularities can cause on the propagation of the waves. It is divided into three subsections at the same time. The first subsection presents simulations of propagation that consider the relationship between the source risetime and the size of the obstacles in the propagation path. The second subsections considers the effect of the ionosphere in relation to the obstacles size. Finally, the third subsection considers the propagation effects for the six profiles of Figures 2.5 to 2.10.

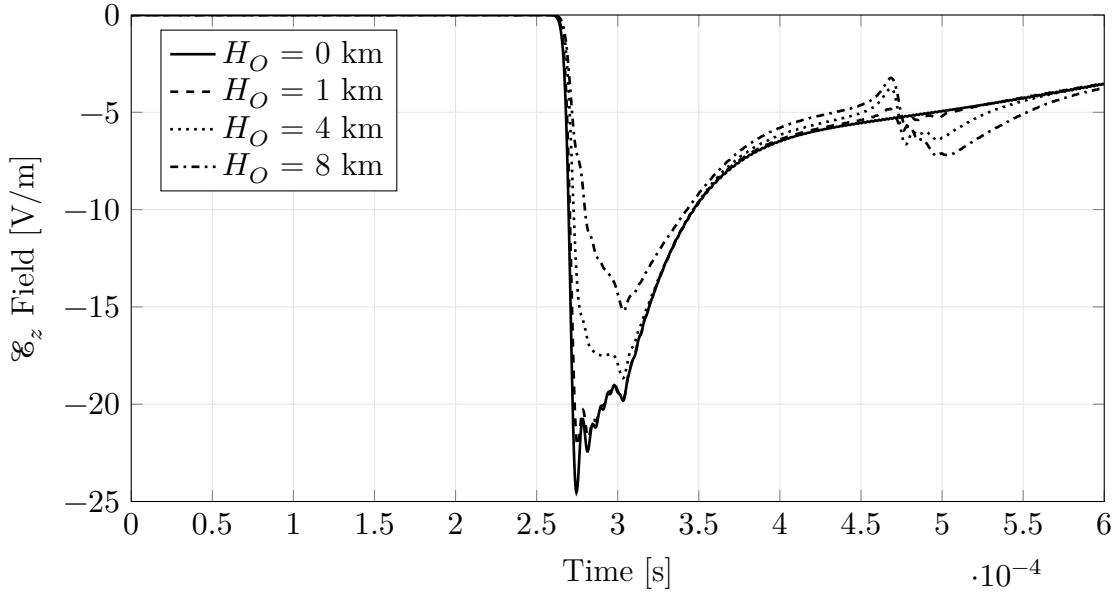


Figure 3.4: Electric field intensity at 80 km from a lightning discharge and propagation in an empty space with rectangular obstacle of different heights.

3.2.1 Source Wavelength-Obstacle Height Relationship

Two particular questions were stated during the introduction of this document: What is the maximum height of a mountain range such that it can be considered to have no effect on the propagation of LEMP? When do the ground irregularities introduced by mountains are worth to be included in a propagation model for lightning localization? The simulations presented here are meant to try to answer these questions.

Knowing that the effect of the obstacles is directly related to the source wavelength, two different sources were chosen with the aim to consider the effects of the same obstacle on them. The first source is the same lightning return-stroke used for the simulations of the previous section, it is, a 10/100 μ s, 30 kA, waveform. The second source is a 0.5/30 μ s, 30 kA waveform. These two waveforms have a frequency spectrum with the shortest wavelength around 5000 m and 790 m, respectively.

The obstacle introduced in the simulation space is the same rectangle-shaped obstacle used in the previous section. It was located in the region $30 \text{ km} \leq r \leq 60 \text{ km}$, $0 \leq z \leq 4000 \text{ m}$. As it can be seen, the obstacle height is around 0.8 times the wavelength of the first source (the 10/100 μ s, 30 kA waveform), and around 5 times the wavelength of the

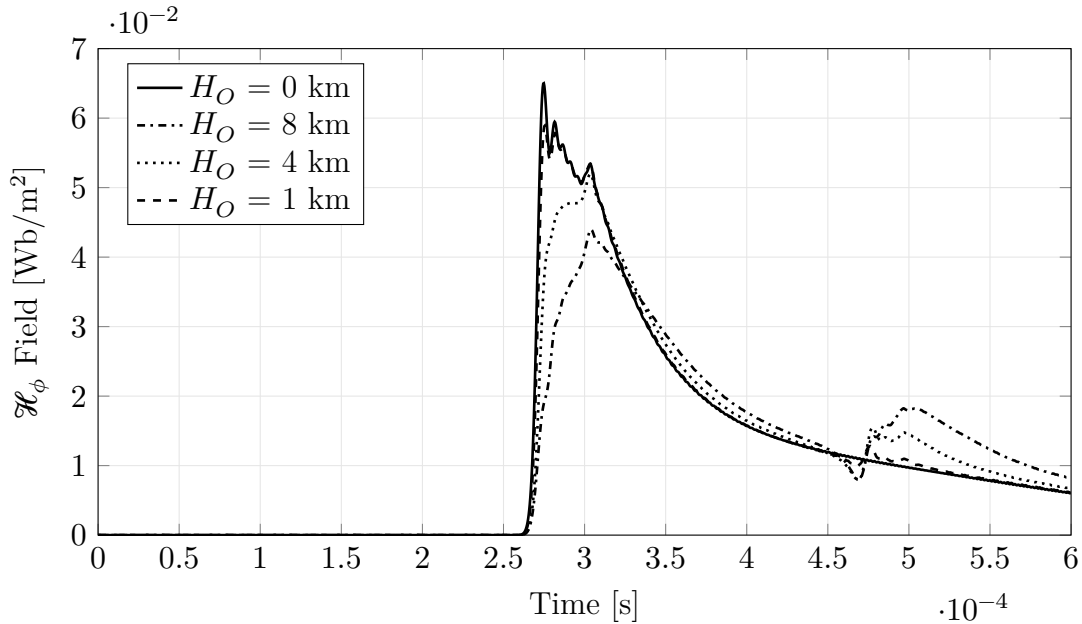


Figure 3.5: Magnetic field intensity at 80 km from a lightning discharge and propagation in an empty space with rectangular obstacle of different heights.

second source (the $0.5/30 \mu\text{ s}$, 30 kA waveform).

The results of the simulation are shown in Figures 3.6 and 3.7. The observation point is at $r = 80 \text{ km}$, beyond the obstacle. It can be observed that the reduction in the amplitude of the waves is much more considerable for the waveform with the shortest wavelength. The parameters used for the simulation are given below.

The return-stroke current model used was the MTL with the Nucci channel-base current of Equation (C.2). The channel height was fixed to $H = 7 \text{ km}$. The parameters for the two channel base currents are:

- Waveform with $\lambda \approx 5000 \text{ m}$: $I_1 = 46300 \text{ A}$, $I_2 = 35000 \text{ A}$, $\tau_1 = 7.2 \times 10^{-6} \text{ s}$, $\tau_2 = 5 \times 10^{-6} \text{ s}$, $\tau_3 = 100 \times 10^{-6} \text{ s}$, $\tau_4 = 6 \times 10^{-6} \text{ s}$, $\eta = 0.845$.
- Waveform with $\lambda \approx 790 \text{ m}$: $I_1 = 27000 \text{ A}$, $I_2 = 25000 \text{ A}$, $\tau_1 = 7.2 \times 10^{-8} \text{ s}$, $\tau_2 = 5 \times 10^{-6} \text{ s}$, $\tau_3 = 60 \times 10^{-6} \text{ s}$, $\tau_4 = 6 \times 10^{-6} \text{ s}$, $\eta = 0.845$.

Given the above parameters, the FDTD simulation was run with the values described in Table 3.3.

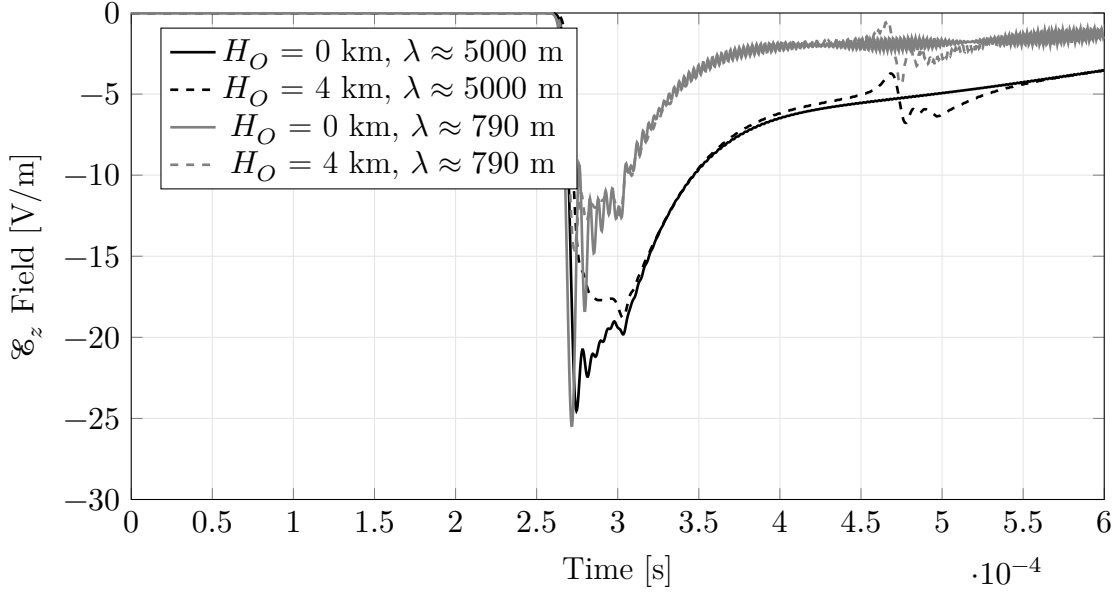


Figure 3.6: Electric field intensity at 80 km from a lightning discharge and propagation in an empty space with rectangular obstacle of different heights: risetime effect.

Table 3.3: Simulation parameters for FDTD simulation of Figures 3.6 and 3.7.

Source Wavelength λ [m]	Δr [m]	Δz [m]	Δt [s]
4000	$\frac{\lambda}{20}$	$\frac{\lambda}{20}$	$\frac{\Delta r}{2c}$
1000	$\frac{\lambda}{10}$	$\frac{\lambda}{10}$	$\frac{\Delta r}{2c}$

3.2.2 Effect of Ionospheric Reflections

The purpose of this part of the results was to show the effect that the ionosphere has on the propagation of the LEMP. Specifically, there is a question concerning the combined effect of the ionosphere and obstacles in the propagation path. The question is whether an obstacle could change the direction of propagation and then, the ionosphere could produce more wave reflections than the case where it is not present.

In order to answer this question, the FDTD model developed in this thesis was tested to see if it was able to reproduce the ionospheric reflections reported in the literature as skywaves; see for example, (Thang et al., 2017) and (Thang et al., 2016). The results are shown in Figures 3.8 and 3.9, where the vertical electric field and azimuthal magnetic field were calculated both for propagation in free space (FS) and propagation in the EIWG. As it is shown, the model is able to predict skywaves when the ionosphere is present. The

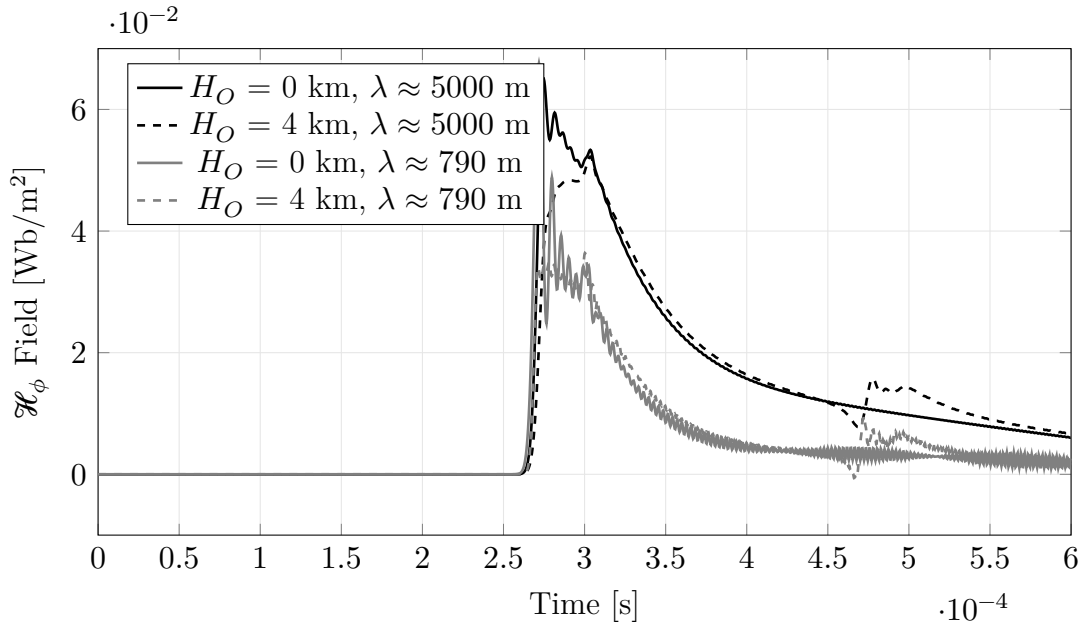


Figure 3.7: Magnetic field intensity at 80 km from a lightning discharge and propagation in an empty space with rectangular obstacle of different heights: risetime effect.

parameters for this simulation are given below.

For this case, the simulation was run with the same parameters used for the simulations that produced Figure 3.4 and 3.5. The ionosphere was modelled as a PEC at an altitude of 80 km. This is the reason for the relatively high magnitudes of the skywaves observed; and the reason for modelling the ionosphere as a PEC is that including a variable conductivity model required much more computer RAM as all the electric parameters of each Yee cell would have had to be stored. Given that the aim of this thesis is not a precise modelling of the ionosphere, the assumption made in order to save computer RAM is considered to be justified.

Once the model was tested for the prediction of skywaves, it was used to see the combined effects of obstacles and the ionosphere. For this test, two simulations were run using the same rectangular-shaped obstacle of 4000 m of altitude that was used in the previous simulations. Two channel base current waveforms were used because the source wavelength had to be considered. The two waveforms are the same ones used for the simulation of Figures 3.6 and 3.7; and the FDTD simulation parameters were the same ones presented in Table 3.3. The results are shown in Figures 3.10 and 3.11.

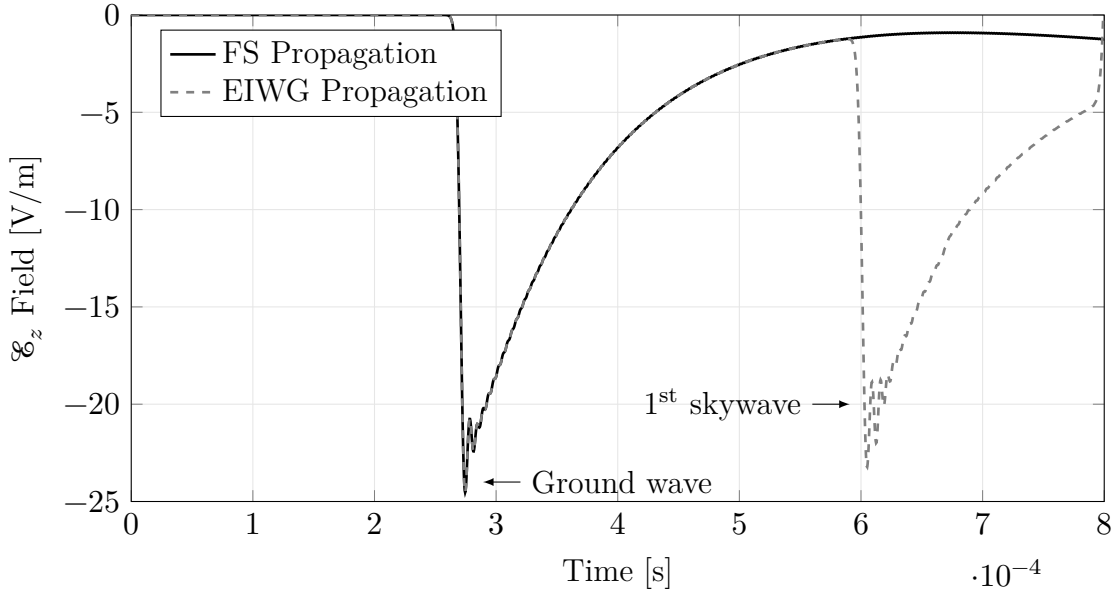


Figure 3.8: Electric field intensity at 80 km from a lightning discharge. Difference between propagation in Free Space and EIWG.

3.2.3 Effects of Propagation Over Relief Profiles in Colombia

Finally, this subsection shows the results that compare the effects of propagation over six different real relief profiles in Colombia, as opposed to propagation over flat ground between the same two points. The propagation cases correspond to the ones explained in Chapter 2.

The source waveform used in the six cases was represented by the MTL model, with Nucci channel base current of Equation (C.2) and the following parameters: $I_1 = 46300$ A, $I_2 = 35000$ A, $\tau_1 = 7.2 \times 10^{-6}$ s, $\tau_2 = 5 \times 10^{-6}$ s, $\tau_3 = 100 \times 10^{-6}$ s, $\tau_4 = 6 \times 10^{-6}$ s, $\eta = 0.845$, $v = c/2$. These parameters create a return-stroke waveform of a wavelength equal to $\lambda \approx 5000$ m. The parameters used to run the FDTD simulation were the same of Table 3.2.

It is worth noticing here that the source waveform used has a wavelength of about the maximum height of the obstacles to be examined. Of course this is not convenient in terms of showing that the mountainous terrain has an important effect on the propagation of the waves; the reason being that a 1000 m-wavelength source would have been more affected by a 5000 m-height mountain. However, the computer RAM needed for simulating the

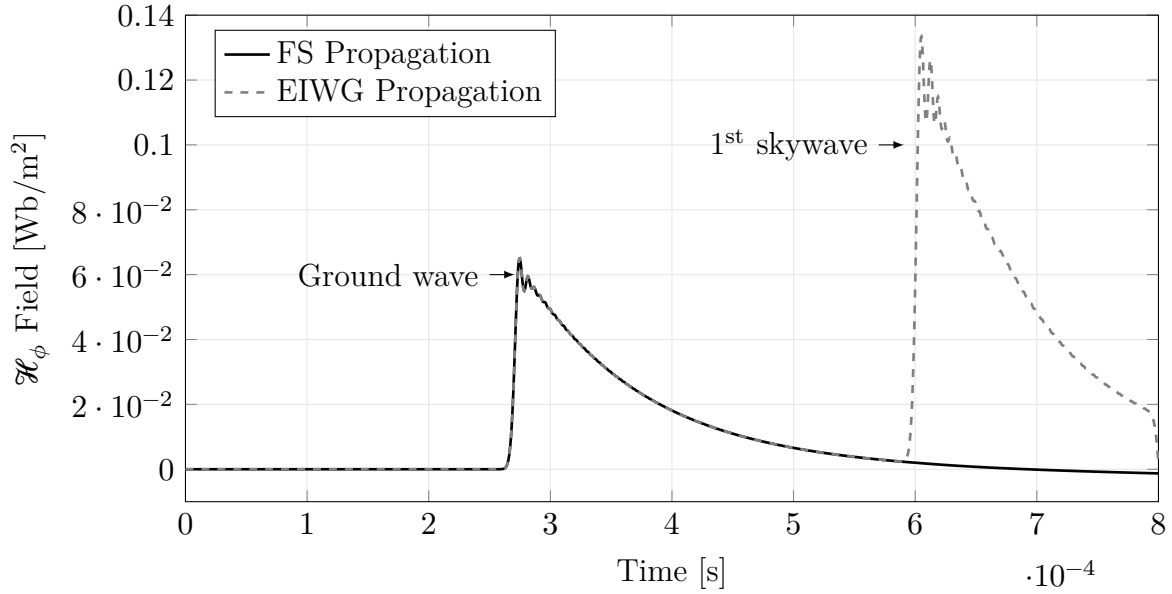


Figure 3.9: Magnetic field intensity at 80 km from a lightning discharge. Difference between propagation in Free Space and EIWG.

propagation of a 1000 m-wavelength source along more than 500 km is unthinkable at the present moment.

Case P_1

The first case corresponds to propagation in the presence of a mountain of 5000 m of altitude. The results are shown in Figures 3.12 and 3.13. The observation point at 80 km is before the mountain, and the observation point at 300 km is beyond the mountain range in the propagation path. There is a very small propagation delay and the main difference in propagation is obtained for the point before the mountain range. There is a reflection of the wave in the mountain at this point. For the point beyond the obstacle, there is a small reduction in the wave amplitude, as expected given that the source wavelength is of about the same height of the mountain.

Case P_2

The second relief profile is for a lightning discharge at ground level and the observation point over a mountain of 3000 m. The results are shown in Figures 3.14 and 3.15. The

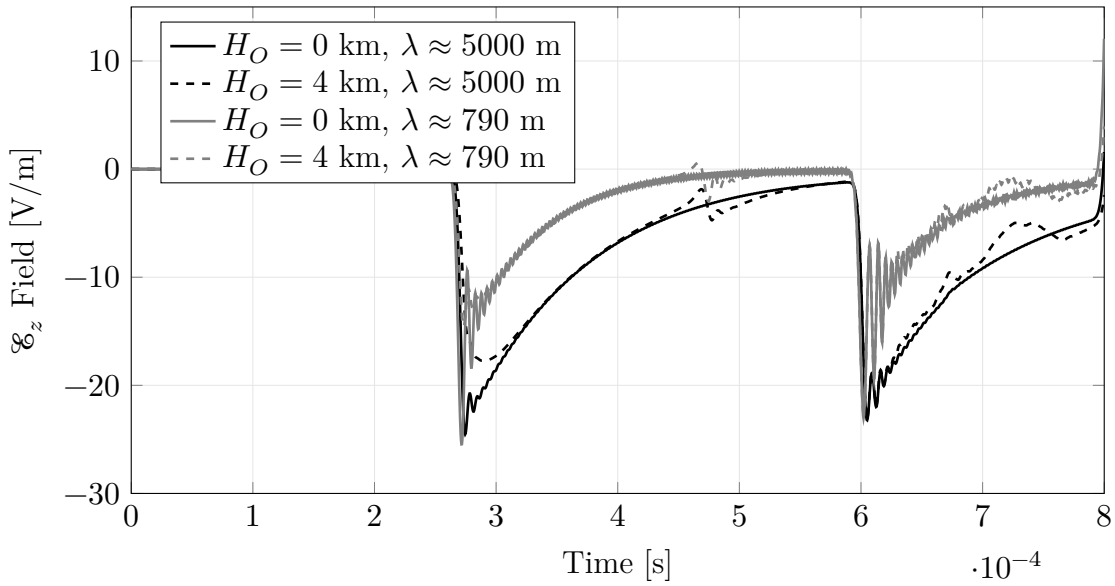


Figure 3.10: Electric field intensity at 80 km from a lightning discharge. Ionospheric Effects.

electric and magnetic fields have opposite behaviours. As shown, the electric field has a larger peak value in the presence of the mountain. The magnetic field instead has a lower peak value in the presence of the mountain. In order to show that these characteristics are due only to the presence of the mountain, the fields were also plotted at the same altitude when the mountain was not present in the simulation space.

Case P_3

In the third relief profile there is kind of a valley that the electromagnetic wave has to get over. The observation point is beyond the second mountain, and the results are shown in Figures 3.16 and 3.17. Also, the propagation distance here is the longest one, with 500 km of distance between the source and the observation point. As expected, both the electric and magnetic fields suffer a considerable reduction in amplitude (around 25%), even though the source wavelength is larger than the tallest mountain.

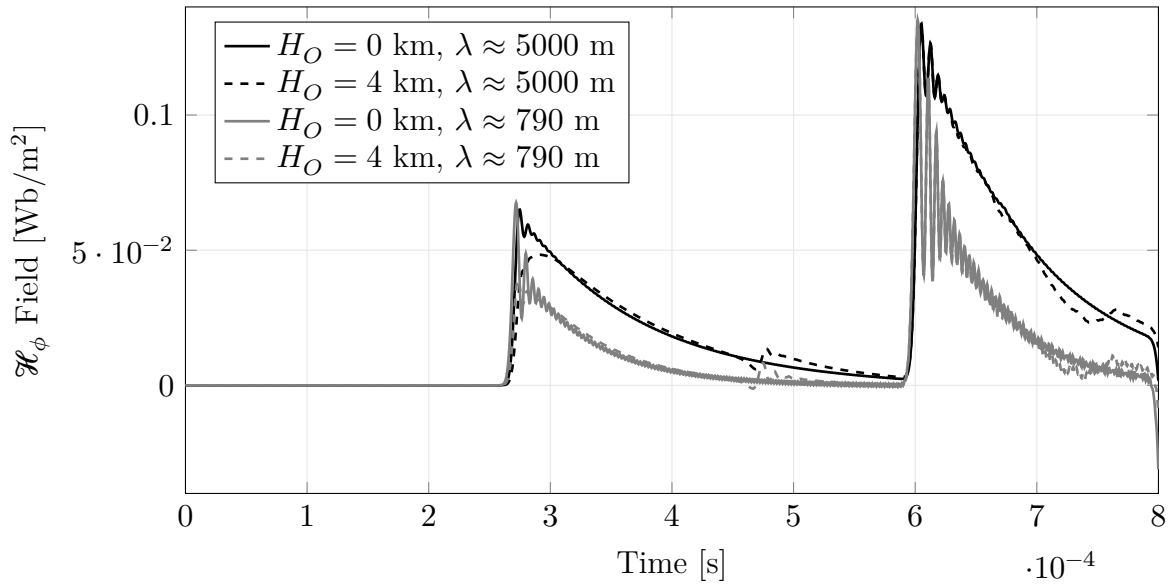


Figure 3.11: Magnetic field intensity at 80 km from a lightning discharge. Ionospheric Effects.

Case P_4

The fourth case of relief profiles corresponds to a lightning discharge that impacts in the top of a mountain of 5000 m in altitude. The wave then has to propagate to an observation point at ground level. The results are shown in Figures 3.18 and 3.19. Both the electric and magnetic fields suffer a small delay and also a small reduction in their amplitude.

Case P_5

The fifth case of propagation shows a relief profile where the wave has to descend again from the source located at the top of a mountain to an observation point at another mountain of about 3000 m tall. The results are shown in Figures 3.20 and 3.21. There is also a small time delay and amplitude reduction, but the propagation over irregular ground shows also some oscillations after the first peak, which are due to reflections of the wave in the PEC mountains.

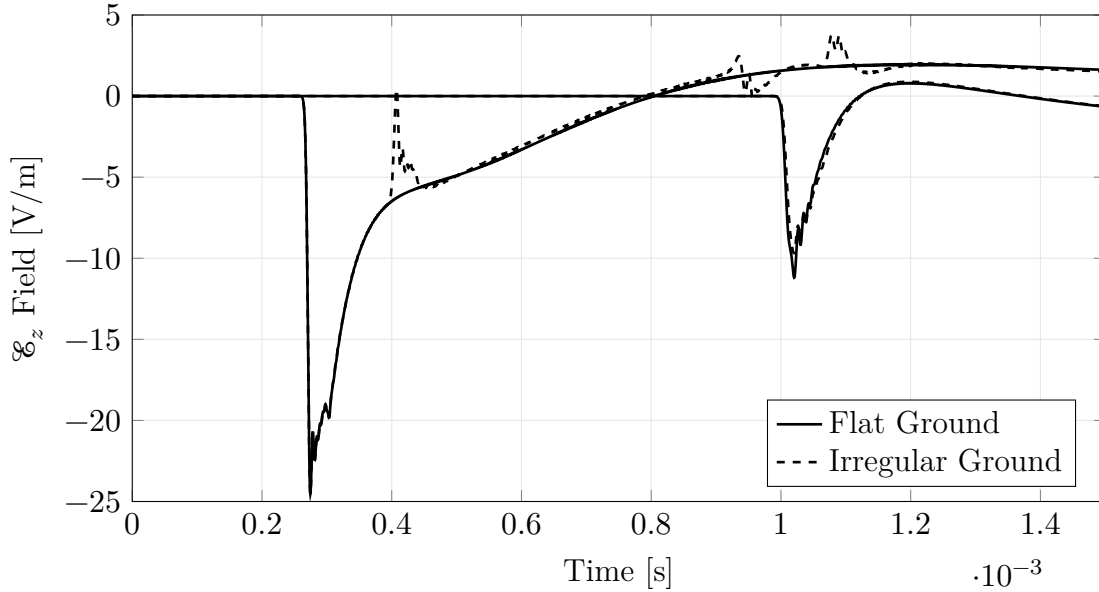


Figure 3.12: Electric field intensity at 80 km and 300 km from a lightning discharge. Difference between propagation over flat ground and over relief profile: Case P_1 . Source wavelength $\lambda \approx 5000$ m.

Case P_6

The sixth and final case of relief profile is very interesting, as the observation point is located under the source and it is hidden by the mountain profile. The results are shown in Figures 3.22 and 3.23. For this particular case, the electric field suffers a reduction of about 50% its peak value. The magnetic field suffers a reduction as well, but it is not as dramatic as the one presented by the electric field.

3.3 Evaluation of the Onset Time for the Relief Profiles Examined

Given that the accuracy of the time-of-arrival technique is directly determined by the electromagnetic wave onset times calculated at each sensor, they were calculated for each of the six relief profiles simulated before. The onset time was calculated for both the flat ground propagation case, and the corresponding irregular ground propagation case. That calculation was made for each relief profile and the values were compared to see the error

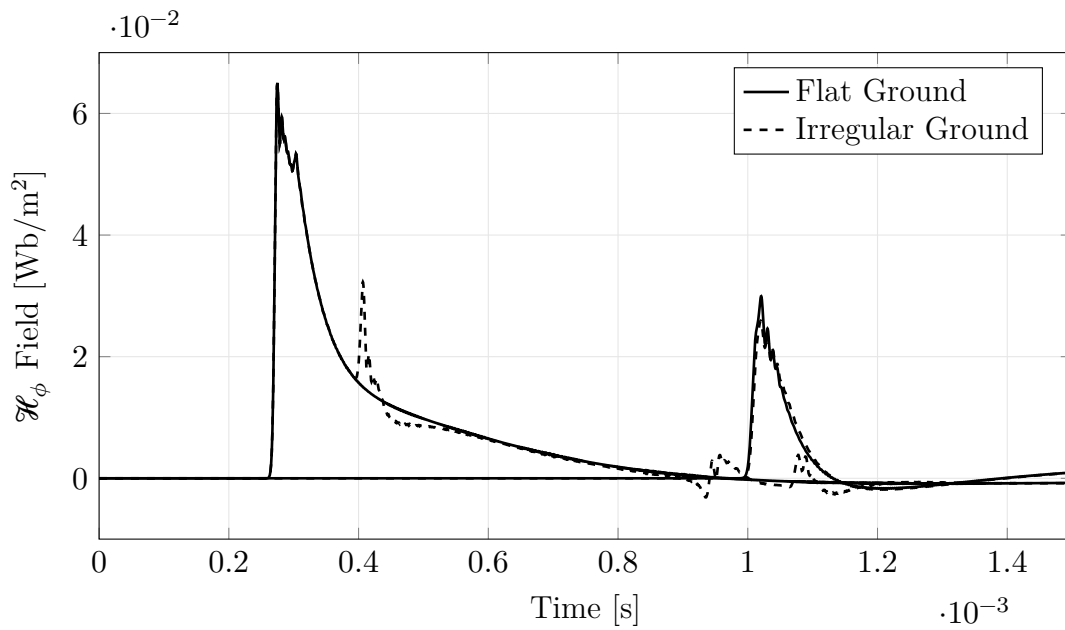


Figure 3.13: Magnetic field intensity at 80 km and 300 km from a lightning discharge. Difference between propagation over flat ground and over relief profile: Case P_1 . Source wavelength $\lambda \approx 5000$ m.

of the flat ground model with respect to the real irregular ground propagation model. The results are shown in Figure 3.24.

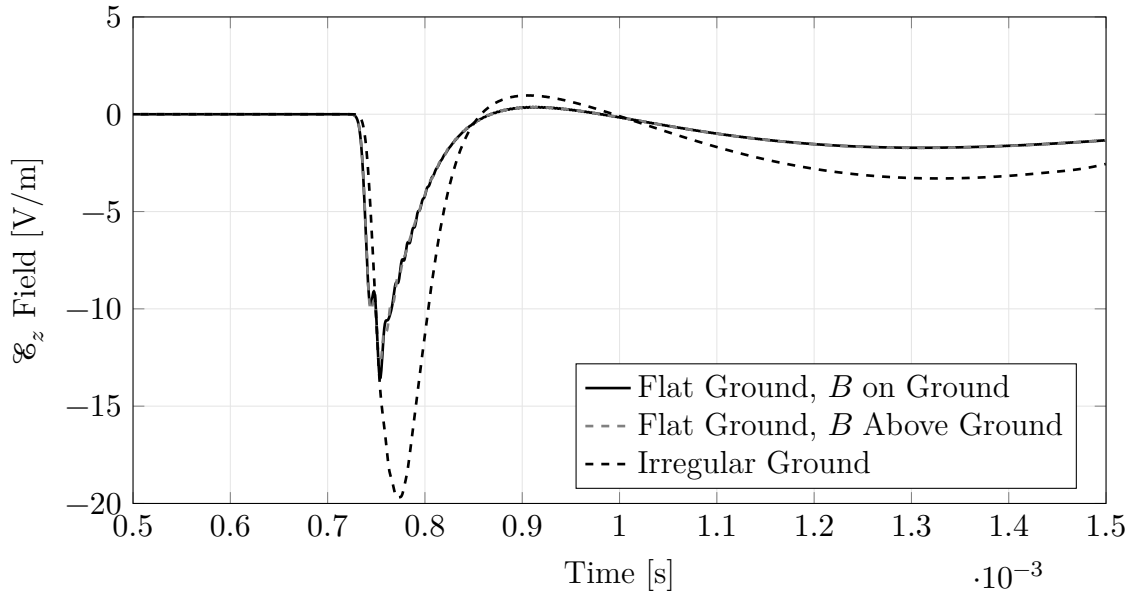


Figure 3.14: Electric field intensity at 220 km from a lightning discharge. Difference between propagation over flat ground and over relief profile: Case P_2 . Source wavelength $\lambda \approx 5000$ m.

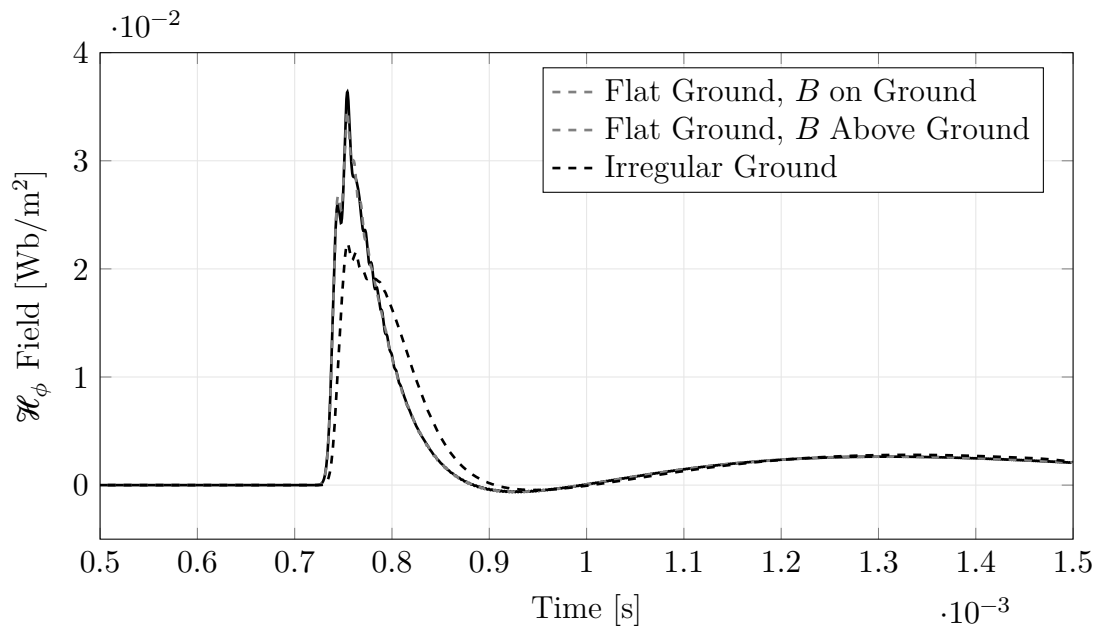


Figure 3.15: Magnetic field intensity at 220 km from a lightning discharge. Difference between propagation over flat ground and over relief profile: Case P_2 . Source wavelength $\lambda \approx 5000$ m.

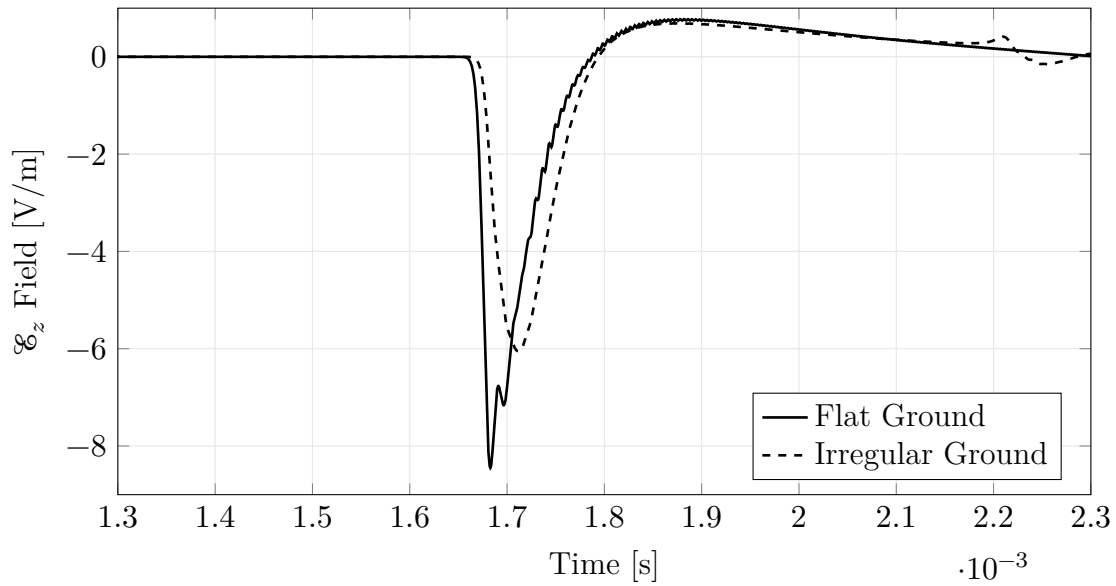


Figure 3.16: Electric field intensity at 500 km from a lightning discharge. Difference between propagation over flat ground and over relief profile: Case P_3 . Source wavelength $\lambda \approx 5000$ m.

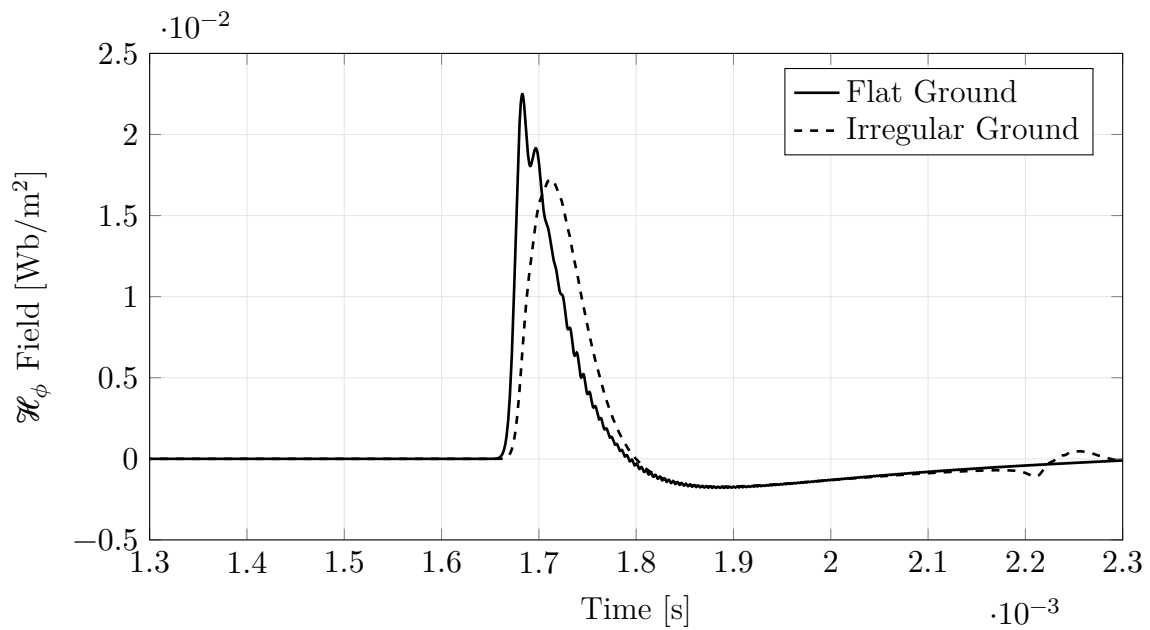


Figure 3.17: Magnetic field intensity at 500 km from a lightning discharge. Difference between propagation over flat ground and over relief profile: Case P_3 . Source wavelength $\lambda \approx 5000$ m.

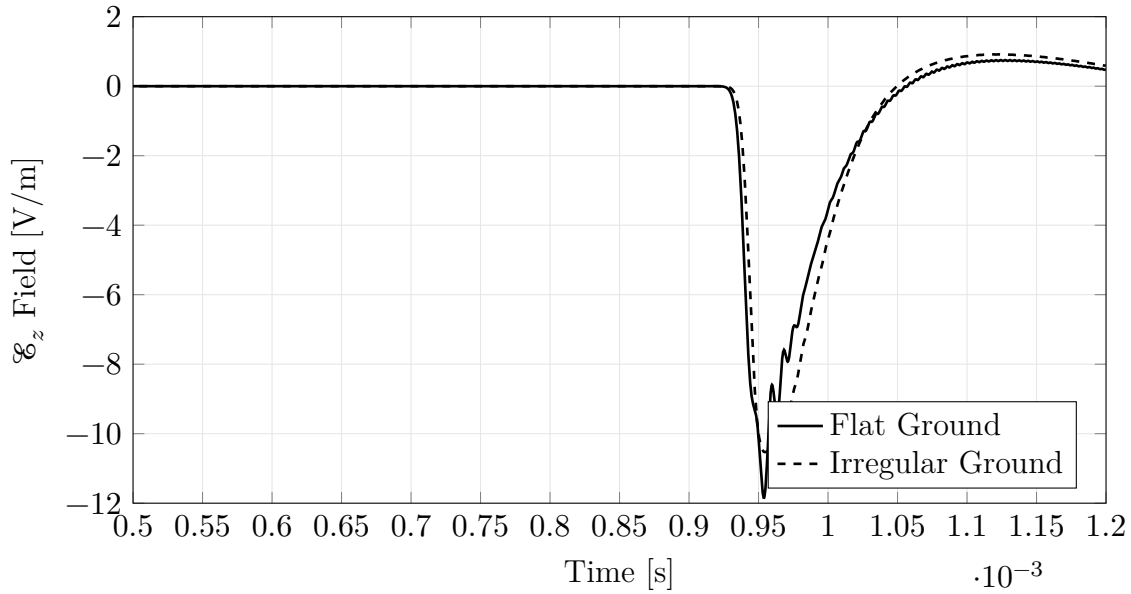


Figure 3.18: Electric field intensity at 280 km from a lightning discharge. Difference between propagation over flat ground and over relief profile: Case P_4 . Source wavelength $\lambda \approx 5000$ m.

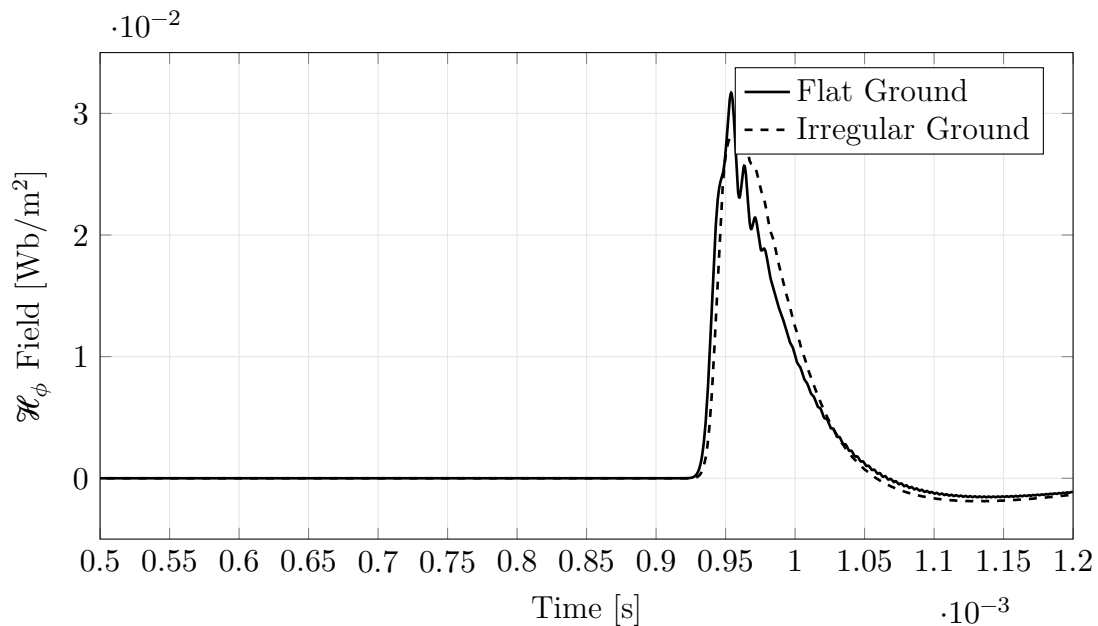


Figure 3.19: Magnetic field intensity at 280 km from a lightning discharge. Difference between propagation over flat ground and over relief profile: Case P_4 . Source wavelength $\lambda \approx 5000$ m.

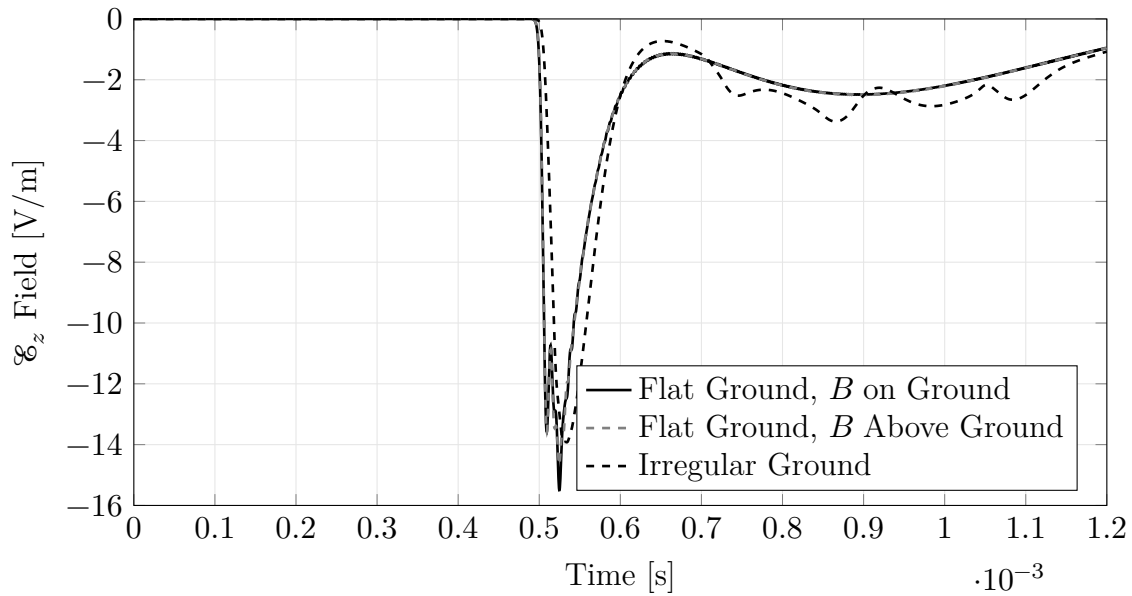


Figure 3.20: Electric field intensity at 150 km from a lightning discharge. Difference between propagation over flat ground and over relief profile: Case P_5 . Source wavelength $\lambda \approx 5000$ m.

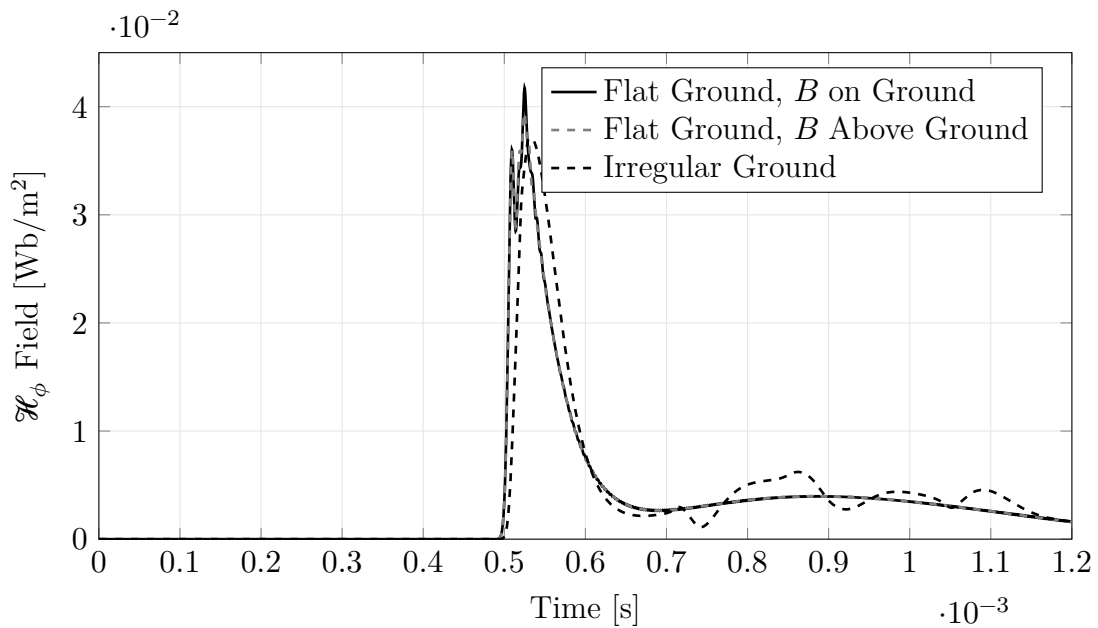


Figure 3.21: Magnetic field intensity at 150 km from a lightning discharge. Difference between propagation over flat ground and over relief profile: Case P_5 . Source wavelength $\lambda \approx 5000$ m.

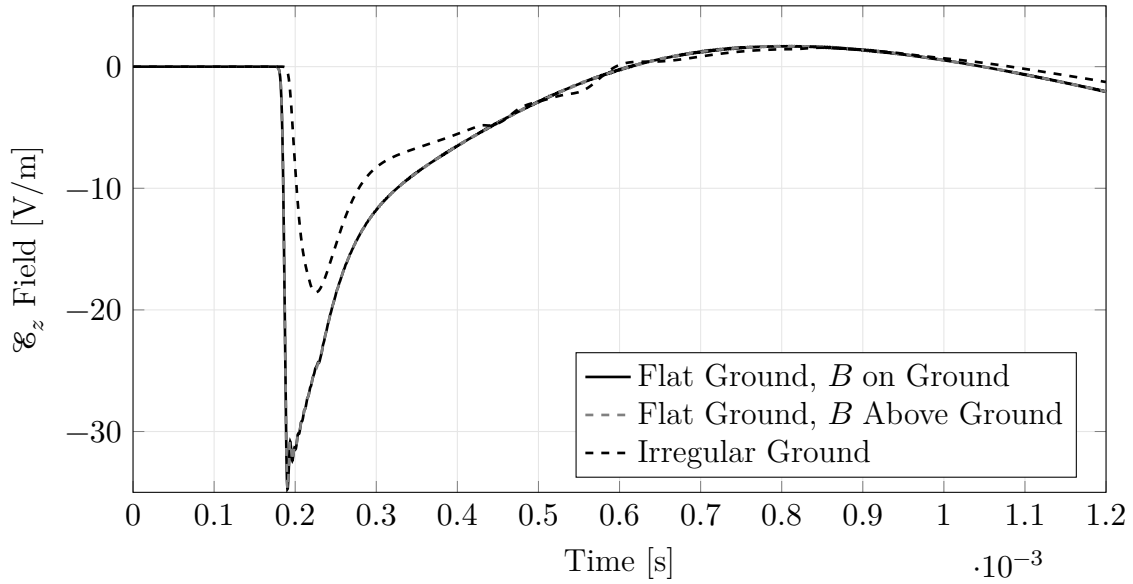


Figure 3.22: Electric field intensity at 55 km from a lightning discharge. Difference between propagation over flat ground and over relief profile: Case P_6 . Source wavelength $\lambda \approx 5000$ m.

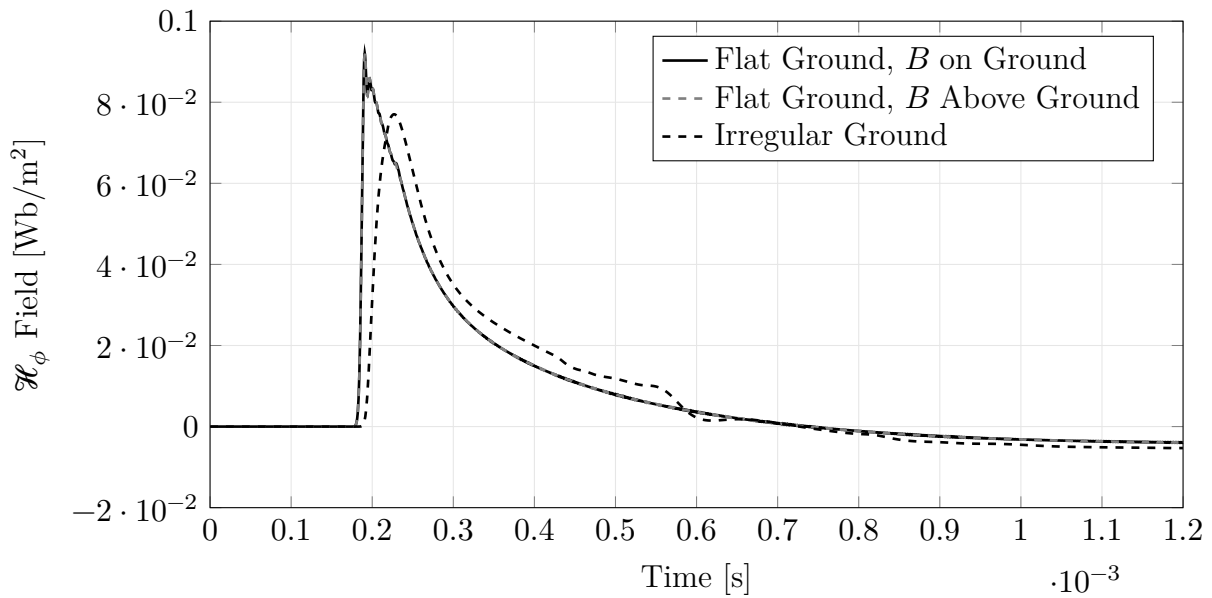


Figure 3.23: Magnetic field intensity at 55 km from a lightning discharge. Difference between propagation over flat ground and over relief profile: Case P_6 . Source wavelength $\lambda \approx 5000$ m.

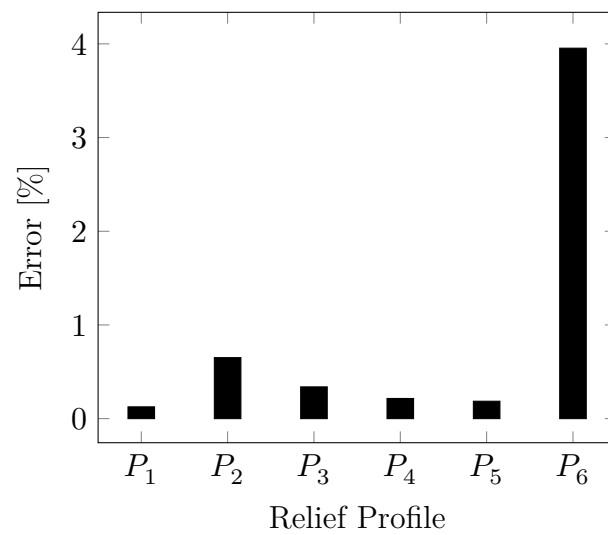


Figure 3.24: Absolute error in the onset time due to propagation effects of different relief profiles.

Chapter 4

Discussion

This chapter is an academic discussion of the results presented in Chapter 3, and its significance in the light of the existing theory in the state of the art literature. The chapter is divided itself into several sections that present first the interpretation of the results; then, the weaknesses of the model developed and a discussion of the possible inconsistent results; finally, the contributions of the work are summarized, further studies and approaches are suggested, and a summary and main conclusions of the whole work are given.

4.1 Interpretation of Results

This section presents the interpretation of the results in the same order that they are shown in Chapter 3. First, the numerical validation of the model, then the simulations for propagation effects, and finally the evaluation of the onset time obtained with the different cases of propagation.

4.1.1 Numerical Validation of the Model

Comparison with Canonical Model

The first validation strategy was to compare the results of the FDTD model developed with those of the canonical model presented by Uman et al. (1975). The results are shown

in Figures 3.1 and 3.2. As it is shown, they are in good agreement. There are however two particular differences: the presence of high frequency oscillations in the FDTD model developed and a difference of about 1% in the magnitude of the electric field only. An explanation of these is given next.

The presence of the high frequency oscillations is explained by the fact that the current source used by Uman et al. (1975) was a piecewise function that has a very sharp peak. This causes the waveform to have very high frequencies along its frequency spectrum. In fact, when this waveform was analysed in order to find its shortest wavelength, it was about $\lambda \approx 1000$ m. In order to eliminate these very high frequency components of the results, a very short length of the Yee cells would have to be used. Of course this is not practical, because it would require prohibitive amounts of computer RAM. This argument is further demonstrated in the next validation strategy, where the source waveform was a softer one and the high frequency components disappeared from the plots (see Figure 3.4).

Now, the difference of about 1% in the electric field amplitude is explained by the fact that the FDTD model needs the use of absorbing boundary conditions in order to truncate the simulation space. For the case of the simulations carried out in this thesis, all the electric field positions were along the borders of the simulation space. Consequently and according to the Yee algorithm, all the magnetic field positions were inside the simulation space. This means that the boundary conditions were only enforced to the electric field components along the boundaries. This is the reason why the magnetic field simulated seems to follow the structure of the canonical model almost perfectly.

Given the above explanations, it was concluded that the FDTD model developed during the development of this thesis is correct and can be used to obtain further results.

Validation of the Obstacle Effect

This second strategy of validation was to show that the model actually reproduced the effect of obstacles in the propagation path. In order to do this, a rectangular obstacle was placed in the simulation space and its altitude was the only parameter that changed

in the simulations for this part. The results are shown in Figures 3.4 and 3.5. It is very clear from these figures that the obstacle has an important effect on the propagation of the waves. Both the electric and magnetic field peaks are reduced as the wave travels from the source to an observation point beyond the obstacle. Also, the waveform is modified at an important extent.

There is another important aspect from these simulations, and it is the fact that the source waveform used here had a wavelength of about $\lambda \approx 5000$ m. That is the reason why the obstacle height was varied to 1 km, 4 km, and 8 km; this values correspond to 0.2, 0.8, and 1.6 times the source wavelength. I want to emphasize this fact because the discussion about the effects of mountains—or any obstacle in general—on the propagation of waves, can only be made in terms of wavelengths comparison. For the case of Figures 3.4 and 3.5, it is clear that the higher the obstacle, the more important its effect on the propagation. By looking at Figure 3.4 one can see, for example, a reduction of about 60% in the peak value of the electric field when the obstacle height is about 1.6 times the wavelength. Of course this relationship has no to be linear, but it gives a number to think of in terms of wavelengths.

As a final note here, the source wavelength used in the simulations that followed this part were made by using the source waveform of the same $\lambda \approx 5000$ m. This may seem contradictory at this point, but the reason was that simulating a source waveform of $\lambda \approx 1000$ m was impractical. The reasons being, again, the fact that there is a limitation in computer RAM; more importantly a limitation when the propagation distances used in this thesis were in the order of hundreds of kilometres.

4.1.2 Numerical Experiments for Propagation Effects

The numerical experiments shown in this part of the results (Chapter 3) were developed in order to achieve the second specific objective of the work. These results are then part of the answer to the research question stated at the beginning in Chapter 1. Before giving the answer to this part of the research question, a discussion of the main findings will be presented.

Source Wavelength-Obstacle Height Relationship

The simulations of this part were made in order to further validate the fact that the present discussion has to be given in terms of wavelengths. The results shown by Figures 3.6 and 3.7 show the effect that the same obstacle has on two sources of different wavelengths. One of the sources has a $\lambda \approx 5000$ m and the other one has $\lambda \approx 790$ m. The obstacle is 4000 m height. There are high frequency components in the plot for the 790 m-wavelength signal, but that is due to the reasons already explained.

As an example, Table 4.1 summarizes the effect that the obstacle has on the peak electric fields, in terms of the source wavelength. The wavelength is directly related to the risetime of the channel base current. Then, it will vary for every event, because lightning is a statistical phenomenon.

Table 4.1: Effect of Obstacle Height on Electric Field in Terms of Source Wavelengths

λ_s [m]	Obstacle [m]	\mathcal{E}_z Peak 1 [V/m]	\mathcal{E}_z Peak 2 [V/m]	Reduction [%]
5000	$0.8 \times \lambda_s$	24	18.74	22
790	$5.1 \times \lambda_s$	25.5	14.5	43

It is concluded then, that each particular lightning discharge will produce electromagnetic waves in a different portion of the LF and VLF ranges, and then the effect of irregular terrain on the propagation of such waves will have to be modelled by considering a stochastic approach.

Effect of Ionospheric Reflections

One of the questions that emerged during the development of this thesis, was whether the effect of the ionosphere would play an important role in the propagation, given also the combined effects of the obstacles. To be more specific, given that the obstacles could reflect portions of the incident electromagnetic wave, those reflections could be in a direction towards the ionosphere, which in turn would also reflect them back. In order to answer this question, different wavelength sources were simulated in the presence of very big obstacles (big in terms of source wavelengths) and the reflections from the ionosphere

were considered.

The results shown in Figures 3.8 and 3.9 are consistent with the results presented in (Thang et al., 2016) and (Thang et al., 2017), where the authors showed that the effect of the ionosphere is to produce skywaves that appear at the observation point and sum up with the ground wave. In the results shown by Figures 3.8 and 3.9, the magnitude of the skywaves is greater than the magnitude of the skywaves presented in (Thang et al., 2016) and (Thang et al., 2017), but this is due to the fact that in this work the ionosphere was modelled also like a perfect electric conductor, so no part of the incident wave is transmitted.

Finally, Figures 3.10 and 3.11 show the ground waves and skywaves that are predicted by the model when the propagation of two sources—wavelengths of 5000 m and 790 m—is considered also in the presence of an obstacle of 4000 m of altitude. The results show that no additional reflections are made towards the ionosphere from the obstacles, as the only skywaves that are present are the same ones given by the flat ground propagation scenario. Also, the shortest wavelength source is not affected in this particular way by the presence of the ionosphere.

Then, in order to answer this question, it can be said that the presence of the ionosphere is not needed to be taken into account when the interest is to predict the effect of obstacles on the ground wave propagation. This is the case for lightning localization, where the algorithms work with the waveform that arrives first, which is precisely the ground wave. Because of this reason, the ionosphere was not considered in the simulations that followed.

Effects of Propagation Over Relief Profiles in Colombia

The aim of this part was to test the validity of the conclusions given above for more realistic cases of propagation. The six relief profiles chosen over the Colombian territory helped to answer the question of how was the propagation over mountainous terrains of important altitude. The results shown by Figures from 3.12 to 3.23 are among the most important ones of this thesis.

In the first place it is important to say that these results are in agreement with previous

analyses reported in the scientific literature. Specially, the results shown by (Li, Azadifar, Rachidi, Rubinstein, Diendorfer, et al., 2016), and (Li, Azadifar, Rachidi, Rubinstein, Paolone, et al., 2016). The mentioned authors have reported similar results in terms of time delays, waveform and amplitude changes for different idealistic and real propagation path geometries. It can then be said that the results obtained in this thesis, further validate, complement and expand those obtained by previous studies.

As stated before, the propagation effects will be different depending on the source wavelength and the size of the obstacle. This means that every particular case has to be evaluated and simulated. But in general, it is being shown that the propagation model has to consider the terrain elevation if a precise model is required. There are dramatic changes undergone by the waves, as for example the ones shown by Figures 3.14 or 3.22. It is also important to notice that these propagation effects would be even more notable for a source waveform of shorter wavelength.

As a final conclusion of this part, the electromagnetic waves produced during the return stroke part of the lightning discharge have frequencies that belong to the LF and VLF part of the electromagnetic spectrum, thus having kilometric wavelengths which are comparable in size to the obstacles that could appear in the propagation path when these phenomena occur over regions with important mountain ranges, as it is the case of Colombia. Then, if a precise prediction is to be made, the propagation effects produced by such obstacles have to be taken into account. For the application to LLS, this is specially important, as these systems make their predictions according to the signal that they measure.

4.1.3 Evaluation of the Onset Time for the Relief Profiles Examined

The final specific objective of this thesis was fulfilled by evaluating the effect of irregular ground on the location accuracy of the time-of-arrival technique. Given that the accuracy of this technique is directly related to the onset times of the electromagnetic wave to the sensors, those times were measured for each of the six cases of relief profiles. After that, the onset times corresponding to flat ground propagation and irregular ground propagation

were compared for each of the six reliefs. It was found that the absolute errors were actually very small. As it can be appreciated in Figure 3.24, all the absolute errors were below 4%; in fact, all of them were below 1% with exception of Case P_6 .

Now comes the following question: why if the propagation is affected by the ground irregularities at an important extent, the onset times present small errors when the real propagation path is considered? The answer is that the onset time greatly depends on the risetime of the electromagnetic wave, and ground irregularities do not affect this parameter in an appreciable way as the wave propagates. See for example Case P_2 , which has one of the bigger changes in the wave amplitude due to the propagation effects. Even though, the risetime seems not to be affected by the propagation effects and then, the onset time error is under 1%.

These results suggest that the location accuracy of lightning locating systems based on the time-of-arrival technique is not affected by propagation effects due to terrain irregularities in an important manner. The reason being that in the presence of perfectly conducting ground, no part of the waves is transmitted but all the waves is reflected and then, the characteristic aspects of the waves do not change as to have a significant effect on the slope that defines the onset times. However, this conclusion needs further consideration due to the fact that the parameter evaluated was the onset time, but the actual localization of the discharges might be affected at a greater extent.

4.2 Weaknesses

During the development of the work there were not any inconsistent or unexpected results; in fact, all of them were in perfect agreement with previous findings of other authors. On the other hand, the model developed here has some limitations. They are explained to continue.

In the first place, the two-dimensional approximation considered does not allow to model completely the propagation over a real three-dimensional terrain. This is a limitation of the model, but it was not possible to consider the three-dimensional version because

the FDTD method requires to store the whole space of simulation at the beginning of the algorithm.

Another important limitation is not due to the model itself, but due to the hardware available for the simulations. It would be interesting to develop simulations of lightning sources with shorter wavelengths by means of online services that are available nowadays. These online services can provide hardware capacities of about 1 or 2 TB of computer RAM.

4.3 Contribution

The contributions of this thesis are mainly theoretical. First of all, a numerical propagation model was developed by making a two-dimensional approximation to Maxwell's equations. The model is able to predict the propagation of lightning electromagnetic waves when considering propagation in free space, in the Earth-Ionosphere waveguide, over flat ground, and over irregular ground of any form.

The results contributed to show that the effect of the ionosphere in the propagation model do not have to be taken into account as it only produces skywaves that are not needed by the lightning locating systems. However, if a precise modelling of the propagation in the Earth-Ionosphere waveguide is needed, the model is able to include this effect for any model of conductivity of the atmosphere.

Another important contribution is the knowledge that the propagation effects due to propagation over irregular ground, greatly depend on the wavelengths involved. For the case of lightning electromagnetic pulse propagation over mountains, the wavelengths of the source and obstacles are comparable and then, these effects are considerable.

Finally, the thesis contributed to show that the propagation effects due to irregular ground (without considering the ground conductivity) seem to be of not considerable interest in regards to the location accuracy of LLS that use the ToA technique. Furthermore, according to the results, it seems that the detection efficiency and the lightning parameters calculated by means of LLS are more dependent on the effects of propagation due to

irregular ground alone.

4.4 Further Studies

During the development of this work, several other questions arose. Also, some suggestions for future work are important to mention. First, the questions that would be important to answer given the results obtained are:

1. How is the detection efficiency of lightning locating systems affected by the propagation effects caused by terrain irregularities?
2. How are the lightning parameters calculated with lightning locating systems information affected by the propagation effects of terrain irregularity?

And finally, some suggestions for future work:

1. Experimental validation of the results obtained would be very important. These experimental measurements are being carried out right now in Colombia and they will be used to obtain further conclusions.
2. Including a stochastic model of the lightning parameters and running several simulations in order to extract patterns of propagation effects is another important work to be done. It would allow to characterize the propagation effects of a lightning locating system over a particular region and to have better results of lightning detection and localization.
3. To test the effect of different absorbing boundary conditions would be important when assessing the precision of the results obtained by the present model.
4. The use of online services for more advanced processing power is another important work that will be carried out in the near future.
5. A design of experiments would be useful as well in order to find relationships between the different variables of interest. For example, the relationship between obstacle height, source wavelength and peak value modification.

6. Information of terrain shape (irregularities) might be contained in the field waveforms observed at a certain point.
7. The use of other types of lightning return-stroke waveforms could improve the performance of the numerical simulation model. For example, the use of only Heidler-type waveform for the channel base current is suggested.
8. Analysis of propagation effects, and specially the effect of the ionosphere in the modelling of intra-cloud lightning generated fields could also be important.
9. The implementation of the time-of-arrival algorithm to further validate the conclusion relative to the effect of ground irregularities on the location accuracy is very important. It will allow to see the localization errors in meters and make an assessment of the real effect of these kind of propagation effects.
10. The development of a time-of-arrival algorithm that includes information of the skywaves for the improvement of location accuracies is another promising application.
11. The use of the present model for optimization of lightning sensors positioning over mountainous regions would be useful in order to reduce the errors in lightning parameters estimation, and location accuracy due to propagation effects of terrain irregularities.

4.5 Summary and Conclusions

This research question of this dissertation was about the propagation effects of irregular ground on the propagation of lightning-generated electromagnetic waves. In order to answer the questions, a FDTD numerical model was developed from Maxwell's equations in the cylindrical coordinate system.

The results showed that the propagation over irregular ground has a significant effect on the propagation phenomenon, specially if the source wavelength is short as compared to the size of the obstacles. It was also shown that although the propagation effects are

important, they affect the onset time that the sensors measure to a limited extent. Then, there is the suggestion that the propagation effects due to irregular ground are not of considerable importance for the location accuracy of LLS.

However, the results also showed that the propagation effects due to terrain irregularities alone (without considering the conductivity of the ground) might be more important in regards to the detection efficiency and to the calculation of lightning parameters by means of information obtained from LLS. This final conclusion is a change of direction with respect to what was originally thought at the beginning of the research, when it was believed that the propagation effects of terrain irregularities would affect the location accuracies very strongly.

If the conclusion of the whole study had to be said very shortly, it would have to be remarked that the presence of the obstacles examined (irregular ground) has an important effect on the magnitudes of the field signals observed: there is attenuation and there is also increase of the peak values as compared to the propagation over flat ground. The reason for this being due to two main phenomena: constructive interference (increase of the peak value) and reflection of part of the waves over the obstacles (peak attenuation). On the other hand, when the propagation effects of irregularities were considered alone, the derivatives of the field signals did not change considerably due to the fact that the propagation was modelled over perfectly conducting ground.

Appendix A

Classical Electrodynamics

A.1 Maxwell's Equations

Maxwell's equations are a set of four coupled partial differential equations that describe all—at least the classical—electromagnetic phenomena. The basic laws of nature associated with this set of equations were established mostly experimentally by several scientists during the nineteenth century, mainly Coulomb's law (associated to Equations (A.4) or (A.8)); Ampère's law (associated to Equations (A.2) or (A.6)) and Faraday's law (associated to Equations (A.1) or (A.5)). These basic laws were the starting point from which James Clerk Maxwell departed to develop the final form of what is known as Maxwell's equations. In part III (entitled “General Equations of the Electromagnetic Field”) of his classic paper (Maxwell, 1865), Maxwell formulated a set of twenty simultaneous equations with 20 variables. In his work Maxwell imagined and introduced the concept of displacement current, inferred the electromagnetic nature of light and predicted the existence of electromagnetic waves that can propagate through empty space. Later, in 1887, Heinrich Hertz confirmed experimentally Maxwell's hypotheses (Hertz, 1888). According to historian Hunt (2005), it was not until 1884 that Oliver Heaviside, concurrently with Josiah Willard Gibbs and Heinrich Hertz, grouped the twenty original Maxwell's equations into a set of only four, which were obtained by using modern vector notation.

Maxwell's equations are based on experimentally established facts. The validity of

these equations is based on their accuracy in describing electromagnetic phenomena associated with physical experiments in a wide range of the electromagnetic spectrum. The description to follow is pretty concise to the needs of this thesis.

A.2 Integral Form of Maxwell's Equations

The physical meaning of Maxwell's equations is more easily understood from their integral form. They are listed below:

$$\oint_{\mathcal{L}} \overline{\mathcal{E}}(\bar{r}, t) \cdot d\bar{\ell} = -\frac{\partial}{\partial t} \iint_{\mathcal{S}} \overline{\mathcal{B}}(\bar{r}, t) \cdot d\bar{s}, \quad (\text{A.1})$$

$$\oint_{\mathcal{L}} \overline{\mathcal{H}}(\bar{r}, t) \cdot d\bar{\ell} = \iint_{\mathcal{S}} \overline{\mathcal{J}}(\bar{r}, t) \cdot d\bar{s} + \frac{\partial}{\partial t} \iint_{\mathcal{S}} \overline{\mathcal{D}}(\bar{r}, t) \cdot d\bar{s}, \quad (\text{A.2})$$

$$\oiint_{\mathcal{S}} \overline{\mathcal{B}}(\bar{r}, t) \cdot d\bar{s} = 0, \quad (\text{A.3})$$

$$\oiint_{\mathcal{S}} \overline{\mathcal{D}}(\bar{r}, t) \cdot d\bar{s} = \iiint_{\mathcal{V}} \rho(\bar{r}, t) d\mathbf{v}. \quad (\text{A.4})$$

Where $\overline{\mathcal{E}}(\bar{r}, t)$, $\overline{\mathcal{B}}(\bar{r}, t)$, $\overline{\mathcal{H}}(\bar{r}, t)$, $\overline{\mathcal{D}}(\bar{r}, t)$, $\overline{\mathcal{J}}(\bar{r}, t)$ and $\rho(\bar{r}, t)$ are real functions of space (position) and time.

$\overline{\mathcal{E}}(\bar{r}, t)$ = electric field strength (volts/m).

$\overline{\mathcal{B}}(\bar{r}, t)$ = magnetic flux density (webers/m²).

$\overline{\mathcal{H}}(\bar{r}, t)$ = magnetic flux strength (amperes/m).

$\overline{\mathcal{D}}(\bar{r}, t)$ = electric displacement (coulombs/m²).

$\overline{\mathcal{J}}(\bar{r}, t)$ = electric current density (amperes/m²).

$\rho(\bar{r}, t)$ = electric charge density (coulombs/m³)

Equation (A.1) is Faraday's law of induction, which states that time-changing magnetic flux induces an electromotive force. In this equation the line integral showing a counterclockwise rotation means that it has to be made consistent with the direction of

the differential surface element $d\bar{s}$ in accordance with the right-hand rule. Equation (A.2) is the generalized Ampère's circuit law, which states that magnetic fields can be produced by either conduction currents ($\bar{\mathcal{J}}(\bar{r}, t)$) or by displacement currents (time-changing electric fields $\frac{\partial}{\partial t}\bar{\mathcal{D}}(\bar{r}, t)$). Equations (A.3) and (A.4) are Gauss's laws for magnetic and electric fields, respectively. Gauss's law for the magnetic field states that there are no magnetic charges (magnetic monopoles), and Gauss's law for the electric field states that the total electric flux through a closed surface equals the total electric charge enclosed by that surface; it is also reminiscent of Coulomb's law, stating that electric charges attract or repel one another with a force that is inversely proportional to the squared of the separation distance between them. In all the equations \mathcal{S} is the surface enclosing the volume \mathcal{V} and \mathcal{L} is the contour enclosing the surface \mathcal{S} .

A.3 Differential Form of Maxwell's Equations

By using either the Stokes's or the divergence theorem, all of the Equations (A.1)–(A.4) can be expressed in differential form:

$$\nabla \times \bar{\mathcal{E}}(\bar{r}, t) + \frac{\partial}{\partial t}\bar{\mathcal{B}}(\bar{r}, t) = 0, \quad (\text{A.5})$$

$$\nabla \times \bar{\mathcal{H}}(\bar{r}, t) - \frac{\partial}{\partial t}\bar{\mathcal{D}}(\bar{r}, t) = \bar{\mathcal{J}}(\bar{r}, t), \quad (\text{A.6})$$

$$\nabla \cdot \bar{\mathcal{B}}(\bar{r}, t) = 0, \quad (\text{A.7})$$

$$\nabla \cdot \bar{\mathcal{D}}(\bar{r}, t) = \rho(\bar{r}, t). \quad (\text{A.8})$$

These are the basic equations primarily used in this thesis.

Appendix B

Basics of the FDTD Method

This chapter is a quick guide to the FDTD numerical method. It is intended to be a self-contained explanation of the Yee algorithm, and its implementation for the solution of a two-dimensional propagation example. As such, the chapter is strongly based on the paper written by Yee (1966).

B.1 Finite Difference Schemes

The FDTD numerical technique is mainly a methodology for the discretization of the continuous physical space and time. The solution of Maxwell's equations in this discrete domain implies the approximation of the exact partial derivatives with a finite difference scheme. The different schemes available can be obtained from the Taylor series expansion of a general function $f(x)$ about $x = a$; the Taylor series being defined by the following well-known expression:

$$f(x) = \sum_{m=0}^{\infty} \frac{f^{(m)}(a)}{m!} (x - a)^m. \quad (\text{B.1})$$

If the Taylor series expansion is used to expand $f(x)$ about $x = x_0$, the result is:

$$f(x) = f(x_0) + (x - x_0)f'(x_0) + \frac{1}{2!}(x - x_0)^2 f''(x_0) + \frac{1}{3!}(x - x_0)^3 f'''(x_0) + \dots \quad (\text{B.2})$$

which is the expression for function $f(x)$ in the vicinity of $x = x_0$.

A common way to obtain expressions for different finite-difference schemes is to evaluate Equation (B.2) in the points $x = (x_0 + \Delta x)$ and $x = (x_0 - \Delta x)$:

$$f(x_0 + \Delta x) = f(x_0) + (\Delta x)f'(x_0) + \frac{1}{2!}(\Delta x)^2 f''(x_0) + \frac{1}{3!}(\Delta x)^3 f'''(x_0) + \dots \quad (\text{B.3})$$

and

$$f(x_0 - \Delta x) = f(x_0) - (\Delta x)f'(x_0) + \frac{1}{2!}(\Delta x)^2 f''(x_0) - \frac{1}{3!}(\Delta x)^3 f'''(x_0) + \dots \quad (\text{B.4})$$

Rearranging these equations, two expressions for $f'(x)$ are obtained:

$$f'(x_0) = \frac{f(x_0 + \Delta x) - f(x_0)}{\Delta x} - \frac{1}{2!}(\Delta x)f''(x_0) - \frac{1}{3!}(\Delta x)^2 f'''(x_0) - \dots \quad (\text{B.5})$$

and

$$f'(x_0) = \frac{f(x_0) - f(x_0 - \Delta x)}{\Delta x} + \frac{1}{2!}(\Delta x)f''(x_0) - \frac{1}{3!}(\Delta x)^2 f'''(x_0) + \dots \quad (\text{B.6})$$

Another common way to obtain an expression for $f'(x_0)$ is by subtracting Equation (B.4) from Equation (B.3) and rearranging to obtain:

$$f'(x_0) = \frac{f(x_0 + \Delta x) - f(x_0 - \Delta x)}{2\Delta x} - \frac{1}{3!}(\Delta x)^2 f'''(x_0) - \frac{1}{5!}(\Delta x)^4 f^{(5)}(x_0) - \dots \quad (\text{B.7})$$

The expressions given by Equations (B.5), (B.6), and (B.7) for the first derivative of a general function $f(x)$ about a point $x = x_0$ can be written in terms of the error that would result if the expressions were truncated to their first terms:

$$f'(x_0) = \frac{f(x_0 + \Delta x) - f(x_0)}{\Delta x} + O(\Delta x), \quad (\text{B.8})$$

$$f'(x_0) = \frac{f(x_0) - f(x_0 - \Delta x)}{\Delta x} + O(\Delta x), \quad (\text{B.9})$$

and

$$f'(x_0) = \frac{f(x_0 + \Delta x) - f(x_0 - \Delta x)}{2\Delta x} + O((\Delta x)^2) \quad (\text{B.10})$$

The order of Δx in the most significant term of the error $O(\Delta x)$ of Equations (B.8) and (B.9) is one; therefore, the approximations obtained by truncating these equations to their first term is said to be *first-order accurate*. On the other hand, when the same analysis is carried out on the error $O((\Delta x)^2)$ of Equation (B.10), the approximation happens to be *second-order accurate*.

Function $f(x)$ can be further generalized to a three-variable function, and its derivative at a general point (x, y, z) , with respect to x can be approximated by different formulas:

$$\left. \frac{\partial f(x, y, z)}{\partial x} \right|_{i, j, k} \approx \frac{f|_{i+1, j, k} - f|_{i, j, k}}{\Delta x} \quad (\text{B.11})$$

$$\left. \frac{\partial f(x, y, z)}{\partial x} \right|_{i, j, k} \approx \frac{f|_{i, j, k} - f|_{i-1, j, k}}{\Delta x} \quad (\text{B.12})$$

$$\left. \frac{\partial f(x, y, z)}{\partial x} \right|_{i, j, k} \approx \frac{f|_{i+1, j, k} - f|_{i-1, j, k}}{2\Delta x} \quad (\text{B.13})$$

In these equations, a convenient notation has been used: the three-dimensional space was divided into several cubes of equal sides Δx , Δy , and Δz ; then, the coordinates of a point (x, y, z) are given by $x = i\Delta x$, $y = j\Delta y$, and $z = k\Delta z$. Where variables i , j , and k are integer numbers. This means that $f(x, y, z)$ is written as $f(i\Delta x, j\Delta y, k\Delta z)$, or as $f|_{i, j, k}$ for short.

It is worth noticing that function $f(x, y, z)$ can only be evaluated at discrete points or nodes when the above notation is used. Furthermore, Equations (B.11), (B.12), and (B.13) are called forward difference, backward difference, and central difference schemes; respectively. As stated before, the forward difference and backward difference schemes are first-order accurate, and the central difference scheme is second order accurate. Thus, the last one is preferred for better accuracy.

B.2 The Yee Algorithm

The Yee algorithm was introduced in 1966 by Kane S. Yee (Yee, 1966). In this algorithm, the Maxwell's *partial differential equations* are replaced by a set of *finite difference equations*. Additionally, the Yee algorithm uses the central difference scheme for the approximation of the two Maxwell's curl equations (Equations (A.5) and (A.6)). The reason why the Yee algorithm does not need the divergence equations, is because they can be satisfied by the developed FDTD updating equations from the curl equations.

Before discretizing Maxwell's vector equations, they need to be expressed in scalar form. In the Cartesian coordinate system, an arbitrary vector field has three space components, which are denoted: $\vec{\mathcal{A}} = \mathcal{A}_x \hat{x} + \mathcal{A}_y \hat{y} + \mathcal{A}_z \hat{z}$. Then, by taking the curl of Equations (A.5) and (A.6), and after separating each of their field components, the following set of scalar equations is obtained:

$$\frac{\partial \mathcal{B}_x}{\partial t} = \frac{\partial \mathcal{E}_y}{\partial z} - \frac{\partial \mathcal{E}_z}{\partial y}, \quad (\text{B.14a})$$

$$\frac{\partial \mathcal{B}_y}{\partial t} = \frac{\partial \mathcal{E}_z}{\partial x} - \frac{\partial \mathcal{E}_x}{\partial z}, \quad (\text{B.14b})$$

$$\frac{\partial \mathcal{B}_z}{\partial t} = \frac{\partial \mathcal{E}_x}{\partial y} - \frac{\partial \mathcal{E}_y}{\partial x}, \quad (\text{B.14c})$$

$$\frac{\partial \mathcal{D}_x}{\partial t} = \frac{\partial \mathcal{H}_z}{\partial y} - \frac{\partial \mathcal{H}_y}{\partial z} - \mathcal{J}_x, \quad (\text{B.14d})$$

$$\frac{\partial \mathcal{D}_y}{\partial t} = \frac{\partial \mathcal{H}_x}{\partial z} - \frac{\partial \mathcal{H}_z}{\partial x} - \mathcal{J}_y, \quad (\text{B.14e})$$

$$\frac{\partial \mathcal{D}_z}{\partial t} = \frac{\partial \mathcal{H}_y}{\partial x} - \frac{\partial \mathcal{H}_x}{\partial y} - \mathcal{J}_z. \quad (\text{B.14f})$$

Now, by means of the expression for the central difference approximation given by Equation (B.13) the space and time derivatives of any scalar field can be approximated

as:

$$\left. \frac{\partial F}{\partial x} \right|_{i,j,k}^n \approx \frac{F|_{i+\frac{1}{2},j,k}^n - F|_{i-\frac{1}{2},j,k}^n}{\delta}, \quad (\text{B.15a})$$

$$\left. \frac{\partial F}{\partial y} \right|_{i,j,k}^n \approx \frac{F|_{i,j+\frac{1}{2},k}^n - F|_{i,j-\frac{1}{2},k}^n}{\delta}, \quad (\text{B.15b})$$

$$\left. \frac{\partial F}{\partial z} \right|_{i,j,k}^n \approx \frac{F|_{i,j,k+\frac{1}{2}}^n - F|_{i,j,k-\frac{1}{2}}^n}{\delta}, \quad (\text{B.15c})$$

$$\left. \frac{\partial F}{\partial t} \right|_{i,j,k}^n \approx \frac{F|_{i,j,k}^{n+\frac{1}{2}} - F|_{i,j,k}^{n-\frac{1}{2}}}{\Delta t}. \quad (\text{B.15d})$$

Where F is a general scalar function representing either the electric or magnetic field, δ is the space increment (assumed to be the same along the three Cartesian coordinate axes), and Δt is the time increment.

Equation (B.15) was written for a general scalar field F , which is supposed to be defined at space points with integer and half-integer indexes: (i, j, k) , and $(i \pm 1/2, j \pm 1/2, k \pm 1/2)$. For the particular case of the scalar electric and magnetic field components, this is not applicable. Therefore, before applying Equation (B.15) to make the discretization of Equation (B.14), it is important to identify the points at which Yee positions the components of $\vec{\mathcal{E}}(\vec{r}, t)$ and $\vec{\mathcal{B}}(\vec{r}, t)$. The positions at which the field components are to be evaluated/stored are shown in Figure B.1. This particular choice of the field points is appropriate for forming a set of difference equations that can be solved, and the solution will satisfy the boundary condition of perfectly conducting surfaces (Yee, 1966), i.e., the tangential components of the electric field and the normal component of the magnetic field vanish on the surface.

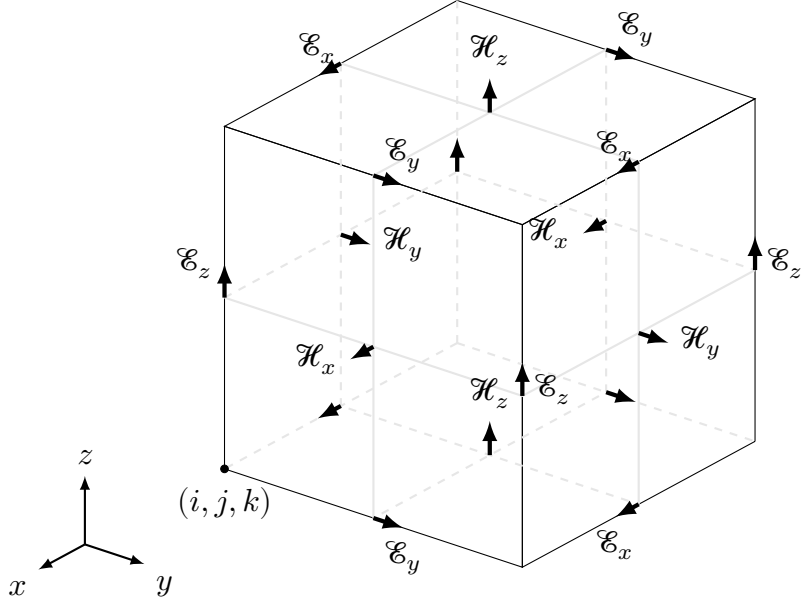


Figure B.1: Positions of the electric and magnetic field components in a unit cell of the Yee's grid in Cartesian coordinates.

B.3 Discretization of Maxwell's Equations

Finally, by evaluating the time derivatives of the electric and magnetic fields at alternate half-integer time steps and with the above considerations, the finite difference approximation of Equation (B.14) is obtained by following this example procedure: Equation (B.14a) needs the approximation of the terms $\frac{\partial \mathcal{B}_x}{\partial t}$, $\frac{\partial \mathcal{E}_y}{\partial z}$, and $\frac{\partial \mathcal{E}_z}{\partial y}$. This can be written as presented below.

$$\begin{aligned} \frac{\partial \mathcal{B}_x}{\partial t} &\approx \frac{\mathcal{B}_x|_{i,j+\frac{1}{2},k+\frac{1}{2}}^{n+\frac{1}{2}} - \mathcal{B}_x|_{i,j+\frac{1}{2},k+\frac{1}{2}}^{n-\frac{1}{2}}}{\Delta t}, \\ \frac{\partial \mathcal{E}_y}{\partial z} &\approx \frac{\mathcal{E}_y|_{i,j+\frac{1}{2},k+1}^n - \mathcal{E}_y|_{i,j+\frac{1}{2},k}^n}{\delta}, \\ \frac{\partial \mathcal{E}_z}{\partial y} &\approx \frac{\mathcal{E}_z|_{i,j+1,k+\frac{1}{2}}^n - \mathcal{E}_z|_{i,j,k+\frac{1}{2}}^n}{\delta}. \end{aligned}$$

After replacing these expressions in Equation (B.14a) and rearranging, $\mathcal{B}_x \Big|_{i,j+\frac{1}{2},k+\frac{1}{2}}^{n+\frac{1}{2}}$ can be written as:

$$\begin{aligned} \mathcal{B}_x \Big|_{i,j+\frac{1}{2},k+\frac{1}{2}}^{n+\frac{1}{2}} &= \mathcal{B}_x \Big|_{i,j+\frac{1}{2},k+\frac{1}{2}}^{n-\frac{1}{2}} + \frac{\Delta t}{\delta} \left[\mathcal{E}_y \Big|_{i,j+\frac{1}{2},k+1}^n - \mathcal{E}_y \Big|_{i,j+\frac{1}{2},k}^n \right. \\ &\quad \left. + \mathcal{E}_z \Big|_{i,j,k+\frac{1}{2}}^n - \mathcal{E}_z \Big|_{i,j+1,k+\frac{1}{2}}^n \right]. \end{aligned} \quad (\text{B.16})$$

In the above equation, the central point in time was chosen to be at n , thus producing magnetic field components evaluated at half-integer time steps and electric field components defined at integer time steps.

The same procedure can be used to obtain the updating equations for the rest of the field components given in Equation (B.14), arriving to the complete set of algebraic equations presented below.

$$\begin{aligned} \mathcal{H}_x \Big|_{i,j+\frac{1}{2},k+\frac{1}{2}}^{n+\frac{1}{2}} &= \mathcal{H}_x \Big|_{i,j+\frac{1}{2},k+\frac{1}{2}}^{n-\frac{1}{2}} + \frac{1}{\mu \Big|_{i,j+\frac{1}{2},k+\frac{1}{2}}} \frac{\Delta t}{\delta} \left[\mathcal{E}_y \Big|_{i,j+\frac{1}{2},k+1}^n - \mathcal{E}_y \Big|_{i,j+\frac{1}{2},k}^n \right. \\ &\quad \left. + \mathcal{E}_z \Big|_{i,j,k+\frac{1}{2}}^n - \mathcal{E}_z \Big|_{i,j+1,k+\frac{1}{2}}^n \right], \end{aligned} \quad (\text{B.17a})$$

$$\begin{aligned} \mathcal{H}_y \Big|_{i+\frac{1}{2},j,k+\frac{1}{2}}^{n+\frac{1}{2}} &= \mathcal{H}_y \Big|_{i+\frac{1}{2},j,k+\frac{1}{2}}^{n-\frac{1}{2}} + \frac{1}{\mu \Big|_{i+\frac{1}{2},j,k+\frac{1}{2}}} \frac{\Delta t}{\delta} \left[\mathcal{E}_z \Big|_{i+1,j,k+\frac{1}{2}}^n - \mathcal{E}_z \Big|_{i,j,k+\frac{1}{2}}^n \right. \\ &\quad \left. + \mathcal{E}_x \Big|_{i+\frac{1}{2},j,k}^n - \mathcal{E}_x \Big|_{i+\frac{1}{2},j,k+1}^n \right], \end{aligned} \quad (\text{B.17b})$$

$$\begin{aligned} \mathcal{H}_z \Big|_{i+\frac{1}{2},j+\frac{1}{2},k}^{n+\frac{1}{2}} &= \mathcal{H}_z \Big|_{i+\frac{1}{2},j+\frac{1}{2},k}^{n-\frac{1}{2}} + \frac{1}{\mu \Big|_{i+\frac{1}{2},j+\frac{1}{2},k}} \frac{\Delta t}{\delta} \left[\mathcal{E}_x \Big|_{i+\frac{1}{2},j+1,k}^n - \mathcal{E}_x \Big|_{i+\frac{1}{2},j,k}^n \right. \\ &\quad \left. + \mathcal{E}_y \Big|_{i,j+\frac{1}{2},k}^n - \mathcal{E}_y \Big|_{i+1,j+\frac{1}{2},k}^n \right], \end{aligned} \quad (\text{B.17c})$$

$$\begin{aligned} \mathcal{E}_x \Big|_{i+\frac{1}{2},j,k}^n &= \mathcal{E}_x \Big|_{i+\frac{1}{2},j,k}^{n-1} + \frac{1}{\epsilon \Big|_{i+\frac{1}{2},j,k}} \frac{\Delta t}{\delta} \left[\mathcal{H}_z \Big|_{i+\frac{1}{2},j+\frac{1}{2},k}^{n-\frac{1}{2}} - \mathcal{H}_z \Big|_{i+\frac{1}{2},j-\frac{1}{2},k}^{n-\frac{1}{2}} \right. \\ &\quad \left. - \mathcal{H}_y \Big|_{i+\frac{1}{2},j,k+\frac{1}{2}}^{n-\frac{1}{2}} + \mathcal{H}_y \Big|_{i+\frac{1}{2},j,k-\frac{1}{2}}^{n-\frac{1}{2}} \right] - \frac{\Delta t}{\epsilon \Big|_{i+\frac{1}{2},j,k}} \mathcal{J}_x \Big|_{i+\frac{1}{2},j,k}^{n-\frac{1}{2}}, \end{aligned} \quad (\text{B.17d})$$

$$\begin{aligned} \mathcal{E}_y \Big|_{i,j+\frac{1}{2},k}^n &= \mathcal{E}_y \Big|_{i,j+\frac{1}{2},k}^{n-1} + \frac{1}{\epsilon \Big|_{i,j+\frac{1}{2},k}} \frac{\Delta t}{\delta} \left[\mathcal{H}_x \Big|_{i,j+\frac{1}{2},k+\frac{1}{2}}^{n-\frac{1}{2}} - \mathcal{H}_x \Big|_{i,j+\frac{1}{2},k-\frac{1}{2}}^{n-\frac{1}{2}} \right. \\ &\quad \left. - \mathcal{H}_z \Big|_{i+\frac{1}{2},j+\frac{1}{2},k}^{n-\frac{1}{2}} + \mathcal{H}_z \Big|_{i-\frac{1}{2},j+\frac{1}{2},k}^{n-\frac{1}{2}} \right] - \frac{\Delta t}{\epsilon \Big|_{i,j+\frac{1}{2},k}} \mathcal{J}_y \Big|_{i,j+\frac{1}{2},k}^{n-\frac{1}{2}}, \end{aligned} \quad (\text{B.17e})$$

$$\begin{aligned} \mathcal{E}_z \Big|_{i,j,k+\frac{1}{2}}^n &= \mathcal{E}_z \Big|_{i,j,k+\frac{1}{2}}^{n-1} + \frac{1}{\epsilon \Big|_{i,j,k+\frac{1}{2}}} \frac{\Delta t}{\delta} \left[\mathcal{H}_y \Big|_{i+\frac{1}{2},j,k+\frac{1}{2}}^{n-\frac{1}{2}} - \mathcal{H}_y \Big|_{i-\frac{1}{2},j,k+\frac{1}{2}}^{n-\frac{1}{2}} \right. \\ &\quad \left. - \mathcal{H}_x \Big|_{i,j+\frac{1}{2},k+\frac{1}{2}}^{n-\frac{1}{2}} + \mathcal{H}_x \Big|_{i,j-\frac{1}{2},k+\frac{1}{2}}^{n-\frac{1}{2}} \right] - \frac{\Delta t}{\epsilon \Big|_{i,j,k+\frac{1}{2}}} \mathcal{J}_z \Big|_{i,j,k+\frac{1}{2}}^{n-\frac{1}{2}}. \end{aligned} \quad (\text{B.17f})$$

Some final comments are important:

- a) The electric and magnetic fields were written in terms of the electric permittivity and magnetic permeability, respectively. This is, $\overline{\mathcal{B}}(\vec{r}, t) = \mu \overline{\mathcal{H}}(\vec{r}, t)$, $\overline{\mathcal{D}}(\vec{r}, t) = \epsilon \overline{\mathcal{E}}(\vec{r}, t)$.
- b) The material media was assumed to be time-invariant, linear, and isotropic.
- c) The central point in time for the approximation of the time derivatives of Equations (B.14d) – (B.14f) was chosen to be $n - \frac{1}{2}$, so as to produce magnetic field components defined at half-integer time steps and electric field components defined at integer time steps.
- d) The positions of the permittivity and permeability coefficients were chosen to be the same as their respective fields; i.e., ϵ is defined at the same position as \mathcal{E} , and μ is defined at the same position as \mathcal{B} .
- e) The positions of the current density components were chosen to be at the same

points as the electric field components. This is true in conducting material media where the Ohm's law holds: $\overline{\mathcal{J}}(\vec{r}, t) = \sigma \overline{\mathcal{E}}(\vec{r}, t)$.

B.4 Accuracy and Stability of the Method

The accuracy of the FDTD method can be thought intuitively. It is natural to think that in order to ensure the accuracy of the results, the size of the cells in the lattice has to be small compared to the smallest wavelength or the smallest physical dimension of the obstacles involved in the problem. A practical factor of at least ten cells per wavelength has shown to be sufficient (Sadiku, 2018). For a lattice with equal dimensions along the three coordinate axes ($\Delta x = \Delta y = \Delta z = \delta$), this implies $\delta \leq \frac{\lambda_{\min}}{10}$.

On the other hand, the stability of the method is more precisely defined by the Courant-Friedrichs-Lewy (CFL) condition (Courant, Friedrichs, & Lewy, 1967) as:

$$\text{CFL} = \frac{c\Delta t}{\sqrt{(\Delta x)^2 + (\Delta y)^2 + (\Delta z)^2}} \leq 1. \quad (\text{B.18})$$

Here, the constant CFL is a number that must be less than one as a necessary (but not sufficient) condition for the FDTD method to be stable. This has again, an intuitive interpretation. What Equation (B.18) says is that the information cannot travel more than one cell of the lattice during a simulation time step, which is very reasonable from the physical point of view.

B.5 Two-Dimensional FDTD Equations

A two-dimensional (or one-dimensional) version of Equation (B.17) can be obtained for problems in which the field components do not depend on specific coordinates in space. For instance in (Yee, 1966), the two-dimensional version of the FDTD updating equations is obtained under the assumption that the field components do not depend on the z coordinate. Moreover, Yee assumes that the current density equals zero in the region of interest, and also that the material media is homogeneous (ϵ and μ are constant every-

where). This last two assumptions are not necessary for obtaining a two-dimensional (or one-dimensional) version of the FDTD method; however, they are applied by simplicity to the problem used by Yee in order to illustrate the working principle of the FDTD method.

The application of these assumptions to Equation (B.14) produces the following two sets of *uncoupled* partial differential equations:

$$\mu \frac{\partial \mathcal{H}_x}{\partial t} = -\frac{\partial \mathcal{E}_z}{\partial y}, \quad (\text{B.19a})$$

$$\mu \frac{\partial \mathcal{H}_y}{\partial t} = \frac{\partial \mathcal{E}_z}{\partial x}, \quad (\text{B.19b})$$

$$\epsilon \frac{\partial \mathcal{E}_z}{\partial t} = \frac{\partial \mathcal{H}_y}{\partial x} - \frac{\partial \mathcal{H}_x}{\partial y}. \quad (\text{B.19c})$$

$$\epsilon \frac{\partial \mathcal{E}_x}{\partial t} = \frac{\partial \mathcal{H}_z}{\partial y}, \quad (\text{B.20a})$$

$$\epsilon \frac{\partial \mathcal{E}_y}{\partial t} = -\frac{\partial \mathcal{H}_z}{\partial x}, \quad (\text{B.20b})$$

$$\mu \frac{\partial \mathcal{H}_z}{\partial t} = \frac{\partial \mathcal{E}_x}{\partial y} - \frac{\partial \mathcal{E}_y}{\partial x}. \quad (\text{B.20c})$$

Equation (B.19) is called the transverse magnetic to z case TM_z and Equation (B.20) is called the transverse electric to z case TE_z . This is due to the fact that in each case, there are two field components that are transverse to the reference coordinate z .

Now, the FDTD updating equations for the two transverse modes of the waves mentioned above can be written by following a similar procedure to the one used in the three-dimensional case. Nevertheless, in order to obtain the same equations presented in (Yee, 1966), the central point in time must be taken to be $(n + \frac{1}{2})$ when writing the electric field time derivatives. This will allow to obtain electric field components defined at integer time steps. This choice is rather arbitrary, as the central point could also be defined at $(n - \frac{1}{2})$ —as Yee does when he writes the FDTD updating equations for the three-dimensional case—for the discretization of the electric field time derivatives.

Then, the following equations are obtained for the two wave modes. For the TE_z waves:

$$\begin{aligned} \mathcal{H}_z \Big|_{i+\frac{1}{2}, j+\frac{1}{2}}^{n+\frac{1}{2}} &= \mathcal{H}_z \Big|_{i+\frac{1}{2}, j+\frac{1}{2}}^{n-\frac{1}{2}} - \frac{1}{\mu} \frac{\Delta t}{\delta} \left[\mathcal{E}_y \Big|_{i+1, j+\frac{1}{2}}^n - \mathcal{E}_y \Big|_{i, j+\frac{1}{2}}^n \right. \\ &\quad \left. + \mathcal{E}_x \Big|_{i+\frac{1}{2}, j}^n - \mathcal{E}_x \Big|_{i+\frac{1}{2}, j+1}^n \right], \end{aligned} \quad (\text{B.21a})$$

$$\mathcal{E}_x \Big|_{i+\frac{1}{2}, j}^{n+1} = \mathcal{E}_x \Big|_{i+\frac{1}{2}, j}^n + \frac{1}{\epsilon} \frac{\Delta t}{\delta} \left[\mathcal{H}_z \Big|_{i+\frac{1}{2}, j+\frac{1}{2}}^{n+\frac{1}{2}} - \mathcal{H}_z \Big|_{i+\frac{1}{2}, j-\frac{1}{2}}^{n+\frac{1}{2}} \right], \quad (\text{B.21b})$$

$$\mathcal{E}_y \Big|_{i, j+\frac{1}{2}}^{n+1} = \mathcal{E}_y \Big|_{i, j+\frac{1}{2}}^n - \frac{1}{\epsilon} \frac{\Delta t}{\delta} \left[\mathcal{H}_z \Big|_{i+\frac{1}{2}, j+\frac{1}{2}}^{n+\frac{1}{2}} - \mathcal{H}_z \Big|_{i-\frac{1}{2}, j+\frac{1}{2}}^{n+\frac{1}{2}} \right]. \quad (\text{B.21c})$$

And for the TM_z waves:

$$\begin{aligned} \mathcal{E}_z \Big|_{i, j}^{n+1} &= \mathcal{E}_z \Big|_{i, j}^n + \frac{1}{\epsilon} \frac{\Delta t}{\delta} \left[\mathcal{H}_y \Big|_{i+\frac{1}{2}, j}^{n+\frac{1}{2}} - \mathcal{H}_y \Big|_{i-\frac{1}{2}, j}^{n+\frac{1}{2}} \right. \\ &\quad \left. + \mathcal{H}_x \Big|_{i, j-\frac{1}{2}}^{n+\frac{1}{2}} - \mathcal{H}_x \Big|_{i, j+\frac{1}{2}}^{n+\frac{1}{2}} \right], \end{aligned} \quad (\text{B.22a})$$

$$\mathcal{H}_x \Big|_{i, j+\frac{1}{2}}^{n+\frac{1}{2}} = \mathcal{H}_x \Big|_{i, j+\frac{1}{2}}^{n-\frac{1}{2}} - \frac{1}{\mu} \frac{\Delta t}{\delta} \left[\mathcal{E}_z \Big|_{i, j+1}^n - \mathcal{E}_z \Big|_{i, j}^n \right], \quad (\text{B.22b})$$

$$\mathcal{H}_y \Big|_{i+\frac{1}{2}, j}^{n+\frac{1}{2}} = \mathcal{H}_y \Big|_{i+\frac{1}{2}, j}^{n-\frac{1}{2}} + \frac{1}{\mu} \frac{\Delta t}{\delta} \left[\mathcal{E}_z \Big|_{i+1, j}^n - \mathcal{E}_z \Big|_{i, j}^n \right]. \quad (\text{B.22c})$$

B.6 Numerical Computation

Equations (B.21) and (B.22) can now be implemented in a computer, provided that there is a source in a given propagation region. In the original paper written by Yee, the only equations implemented are those of the TM_z waves, i.e., Equation (B.22). The source of excitation is an incident wave, which will be defined below; and the region of propagation is a rectangular surface, also defined below.

First, the propagation of the incident wave is simulated by assuming that there is only empty space in the propagation region; then, a square-shaped Perfect Electric Conductor (PEC) is placed inside the propagation region and the wave is scattered when it encounters the obstacle. The simulation parameters and results are presented in the next sections. The source codes of the numerical implementation in MATLAB[®] are available at the following GitHub repository: [FDTDYeePaper](#).

B.6.1 Simulation Region

The region of interest is a rectangle over the xy plane, with sides $81\Delta x$ and $98\Delta y$. There are four PEC walls placed at $i = 0$, $i = 81$, $j = \frac{1}{2}$, and $j = 97\frac{1}{2}$. The obstacle is taken to be a square made of other four PEC walls placed at $i = 17$, $i = 49$, $j = 33$, and $j = 65$. As it was stated before, the condition of the PEC materials imply zero tangential components of the electric field and zero normal components of the magnetic field at these curves.

B.6.2 Grid Size and Simulation Parameters

The size of the cells in the simulation region was chosen to be $\Delta x = \Delta y = \delta = \frac{\alpha}{8}$, with α being the wavelength of the source defined below. Also, the time step was chosen to be $\Delta t = \frac{\Delta x}{2c} = \frac{\delta}{2c}$.

B.6.3 Definition of the Source

The source in the problem region is a plane electromagnetic wave, which has only \mathcal{E}_z and \mathcal{H}_y components. The profile of the wave is a half sine and its wavelength is taken to

be α units. Furthermore, the initial position of the wave is assumed to be $x_0 = 50\Delta x$. The wave propagates in the negative direction of x with the speed of light, c . Thus, the mathematical representation of this wave can be written as:

$$\mathcal{E}_z(x, y, t) = \begin{cases} \sin \left[\frac{\pi}{\alpha} \left(x - \frac{50\alpha}{8} + ct \right) \right] & \text{if } 0 \leq \phi \leq \pi, \\ 0 & \text{otherwise.} \end{cases} \quad (\text{B.23})$$

With $\phi = \left[\frac{\pi}{\alpha} \left(x - \frac{50\alpha}{8} + ct \right) \right]$.

With the \mathcal{E}_z component of the incident wave so defined, the \mathcal{H}_y component is easily calculated as:

$$\mathcal{H}_y(x, y, t) = \frac{1}{Z} \mathcal{E}_z(x, y, t). \quad (\text{B.24})$$

Where $Z = \sqrt{\frac{\mu}{\epsilon}}$ represents the intrinsic impedance of the material media—the empty space in the present case, with $Z \approx 377\Omega$.

Figure B.2 shows the profile of this wave. The z component of the electric field has been plotted as a function of the x coordinate (in terms of the number of cells along x) for different instants of time, n . It is then shown that the incident wave is a half sine that propagates in the negative direction of x , starting at $x = 50\Delta x$.

B.6.4 Wave Propagation

When the obstacle is not present, the numerical solution of Equation (B.22) must reproduce the propagation of the incident wave towards the left of the x axis without distortion; this is shown in Figure B.3. As it can be seen, the numerical method reproduces the propagation of the wave as expected, with some ripple that may be due to the approximation made by the method and by the presence of the perfect electric conductors that are delimiting the region of simulation.

Now, if the obstacle is included in the simulation region, the electromagnetic wave is scattered and suffers distortion. This is shown in Figures B.4, B.5, and B.6 for different observation points along the y axis and for different time steps.

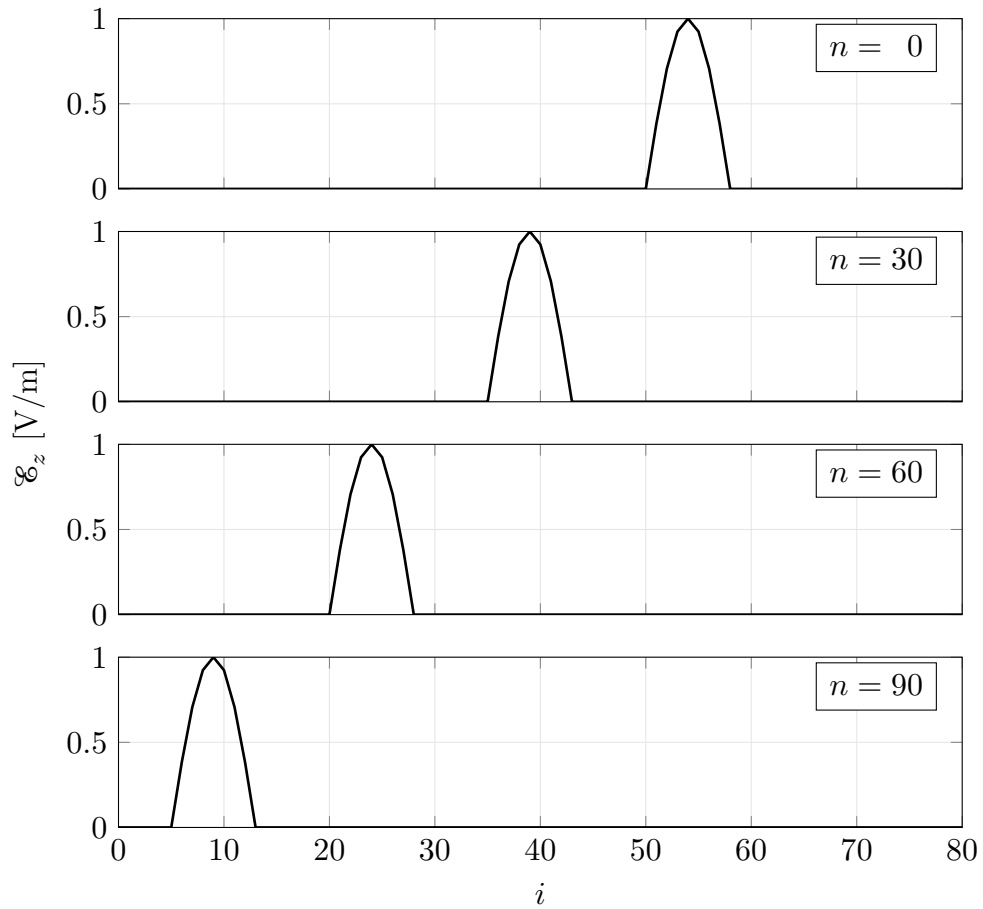


Figure B.2: Profile of the incident wave used by Yee (1966).

Finally, Figures B.7, B.8, and B.9 show an easier-to-visualize version of the propagation phenomena under consideration. They show three snapshots of the incident wave at different time instants, but plotting the \mathcal{E}_z field in the z axis, as a function of x and y .

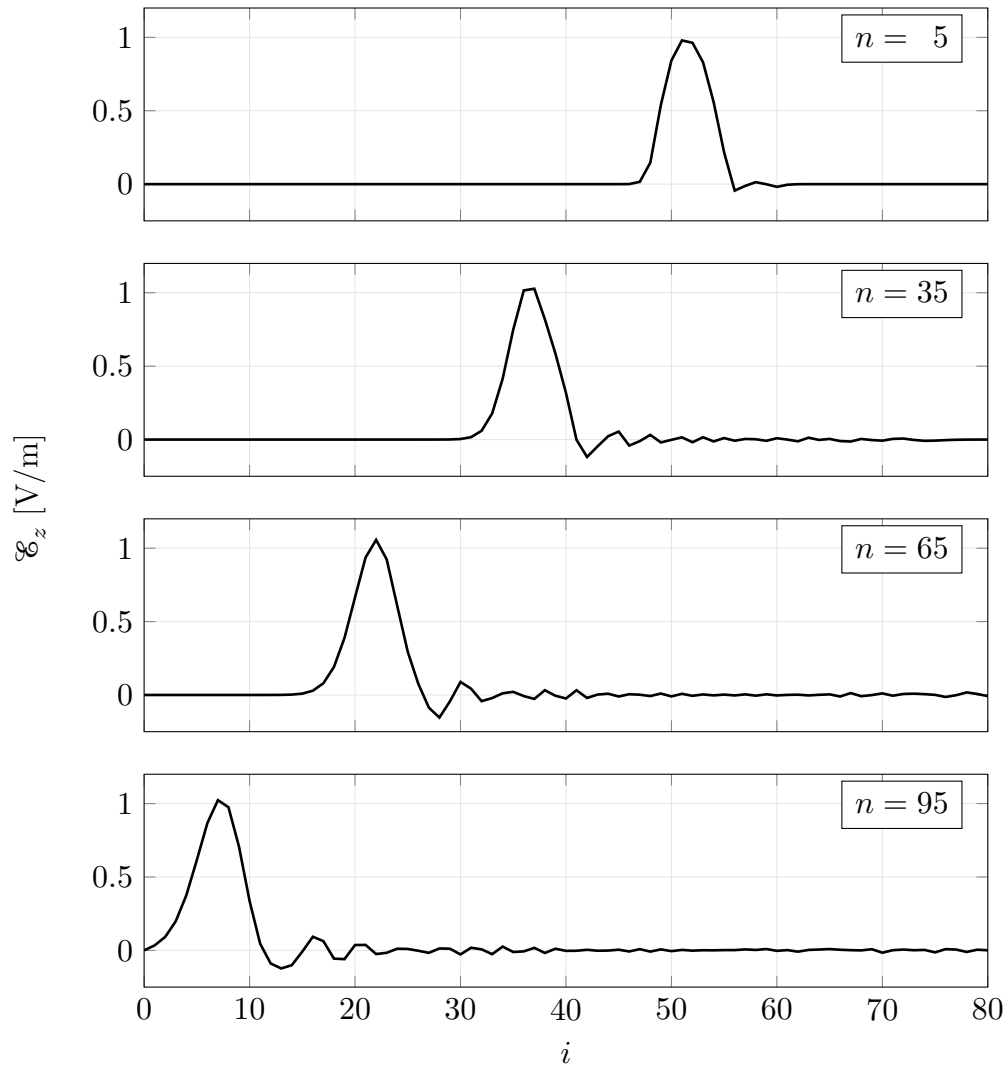


Figure B.3: Calculation of \mathcal{E}_z by means of Equation (B.22) for different time steps in the absence of the obstacle.

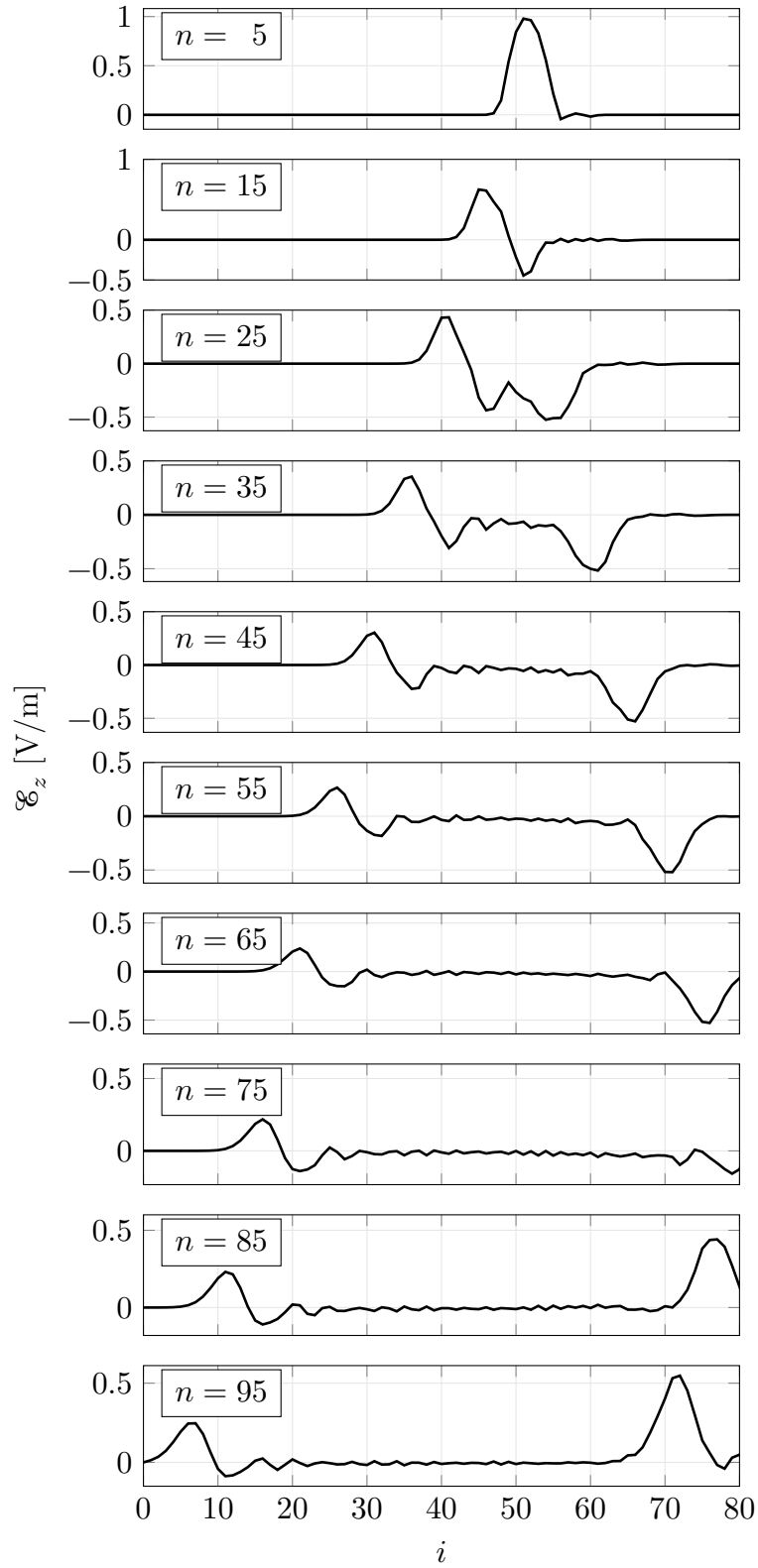


Figure B.4: Calculation of \mathcal{E}_z by means of Equation (B.22) for different time steps in presence of the obstacle. The vertical point of observation is $j = 30$.

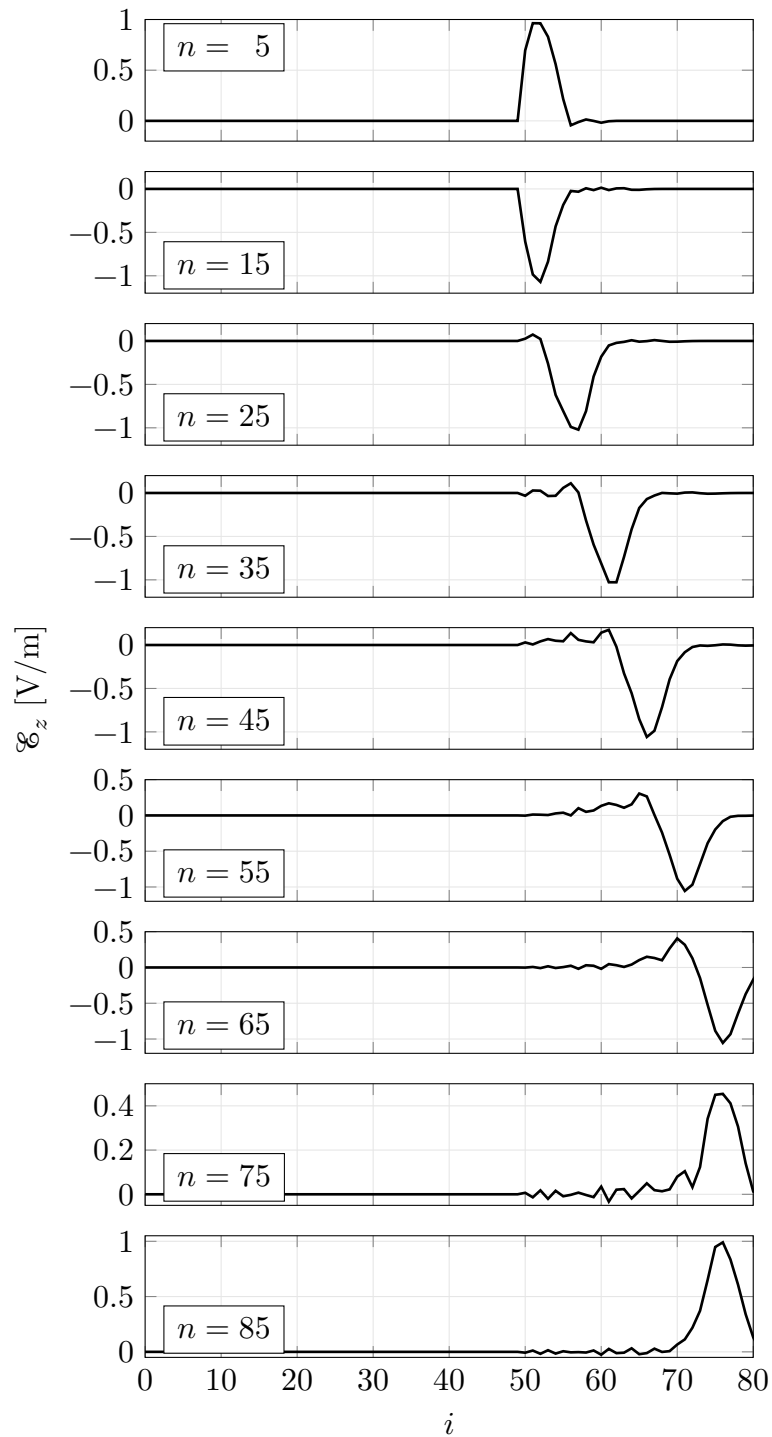


Figure B.5: Calculation of \mathcal{E}_z by means of Equation (B.22) for different time steps in presence of the obstacle. The vertical point of observation is $j = 50$.

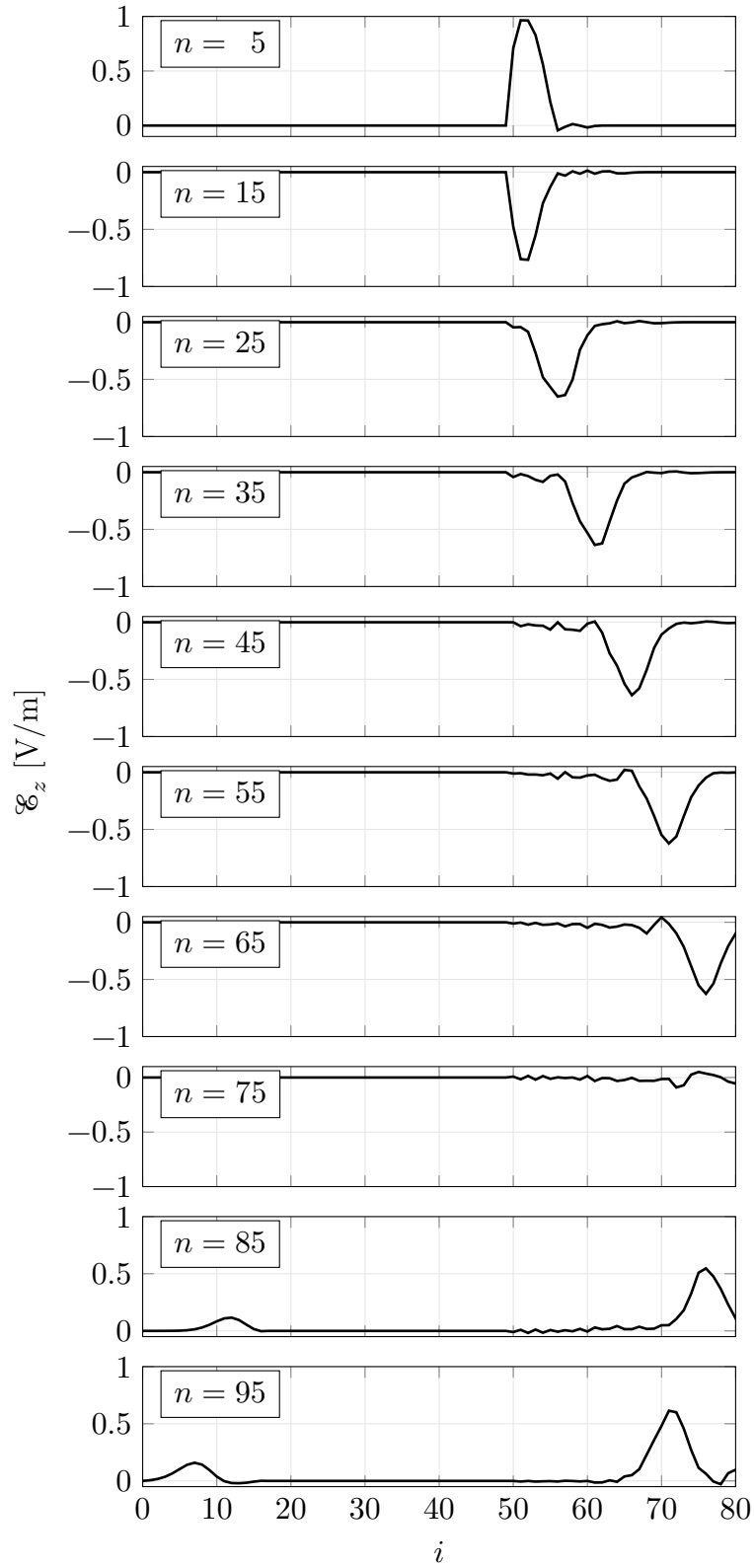


Figure B.6: Calculation of \mathcal{E}_z by means of Equation (B.22) for different time steps in presence of the obstacle. The vertical point of observation is $j = 65$.

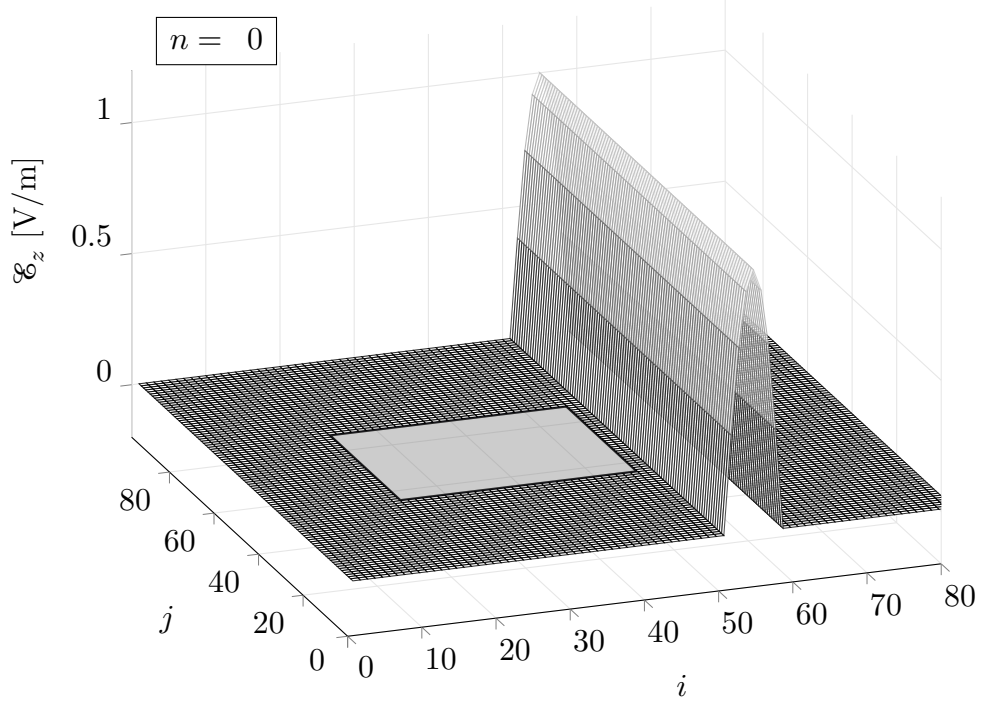


Figure B.7: Three-dimensional view of the wave propagation for time $n = 0$.

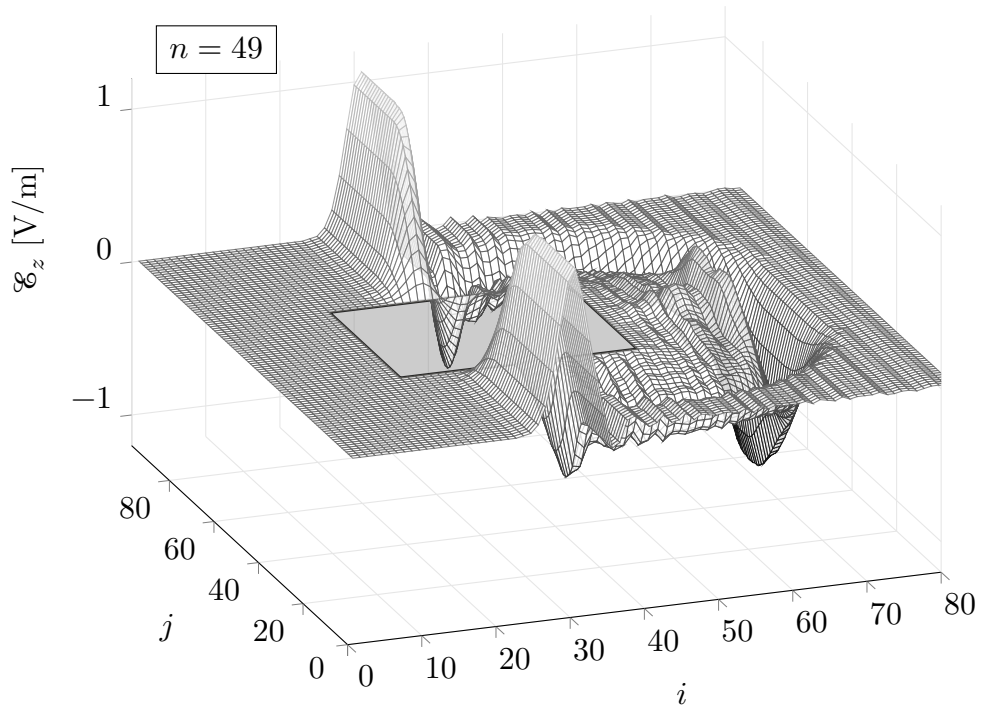


Figure B.8: Three-dimensional view of the wave propagation for time $n = 49$.

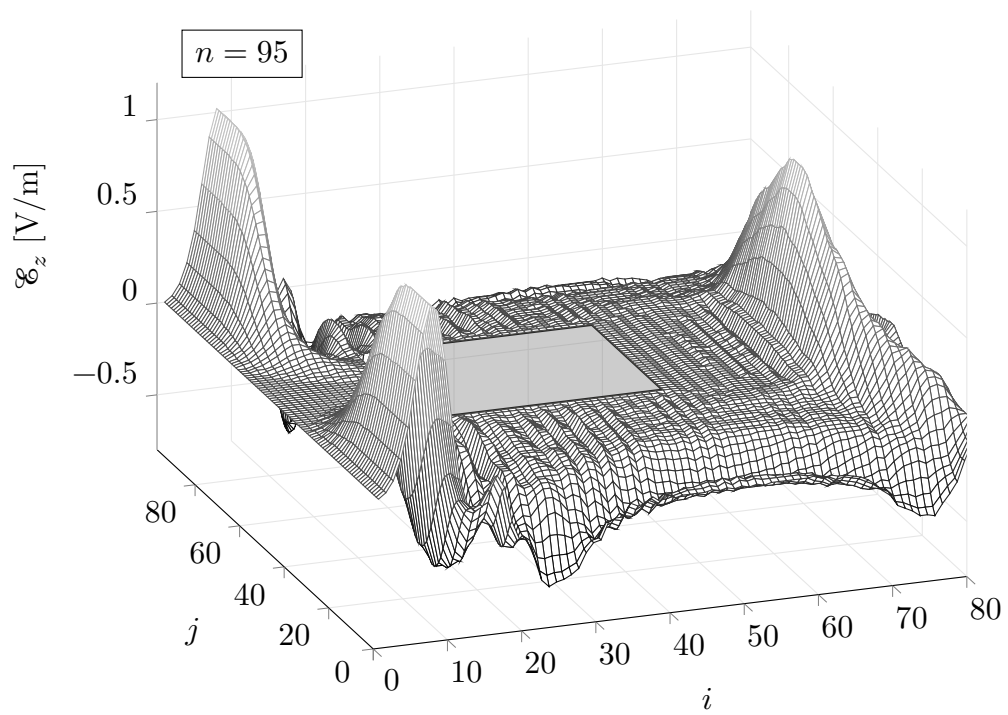


Figure B.9: Three-dimensional view of the wave propagation for time $n = 95$.

Appendix C

Lightning Return-Stroke Modelling

There are different lightning return-stroke models depending on the equations that govern them and on their scope. Rakov and Uman (1998) define four classes of lightning return stroke models: gas dynamic models or “physical models”, electromagnetic models, distributed-circuit models, and “engineering” models. For the purpose of engineering applications, the engineering-type models are adequate and then, they are widely used. These models overlook the lightning physics and instead focus on the development of mathematical expressions that represent experimental observations of the lightning process—mainly from instrumented towers. The validation of these mathematical models is made by comparison with measured data, such as lightning electromagnetic fields, optical emissions, peak and wave-shape of currents, etc. For the purpose of this thesis, the engineering-type models are quite adequate. The main of them are described below and two examples are given.

C.1 Engineering-Type Models

Following the categorization made by Rakov and Uman (1998), the four most widely used engineering-type return-stroke models are: the Transmission Line Model (TL), the Modified Transmission-Line Model with Linear Decay (MTLL), the Modified Transmission Line Model with Exponential Decay (MTLE), and the Bruce-Golde Model (BG). A

mathematical expression that generalizes all of these models is given by (C.1):

$$i(z', t) = P(z') i\left(0, t - \frac{z'}{v}\right) u\left(t - \frac{z'}{v_f}\right). \quad (\text{C.1})$$

Where

$i\left(0, t - \frac{z'}{v}\right)$ is the assumed channel-base current;

u is the Heaviside's unit step function;

$P(z')$ is the height-dependent current attenuation factor;

v_f is the upward-propagating front speed (also called return-stroke speed);

v is the current-wave propagation speed; and

z' is the height along the lightning channel.

The parameters given in Table C.1 differentiate between the engineering-type return-stroke models mentioned above. Where, H is the total channel height; α is the current

Table C.1: $P(z')$ and v parameters for engineering-type return-stroke models.

Model	$P(z')$	v
BG	1	∞
TL	1	v_f
MTLL	$1 - \frac{z'}{H}$	v_f
MTLE	$e^{-\frac{z'}{\alpha}}$	v_f

decay constant (assumed by Nucci et al. (1990) to be 2000 m); and c is the speed of light.

Two illustrative examples are given in the next sections.

C.2 Channel Base Current

Different expressions have been developed with the aim to reproduce the return-stroke currents observed at the channel base by means of instrumented towers. The majority

of them are adaptations of a double exponential function or the Heidler function. The examples given here use the channel base current proposed by Nucci et al. (1990), which is basically the sum of a Heidler, and a double exponential function:

$$i(0, t) = \left(\frac{I_1}{\eta} \right) \left(\frac{t}{\tau_1} \right)^2 \frac{e^{-\frac{t}{\tau_2}}}{1 + \left(\frac{t}{\tau_1} \right)^2} + I_2 [e^{(-t/\tau_3)} - e^{(-t/\tau_4)}] \quad (\text{C.2})$$

Where t represents the time, $I_1 = 9900$ A, $I_2 = 7500$ A, $\tau_1 = 7.2 \times 10^{-8}$ s, $\tau_2 = 5 \times 10^{-6}$ s, $\tau_3 = 60 \times 10^{-6}$ s, $\tau_4 = 6 \times 10^{-6}$ s, and $\eta = 0.845$.

C.3 Examples of Current Distributions

C.3.1 MTLE Model Example

The use of Equation (C.1) for the MTLE model produces the following expression:

$$i(z', t) = \begin{cases} e^{(-z'/\alpha)} i\left(0, t - \frac{z'}{v}\right) & \text{if } t \geq \frac{z'}{v}, \\ 0 & \text{if } t < \frac{z'}{v}. \end{cases} \quad (\text{C.3})$$

The following parameters are used to obtain the plots of current distribution along the lightning channel: $\alpha = 2000$ m and $v = 1.5 \times 10^8$ m/s. The results are presented in Figure C.1.

C.3.2 MTLL Model Example

The use of Equation (C.1) for the MTLL model produces the following expression:

$$i(z', t) = \begin{cases} \left(1 - \frac{z'}{H}\right) i\left(0, t - \frac{z'}{v}\right) & \text{if } t \geq \frac{z'}{v}, \\ 0 & \text{if } t < \frac{z'}{v}. \end{cases} \quad (\text{C.4})$$

The following parameters were used: $H = 6000$ m and $v = 1.5 \times 10^8$ m/s. The results are presented in Figure C.2.

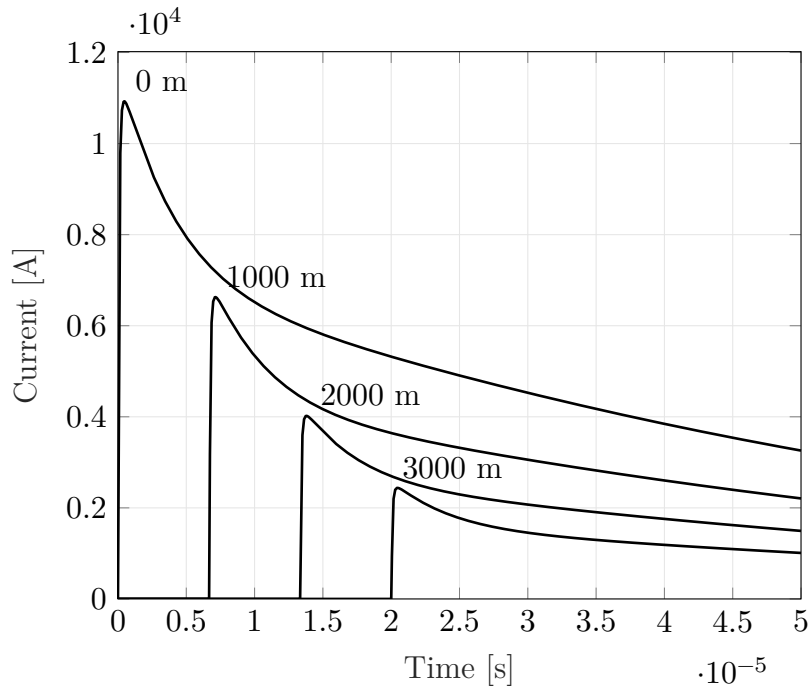


Figure C.1: MTLE model example with Nucci-type channel base current.

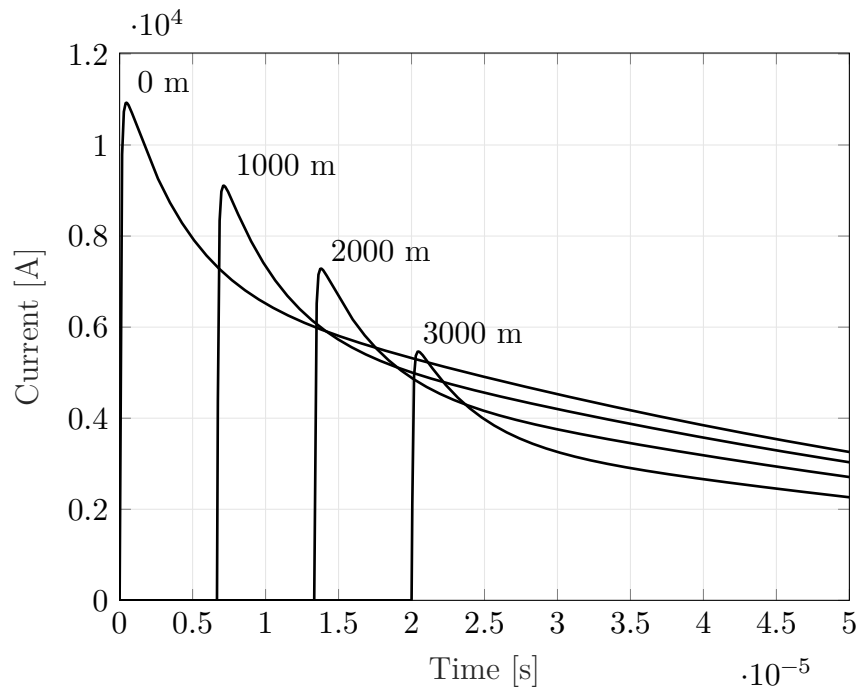


Figure C.2: MTLL model example with Nucci-type channel base current.

It is important to notice that the models exemplified here reproduce two physical characteristics of the lightning return-stroke process: the current peak attenuation with height, and the time delay of the currents with height. These two phenomena are the main differences among the engineering-type return-stroke models. The peak current attenuation is due to the resistivity of the plasma channel of the lightning, and the time delay of currents with height, is due to the finite speed of propagation of current.

Appendix D

Vectorization of the Trapezoidal Rule

D.1 Introduction

The trapezoidal rule of integration is very easy to understand and to implement in a computer program; however, in MATLAB[®] it can be implemented in two ways. Namely, by means of `for` cycles and by means of matrix operations.

The implementation with `for` cycles is very inefficient because it takes many repetitions; therefore, when a problem involves the calculation of thousands or even more integrals, the computer power becomes an issue. On the other hand, MATLAB[®] is optimized for operations involving matrices and vectors, which makes it very efficient for implementing this integration rule—among other kind of numerical computations—by means of matrix operations.

Consequently, the purpose of this appendix is to develop the intuitive idea behind the trapezoidal rule of integration, and further expand the concept to obtain general formulas that will allow the calculation of numerical integrals by means of matrix operations only.

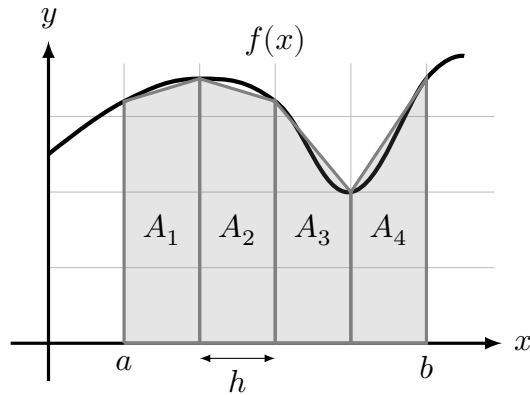


Figure D.1: Trapezoidal Rule: Intuitive Idea

D.2 Functions of One Independent Variable

D.2.1 Intuitive Idea

In the case of functions of one independent variable, the trapezoidal rule consists in approximating the area under a given curve by the sum of the areas of a chosen number of trapezoids. For an intuitive understanding, consider Figure D.1. The numerical integral of the function $f(x)$ between the points a and b can be calculated like this:

$$\int_a^b f(x)dx \approx A_1 + A_2 + A_3 + A_4. \quad (\text{D.1})$$

The areas of trapezoids can be easily calculated if function $f(x)$ is known.

As it can be seen, there is an error associated to the calculation made by means of Equation (D.1); this error can be reduced by reducing the width of the trapezoids h , which is equivalent to increasing the number of divisions n .

$$h = \frac{(b - a)}{n}. \quad (\text{D.2})$$

In the example given in Figure D.1, the number of divisions taken between a and b is $n = 4$.

D.2.2 Worked Example

For function $f(x) = x^2$, calculate the numerical integral between $a = 0$ and $b = 4$ using the trapezoidal rule. Use only 4 divisions for the calculation.

First, the analytical solution is obtained in order to test the validity of the approximation given by the trapezoidal rule:

$$\int_a^b x^2 dx = \frac{x^3}{3} \Big|_a^b = \frac{x^3}{3} \Big|_0^4 = \frac{64}{3} \approx 21.\bar{3}.$$

So now, by means of the trapezoidal rule we have:

$$\int_0^4 x^2 dx \approx A_1 + A_2 + A_3 + A_4.$$

Where A_i is the area of the i -th trapezoid, for $i = 1, \dots, 4$.

Finally, the solution to the problem can be expressed as:

$$\int_0^4 x^2 dx \approx \frac{(b_1 + B_1)h}{2} + \frac{(b_2 + B_2)h}{2} + \frac{(b_3 + B_3)h}{2} + \frac{(b_4 + B_4)h}{2}.$$

Where:

b_i : length of one of the bases of the i -th trapezoid.

B_i : length of the other base of the i -th trapezoid.

All the lengths b_i and B_i needed are calculated by evaluating function $f(x)$ in the corresponding nodes. For this particular example, we have $a = 0$, $b = 4$ and $n = 4$; then:

$$h = \frac{4 - 0}{4} = 1.$$

Hence,

$$b_1 = f(0), \quad b_2 = f(1), \quad b_3 = f(2), \quad b_4 = f(3)$$

$$B_1 = f(1), \quad B_2 = f(2), \quad B_3 = f(3), \quad B_4 = f(4).$$

$$\int_0^4 x^2 dx \approx \frac{(0+1)(1)}{2} + \frac{(1+4)(1)}{2} + \frac{(4+9)(1)}{2} + \frac{(9+16)(1)}{2} \approx 22.$$

The value obtained is relatively far from the exact value, which is $21.\overline{33}$. This is because of the low number of divisions chosen. If the precision of the method were to be increased, it would obviously be necessary to use a computer. As an exercise, it is proposed to make this same calculation but changing the number of divisions to 10, then to 100. The reader will verify that the new values obtained are 21.4400 and 21.3344, respectively.

D.2.3 Generalization of the Idea

Let $f(x)$ be an arbitrary function. The numerical integral of it between two points can be approximated by using the trapezoidal rule as:

$$\int_a^b f(x)dx \approx A_1 + A_2 + A_3 + \dots + A_n.$$

Calculating the areas of the trapezoids:

$$\int_a^b f(x)dx \approx \frac{(f(a) + f(a+h))h}{2} + \frac{(f(a+h) + f(a+2h))h}{2} + \frac{(f(a+2h) + f(a+3h))h}{2} + \dots + \frac{(f(a+(n-1)h) + f(a+nh))h}{2}.$$

Which gives:

$$\int_a^b f(x)dx \approx \frac{h}{2} \sum_{k=1}^n [f(a+(k-1)h) + f(a+kh)]. \quad (\text{D.3})$$

D.2.4 Vectorization for MATLAB[®]

Equation D.3 can be easily implemented in MATLAB[®] by means of one `for` cycle; however, that would be very inefficient. Given that MATLAB[®] is optimized for operations involving matrices and vectors, the vectorized code runs much faster than the code containing loops.

In order to do this, let us take a look at Equation (D.3), which can be expanded like:

$$\int_a^b f(x)dx \approx \frac{h}{2} \left[f(a) + f(a+h) + f(a+h) + \right. \\ \left. f(a+2h) + f(a+2h) + \right. \\ \left. f(a+3h) + f(a+3h) + \dots + \right. \\ \left. f(a+(n-1)h) + \underbrace{f(a+nh)}_{=f(b)} \right].$$

Thereby,

$$\int_a^b f(x)dx \approx \frac{h}{2} \left[f(a) + 2f(a+h) + 2f(a+2h) + \right. \\ \left. 2f(a+3h) + \dots + 2f(a+(n-1)h) + f(b) \right].$$

This same result can be obtained by performing the following vector operations:

$$I := \int_a^b f(x)dx.$$

$$I \approx \frac{h}{2} \underline{B} \underline{W}. \tag{D.4}$$

Equation (D.4) is identical to (D.3), but Equation (D.4) does not need a `for` cycle in order to be implemented in MATLAB®.

In order for Equation (D.4) to be equal to Equation (D.3), the vectors \underline{B} and \underline{W} must be defined as follows:

$$\underline{B} = \left[f(a) \quad f(a+h) \quad f(a+2h) \quad \dots \quad f(b) \right].$$

$$\underline{W} = \begin{bmatrix} 1 \\ 2 \\ 2 \\ \vdots \\ 2 \\ 2 \\ 1 \end{bmatrix} .$$

Both \underline{B} and \underline{W} have dimension equal to the number of nodes ($n + 1$). \underline{B} is a vector that contains the results of evaluating $f(x)$ in all the nodes; therefore, it is a vector of scalar numbers. \underline{W} instead, does not depend on $f(x)$; it is called the *weights vector*.

D.2.5 Numerical Example

Let us try with function $f(x) = x^2$, integrating between 0 and 4, and using 100 divisions:

```
>> f = inline('x.^2','x');
>> I = trap_rule(f,0,4,100);
The numerical integral is: 21.3344
```

Code listings for this example are given in Section D.4.

D.3 Functions of Two Independent Variables

D.3.1 Generalization of the Idea for Functions of Two Variables

Let us suppose that the numerical value of the following integral needs to be calculated:

$$I = \iint_R f(x, y) dA.$$

Where R is the rectangular region of the plane $R = \{(x, y) : a \leq x \leq b, c \leq y \leq d\}$, so that:

$$I = \int_c^d \int_a^b f(x, y) dx dy.$$

The numerical value of this integral can be obtained by applying the trapezoidal rule. Consider the following definitions:

n : number of divisions along the x axis.

m : number of divisions along the y axis.

h : height of the trapezoids along the x axis.

k : height of the trapezoids along the y axis.

Therefore,

$$h = \frac{(b - a)}{n}.$$

$$k = \frac{(d - c)}{m}.$$

The integral can be expressed like:

$$I = \int_c^d \left[\int_a^b f(x, y) dx \right] dy = \int_c^d g(y) dy.$$

Where $g(y) = \int_a^b f(x, y) dx$, taking x as a constant.

Let us now make a parenthesis to see that further generalization of Equation (D.3) can be introduced to obtain the following expression:

$$\int_a^b f(x) dx \approx \frac{h}{2} \left[f(x_1) + 2 \sum_{k=2}^n f(x_k) + f(x_{n+1}) \right]. \quad (\text{D.5})$$

With the values of x_k given by $x_k = a + (k - 1)h \quad \forall \quad k = 1, 2, 3, \dots, (n + 1)$.

With this last expression, we can continue working on the integral $I = \int_c^d g(y)dy$:

$$I = \int_c^d g(y)dy \approx \frac{k}{2} \left[g(y_1) + 2 \sum_{j=2}^m g(y_j) + g(y_{m+1}) \right].$$

Where $y_j = c + (j-1)k \quad \forall \quad j = 1, 2, 3, \dots, (m+1)$. But we know that $g(y)$ is in turn another integral, so that:

$$I \approx \frac{k}{2} \left[\int_a^b f(x, y_1)dx + 2 \sum_{j=2}^m \int_a^b f(x, y_j)dx + \int_a^b f(x, y_{m+1})dx \right].$$

Now, by applying the structure of Equation (D.5) again, we arrive to the following summations:

$$\begin{aligned} I \approx \frac{k}{2} & \left(\frac{h}{2} \left[f(x_1, y_1) + 2 \sum_{i=2}^n f(x_i, y_1) + f(x_{n+1}, y_1) \right] + \right. \\ & \left. 2 \sum_{j=2}^m \left[\frac{h}{2} \left(f(x_1, y_j) + 2 \sum_{i=2}^n f(x_i, y_j) + f(x_{n+1}, y_j) \right) \right] + \right. \\ & \left. \frac{h}{2} \left[f(x_1, y_{m+1}) + 2 \sum_{i=2}^n f(x_i, y_{m+1}) + f(x_{n+1}, y_{m+1}) \right] \right). \end{aligned}$$

With $x_i = a + (i-1)h \quad \forall \quad i = 1, 2, 3, \dots, (n+1)$.

The factorization of the term $\frac{h}{2}$ takes us to the final expression for the numerical calculation of double integrals:

$$\begin{aligned} I \approx \frac{hk}{4} & \left(f(x_1, y_1) + 2 \sum_{i=2}^n f(x_i, y_1) + f(x_{n+1}, y_1) + \right. \\ & 2 \sum_{j=2}^m f(x_1, y_j) + 4 \sum_{j=2}^m \sum_{i=2}^n f(x_i, y_j) + 2 \sum_{j=2}^m f(x_{n+1}, y_j) + \\ & \left. f(x_1, y_{m+1}) + 2 \sum_{i=2}^n f(x_i, y_{m+1}) + f(x_{n+1}, y_{m+1}) \right). \end{aligned} \quad (D.6)$$

D.3.2 Vectorization for MATLAB[®]

Again, Equation (D.6) can be implemented computationally with `for` cycles, which is not very efficient given that it is needed to nest them at least once. The analysis that follows has been mainly adapted from (Cordero-Barbero, Hueso-Pagoaga, Martínez-Molada, & Torregrosa-Sánchez, 2012).

The expansion of the summations given in Equation (D.6) produces:

$$\begin{aligned}
 I \approx \frac{hk}{4} & \left(f(x_1, y_1) + 2f(x_2, y_1) + 2f(x_3, y_1) + \cdots + f(x_n, y_1) + f(x_{n+1}, y_1) + \right. \\
 & 2f(x_1, y_2) + 2f(x_1, y_3) + 2f(x_1, y_4) + \cdots + 2f(x_1, y_m) + \\
 & 4f(x_2, y_2) + 4f(x_3, y_2) + 4f(x_4, y_2) + \cdots + 4f(x_n, y_3) + \\
 & \vdots \\
 & 4f(x_2, y_m) + 4f(x_3, y_m) + 4f(x_4, y_m) + \cdots + 4f(x_n, y_m) + \\
 & 2f(x_{n+1}, y_2) + 2f(x_{n+1}, y_3) + 2f(x_{n+1}, y_4) + \cdots + 2f(x_{n+1}, y_m) + f(x_1, y_{m+1}) + \\
 & \left. 2f(x_2, y_{m+1}) + 2f(x_3, y_{m+1}) + \cdots + 2f(x_n, y_{m+1}) + f(x_{n+1}, y_{m+1}) \right).
 \end{aligned}$$

Grouping these terms by rows:

$$\begin{aligned}
 I \approx \frac{hk}{4} & \left(f(x_1, y_1) + 2f(x_1, y_2) + 2f(x_1, y_3) + \cdots + 2f(x_1, y_m) + f(x_1, y_{m+1}) + \right. \\
 & 2f(x_2, y_1) + 4f(x_2, y_2) + 4f(x_2, y_3) + \cdots + 4f(x_2, y_m) + 2f(x_2, y_{m+1}) + \\
 & 2f(x_3, y_1) + 4f(x_3, y_2) + 4f(x_3, y_3) + \cdots + 4f(x_3, y_m) + 2f(x_3, y_{m+1}) + \\
 & \vdots \\
 & 2f(x_n, y_1) + 4f(x_n, y_2) + 4f(x_n, y_3) + \cdots + 4f(x_n, y_m) + 2f(x_n, y_{m+1}) + \\
 & \left. f(x_{n+1}, y_1) + 2f(x_{n+1}, y_2) + 2f(x_{n+1}, y_3) + \cdots + 2f(x_{n+1}, y_m) + f(x_{n+1}, y_{m+1}) \right).
 \end{aligned}$$

This development gives us a clear understanding of the fact that the numerical integral is just the summation of the evaluations of the two-variable function in all the possible nodes, multiplying these evaluations by some numerical constants that will be called *weights*. Thus, the numerical integration can be compactly expressed as:

$$\int_c^d \int_a^b f(x, y) dx dy \approx \frac{hk}{4} \sum_{j=1}^{m+1} \sum_{i=1}^{n+1} W_{ij} f(x_i, y_i).$$

A matrix of weights can be formed to multiply the evaluations of the function:

$$\underline{\underline{W}}_{(n+1) \times (m+1)} = \begin{bmatrix} 1 & 2 & 2 & \cdots & 2 & 2 & 1 \\ 2 & 4 & 4 & \cdots & 4 & 4 & 2 \\ 2 & 4 & 4 & \cdots & 4 & 4 & 2 \\ \vdots & \vdots & \vdots & & \vdots & \vdots & \vdots \\ 2 & 4 & 4 & \cdots & 4 & 4 & 2 \\ 2 & 4 & 4 & \cdots & 4 & 4 & 2 \\ 1 & 2 & 2 & \cdots & 2 & 2 & 1 \end{bmatrix}. \quad (\text{D.7})$$

Matrix $\underline{\underline{W}}$ can also be put in a simpler way like:

$$\underline{\underline{W}} = \underline{\underline{P}} \underline{\underline{Q}}$$

With,

$$\underline{P}_{(n+1) \times 1} = \begin{bmatrix} 1 \\ 2 \\ 2 \\ \vdots \\ 2 \\ 2 \\ 1 \end{bmatrix}.$$

$$\underline{Q}_{1 \times (m+1)} = \begin{bmatrix} 1 & 2 & 2 & \dots & 2 & 2 & 1 \end{bmatrix}.$$

Finally, if another matrix containing the evaluations of the function in all the nodes is defined, it is easy to obtain the numerical integral by performing only matrix operations.

This is:

$$\underline{F}_{(n+1) \times (m+1)} = \begin{bmatrix} f_{1,1} & f_{1,2} & f_{1,3} & \dots & f_{1,(m+1)} \\ f_{2,1} & f_{2,2} & f_{2,3} & \dots & f_{2,(m+1)} \\ \vdots & & & & \vdots \\ f_{(n+1),1} & f_{(n+1),2} & f_{(n+1),3} & \dots & f_{(n+1),(m+1)} \end{bmatrix}. \quad (\text{D.8})$$

Here, $f_{1,1} = f(x_1, y_1)$, and $f_{(n+1),(m+1)} = f(x_{n+1}, y_{m+1})$. So the final expression is:

$$I = \left(\frac{hk}{4} \right) \underline{Q} \underline{F}^T \underline{P} \quad (\text{D.9})$$

D.3.3 Numerical Example

Let the two-variable function $f(x, y) = x^2y$. In order to validate the formula given by Equation (D.9), let us calculate the integral of $f(x, y)$ like this:

$$\int_0^4 \int_0^4 (x^2y) dx dy = \frac{512}{3} \approx 170.6\bar{6}.$$

```
>> f = inline('x.^2.*y','x','y');
>> I = double_trap_rule(f,0,4,0,4,100,100);
The numerical integral is: 170.6752
```

Code listings used in this example are given in Section D.4.

D.4 MATLAB[®] Code Listings for the Examples

Listing D.1: MATLAB[®] Implementation for One-Variable Functions

```
1 % Trapezoidal rule for numerical integration of one-variable
   functions.
2
3 % f: inline definition of the function to be integrated.
4 % a, b: lower and upper integral limits.
5 % n: number of divisions.
6
7 function I = trap_rule(f,a,b,n)
8 h = (b-a)/n;
9 sp = a:h:b;
10 B = f(sp);
11 w = zeros(1,(n+1)) + 2;
12 w(1,1) = 1;
13 w(1,(n+1)) = 1;
14
15 I = (h/2)*(B*w');
16
17 fprintf('The numerical integral is: %.4f\n',I)
18 end
```

Listing D.2: MATLAB® Implementation for Two-Variable Functions

```

1 % Trapezoidal rule for numerical integration of two-variable
   functions.
2
3 % f: inline definition of the function to be integrated.
4 % a, b: lower and upper integral limits in x.
5 % c, d: lower and upper integral limits in y.
6 % n: number of divisions in x.
7 % m: number of divisions in y.
8
9 function I = double_trap_rule(f,a,b,c,d,n,m)
10 h = (b-a)/n;
11 k = (d-c)/m;
12
13 spx = a:h:b;
14 spy = c:k:d;
15
16 [Y,X] = meshgrid(spy,spx);
17
18 P = zeros((n+1),1) + 2;
19 P(1,1) = 1;
20 P(end,1) = 1;
21
22 Q = zeros(1,(m+1)) + 2;
23 Q(1,1) = 1;
24 Q(1,end) = 1;
25
26 F = f(X,Y);
27

```

```
28 I = (h*k/4)*(Q*F'*P);  
29  
30 fprintf('The numerical integral is: %.4f\n',I)  
31 end
```

References

- Aoki, M., Baba, Y., & Rakov, V. A. (2015). FDTD Simulation of LEMP Propagation Over Lossy Ground: Influence of Distance, Ground Conductivity, and Source Parameters. *Journal of Geophysical Research: Atmospheres*, 120(16), 8043–8051.
- Arzag, K., Azzouz, Z., & Ghemri, B. (2016). Lightning Electromagnetic Pulse Simulation Using 3D-FDTD Method (Comparison Between PEC and UPLM Boundary Conditions). In *2016 33rd International Conference on Lightning Protection (ICLP)* (pp. 1–6).
- Bannister, P. R. (1984). *Extension of Finitely Conducting Earth-Image-Theory Results to Any Range* (Tech. Rep.). Naval Underwater Systems Center, New London Connecticut.
- Bérenger, J.-P. (2002). FDTD Computation of VLF-LF Propagation in the Earth-Ionosphere Waveguide. In *Annales des Télécommunications* (Vol. 57, pp. 1059–1090).
- Carassa, F. (1982, December). On the 80th Anniversary of the First Transatlantic Radio Signal. *IEEE Antennas and Propagation Society Newsletter*, 24(6), 10-19. doi: 10.1109/MAP.1982.27650
- Cooray, V. (2008, July). On the Accuracy of Several Approximate Theories Used in Quantifying the Propagation Effects on Lightning Generated Electromagnetic Fields. *IEEE Transactions on Antennas and Propagation*, 56(7), 1960–1967. doi: 10.1109/TAP.2008.924680
- Cordero-Barbero, A., Hueso-Pagoaga, J. L., Martínez-Molada, E., & Torregrosa-Sánchez, J. R. (2012). *Métodos Numéricos con MATLAB*. Universitat Politècnica de València.

- Courant, R., Friedrichs, K., & Lewy, H. (1967, March). On the Partial Difference Equations of Mathematical Physics. *IBM Journal of Research and Development*, 11(2), 215-234. doi: 10.1147/rd.112.0215
- Cummer, S. A. (2000). Modeling Electromagnetic Propagation in the Earth-Ionosphere Waveguide. *IEEE Transactions on Antennas and Propagation*, 48(9), 1420–1429.
- Cummins, K. L., & Murphy, M. J. (2009). An Overview of Lightning Locating Systems: History, Techniques, and Data Uses, With an In-Depth Look at the U.S. NLDN. *IEEE Transactions on Electromagnetic Compatibility*, 51(3), 499-518.
- Furutsu, K. (1982). A Systematic Theory of Wave Propagation over Irregular Terrain. *Radio Science*, 17(5), 1037–1050.
- Gong, J., Maclean, T. S. M., & Wu, Z. (1989). Radiowave Propagation over Rectangular Plateau. *Electronics Letters*, 25(11), 707–709.
- Google. (2020, January). *Google Earth Pro (Version 7.3) [Computer Software]*. <https://www.google.com/intl/es/earth/download/gep/agree.html>.
- Hertz, H. (1888). On the Finite Velocity of Propagation of Electromagnetic Actions. *Electric Waves*, 110.
- Hufford, G. A. (1952). An Integral Equation Approach to the Problem of Wave Propagation Over an Irregular Surface. *Quarterly of Applied Mathematics*, 9(4), 391–404.
- Hunsucker, R. D., & Hargreaves, J. K. (2003). *The High-Latitude Ionosphere and its Effects on Radio Propagation*. Cambridge University Press.
- Hunt, B. J. (2005). *The Maxwellians*. Cornell University Press.
- Inan, U. S., & Marshall, R. A. (2011). *Numerical Electromagnetics: the FDTD Method*. Cambridge University Press.
- Kissick, W. A., Haakinson, E. J., & Stonehocker, G. H. (1978). *Measurements of LF and MF Radio Propagation over Irregular, Inhomogeneous Terrain* (Vol. 79; Tech. Rep.). NASA STI/Recon Technical Report N.
- Li, D., Azadifar, M., Rachidi, F., Rubinstein, M., Diendorfer, G., Sheshyekani, K., ... Wang, Z. (2016). Analysis of Lightning Electromagnetic Field Propagation in Mountainous Terrain and its Effects on ToA-Based Lightning Location Systems. *Journal*

- of Geophysical Research: Atmospheres*, 121(2), 895–911.
- Li, D., Azadifar, M., Rachidi, F., Rubinstein, M., Paolone, M., Pavanello, D., ... Wang, Z. (2016). On lightning electromagnetic field propagation along an irregular terrain. *IEEE Transactions on Electromagnetic Compatibility*, 58(1), 161–171.
- Liao, Z.-F., Huang, K.-l., Yang, B.-p., & Yuan, Y.-F. (1984). A Transmitting Boundary for Transient Wave Analyses. *Science in China Series A-Mathematics, Physics, Astronomy & Technological Science*, 27(10), 1063–1076.
- Maclean, T. S. M., & Wu, Z. (1993). *Radiowave Propagation over Ground*. Chapman & Hall London.
- Maxwell, J. C. (1865, January). A Dynamical Theory of the Electromagnetic Field. *Philosophical Transactions of the Royal Society of London*, 459–512. doi: 10.1098/rstl.1865.0008
- Monteath, G. D. (1978). *Computation of Groundwave Attenuation Over Irregular and Inhomogeneous Ground at Low and Medium Frequencies* (Vol. 78; Tech. Rep.). Research Department, Engineering Division - THE BRITISH BROADCASTING CORPORATION.
- Noda, T., Yonezawa, R., Yokoyama, S., & Takahashi, Y. (2004, October). Error in Propagation Velocity Due to Staircase Approximation of an Inclined Thin Wire in FDTD Surge Simulation. *IEEE TRANSACTIONS ON POWER DELIVERY*, 19(4), 1913–1918.
- Norton, K. A. (1937). The Propagation of Radio Waves over the Surface of the Earth and in the Upper Atmosphere. *Proceedings of the Institute of Radio Engineers*, 25(9), 1203–1236. doi: 10.1109/JRPROC.1937.228544
- Nucci, C. A., Diendorfer, G., Uman, M. A., Rachidi, F., Ianoz, M., & Mazzetti, C. (1990). Lightning Return Stroke Current Models with Specified Channel-Base Current: A Review and Comparison. *Journal of Geophysical Research: Atmospheres*, 95(D12), 20395–20408.
- Ott, R. H. (1971a). An Alternative Integral Equation for Propagation Over Irregular Terrain, 2. *Radio Science*, 6(4), 429–435.

- Ott, R. H. (1971b). *A New Method for Predicting HF Ground Wave Attenuation over Inhomogeneous, Irregular Terrain* (Tech. Rep.). Office of Telecommunications, Institute for Telecommunication Sciences. Boulder, Colorado.
- Ott, R. H., & Berry, L. A. (1970). An Alternative Integral Equation for Propagation Over Irregular Terrain. *Radio Science*, 5(5), 767-771. doi: 10.1029/RS005i005p00767
- Ott, R. H., Vogler, L., & Hufford, G. (1979). Ground-Wave Propagation Over Irregular Inhomogeneous Terrain: Comparisons of Calculations and Measurements. *IEEE Transactions on Antennas and Propagation*, 27(2), 284-286.
- Pérez-Pérez, D. (2014). *Eficiencia de los sistemas de localización del rayo en zonas montañosas* (M.Sc. Thesis).
- Qin, Z., Chen, M., Zhu, B., & Du, Y.-P. (2017). An Improved Ray Theory and Transfer Matrix Method-based Model for Lightning Electromagnetic Pulses Propagating in Earth-Ionosphere Waveguide and its Applications. *Journal of Geophysical Research: Atmospheres*, 122(2), 712-727.
- Rakov, V. A., & Uman, M. A. (1998). Review and Evaluation of Lightning Return Stroke Models Including Some Aspects of Their Application. *IEEE transactions on Electromagnetic Compatibility*, 40(4), 403-426.
- Rubinstein, M., & Uman, M. A. (1989). Methods for Calculating the Electromagnetic Fields from a Known Source Distribution: Application to Lightning. *IEEE Transactions on Electromagnetic Compatibility*, 31(2), 183-189.
- Sadiku, M. N. (2018). *Computational Electromagnetics with MATLAB*. CRC Press.
- Schulz, W., & Diendorfer, G. (2000). Evaluation of a Lightning Location Algorithm using an Elevation Model. In *25th International Conference on Lightning Protection (ICLP)*, Rhodos.
- Sommerfeld, A. (1909). Über die Ausbreitung der Wellen in der drahtlosen Telegraphie. *Annalen der Physik*, 333(4), 665-736.
- Thang, T. H., Baba, Y., Somu, V. B., & Rakov, V. A. (2017). FDTD Modeling of LEMP Propagation in the Earth-Ionosphere Waveguide With Emphasis on Realistic Representation of Lightning Source. *Journal of Geophysical Research: Atmospheres*,

122(23).

- Thang, T. H., Rakov, V. A., Baba, Y., & Somu, V. B. (2016). 2D FDTD Simulation of LEMP Propagation Considering the Presence of Conducting Atmosphere. In *2016 Asia-Pacific International Symposium on Electromagnetic Compatibility (APEMC)* (Vol. 1, pp. 19–21).
- Thèvenot, M., Bérenger, J. P., Monedièrre, T., & Jecko, F. (1999). A FDTD Scheme for the Computation of VLF-LF Propagation in the Anisotropic Earth-Ionosphere Waveguide. In *Annales des Télécommunications* (Vol. 54, pp. 297–310).
- Uman, M. A. (1987). *The Lightning Discharge*. Academic Press, Inc.
- Uman, M. A., McLain, D. K., & Krider, E. P. (1975). The Electromagnetic Radiation from a Finite Antenna. *American Journal of Physics*, *43*(1), 33–38.
- Watts, M. E. (2003). Perfect Plane-Wave Injection into a Finite FDTD Domain through Teleportation of Fields. *Electromagnetics*, *23*(2), 187–201.
- Wu, Z., Maclean, T. S. M., Bagwell, D. J., & Mehler, M. J. (1988). Propagation over an Inhomogenous Irregular Surface. *Radio Science*, *23*(1), 33–40.
- Yee, K. (1966, May). Numerical Solution of Initial Boundary Value Problems Involving Maxwell's Equations in Isotropic Media. *IEEE Transactions on Antennas and Propagation*, *14*(3), 302–307. doi: 10.1109/TAP.1966.1138693
- Yu, T.-b., Zhou, B.-h., & Liu, S.-h. (2006). A Modified Liao's Absorbing Boundary Condition with Stabilization. In *The 2006 4th Asia-Pacific Conference on Environmental Electromagnetics* (pp. 372–374).